MODELING, SIMULATION, AND CONTROL OF BIOTRICKLING FILTER FOR REMOVAL OF AIR POLLUTANTS

by

Wasim Ahmed

A Thesis Presented to the Faculty of the
American University of Sharjah
College of Engineering
in Partial Fulfillment
of the Requirements
for the Degree of

Master of Science in
Chemical Engineering

Sharjah, United Arab Emirates

June 2012

Approval Signatures

We, the undersigned, approve the Master's Thesis of Wasim Ahmed.

Thesis Title: Modeling, Simulation, and Control of Biotrickling Filter for Removal of Air Pollutants

Signature	**Date of Signature**
_____	_____
Dr. Zarook Shareefdeen Associate Professor, Department of Chemical Engineering Thesis Advisor	
_____	_____
Dr. Nabil Abdel Jabbar Professor, Department of Chemical Engineering Thesis Co-Advisor	
_____	_____
Dr. Rachid Chebbi Professor, Department of Chemical Engineering Thesis Committee Member	
_____	_____
Dr. Ahmed Aidan Lab Instructor, Department of Chemical Engineering Thesis Committee Member	
_____	_____
Dr. Abdul-Rahman Al-Ali Professor, Department of Computer Science and Engineering External Thesis Committee Member	
_____	_____
Dr. Dana Abouelnasr Head, Department of Chemical Engineering	
_____	_____
Dr. Hany El-Kadi Associate Dean, College of Engineering	
_____	_____
Dr. Yousef Al-Assaf Dean of College of Engineering	
_____	_____
Dr. Khaled Assaleh Director of Graduate Studies	

Abstract

Stringent environmental regulations for control of pollutants have led to the use of effective air pollution control strategies. Biotrickling filter, one of the biological reactors, offers a great advantage of being a cost effective and environmental friendly technology. This emerging technology has not yet received widespread application. Moreover, there is still a need to develop an appropriate biotrickling filter model for general acceptance and equally important to design an optimum control strategy before utilizing this technology on a large scale. Hence, this thesis aims to develop a representative dynamic model for the biotrickling filter based on the review of existing models, provide accurate analytical and numerical solution of the model under different conditions, and also select an optimum control strategy amongst the different control systems designed in this study. A theoretical model was selected, validated and modified to account for continuous, larger biotrickling filter. The modified model was solved using the pseudo-steady state assumption to reduce computational effort and time. Based on sensitivity analysis of the modified model, it was found that gas velocity and inlet concentration had strong effect on the outlet concentration of biotrickling filter. To implement the control strategies, simple data driven models were obtained using the data from simulation of the modified model. These data driven models were needed since the modified model simulation would require considerable computational effort and time. In particular, transfer function and neural network models were successfully obtained with R^2 values above 0.97. Five control strategies were designed, implemented and analyzed through set-point and disturbance changes. Three of the five controllers were based on transfer function biotrickling filter model while the rest used steady state neural networks as the biotrickling filter plant model. Overall, it was found that the proportional-integral, proportional-integral with feedforward and the transfer function based model predictive controllers provided satisfactory system performance. In case of the neural network based model predictive controller, excellent set-point tracking had been observed but an offset error had been observed in case of disturbance change. While the addition of an integral controller to the neural network based model predictive controller eliminated the offset errors, large overshoots had been observed in response to both set-point and disturbance changes.

Search Terms: *biotrickling filter, mathematical modeling, step response model, neural network model, biotrickling filter control strategies, conventional control strategies, advanced control*

Table of Contents

List of Figures

List of Tables

Nomenclature

A_{nw} - non-wetted area (m^2)

A_w - wetted area (m^2)

a - specific interfacial area (m^{-1})

a_w - specific wetted area ($m^2/(m^3$ of packed bed))

C - H_2S concentration ($g\ m^{-3}$)

C_{gi1} - gas phase concentration of H_2S at gas-liquid interface ($g\ m^{-3}$)

C_{gi2} - gas phase concentration of H_2S at gas-biofilm interface ($g\ m^{-3}$)

C_{Li2} - liquid phase concentration of H_2S at liquid-biofilm interface ($g\ m^{-3}$)

C_{wb} - concentration of H_2S in the wetted biofilm ($g\ m^{-3}$)

C_{nwb} - concentration of H_2S in the non-wetted biofilm ($g\ m^{-3}$)

D_g - H_2S diffusion coefficient in air ($m^2\ h^{-1}$)

D_L - diffusivity of H_2S in trickling liquid ($m^2\ h^{-1}$)

d - disturbance variable

EBRT - empty bed residence time, $\frac{\text{Bed height}}{u_g}$ (h or sec)

F - volumetric flow rate (m^3h^{-1})

Fr - Froude number

FT - biofilm thickness (m)

ΔFT - discretized biofilm thickness (m)

G - superficial mass velocity of gas ($kgm^{-2}h^{-1}$)

G(s) - transfer function

G_c - controller transfer function

G_d - disturbance transfer function

G_f - feedforward controller transfer function

G_m / G_t - sensor transfer function

G_p - process transfer function

G_v - control valve transfer function

g_c - gravitational constant (mh^{-2})

H - Henry's constant (-)

i, j - index for finite elements in the dynamic model

K - gain

K_c - proportional gain

K_{IP} - current to pressure transducer gain

K_m - measurement gain

K_s - Michaelis-Menten constant ($g\ m^{-3}$)

K_v - control valve gain

k_{g1} - mass transfer coefficient from gas to liquid (mh^{-1})

k_{g2} - mass transfer coefficient from gas to non-wetted biofilm (mh^{-1})

k_L - mass transfer coefficient in liquid (mh^{-1})

L - superficial mass velocity of liquid ($kgm^{-2}h^{-1}$)

N - number of layer subdivisions

Re - Reynolds number

R_m - maximum reaction rate ($gm^{-3}h^{-1}$)

u - manipulated variable

U - input

$U_{L/g}$ - liquid-gas velocity ratio

V - volume (m^3)

$V_{g/L}$ - gas-liquid volume ratio

We - Weber number

WR - wetting ratio

X - test variable or data point

ΔX - deviation variable

Y - output

Greek letters

Δ - deviation

θ - time delay (s)

μ - viscosity ($kgm^{-1}h^{-1}$)

ρ - density (kgm^{-3})

σ_p - surface tension of packing ($kg\ h^{-2}$)

σ - surface tension of water ($kg\ h^{-2}$)

τ - time constant (s)

τ_D - derivative time

τ_I - integral time

Subscripts

g - gas phase

L - liquid phase

max - maximum

min - minimum

nm - nominal

sp - set-point

Superscript

n - normalized

Abbreviations

ANN - artificial neural network

BTF - biotrickling filter

ERN - external neural network

FB - feedback

FF - feedforward

FNN - feedforward neural network

LGVR - liquid-gas velocity ratio

MPC - model predictive control

NN - neural network

ODE - ordinary differential equation

PDE - partial differential equation

PUF - polyurethane foam

TF - transfer function

VOC - volatile organic compound

Chapter 1. Introduction

Stringent environmental regulations for control of pollutants have led to the use of effective air pollution control strategies. Biotrickling filter (BTF), one of the biological reactors, offers a great advantage of being a cost effective and environmental friendly technology [1]. This emerging technology has not yet received widespread application. However, in the future, environmental regulations will become more restricted, forcing industries to implement such environmental friendly technologies. As mentioned by Devinny and Ramesh [2], no single BTF model exists for general acceptance and most of the models are specific to experiments under study. On the other hand, implementing any industrial process without control is impossible by all respect and controlling treatment processes is by itself a necessity to avoid release of pollutants above the legal limits. Hence, accurate model prediction and effective control of a BTF is necessary to render this prospective technology feasible for industrial application.

1.1 Background

Harmful pollutants such as volatile organic compounds and odorous compounds released from several industries pose a serious threat to human health and environment [1]. An even worse situation is the increasing release of these compounds as more industries develop to cope with the increasing population. As a result, there is an increasing demand to control such emissions for the well-being of humans and the environment. Stringent environmental regulations for the emissions of such pollutants have led industries to opt for effective air pollution control technologies to comply with the governmental regulations as well as minimize costs for treatment [1]. Physical and chemical treatment technologies are the conventional methods used in industries to treat these pollutants. However, biological treatment technologies have increasingly become popular due to some major advantages they offer in comparison to the conventional methods. Biological reactors offer greater advantage of being cost-effective as well as environmental friendly [1]. There are three main types of bioreactors: 1) biofilters, 2) biotrickling filters, and 3) bioscrubbers. The basic removal mechanisms are somewhat

similar in all three bioreactors. A biotrickling filter (BTF), the bioreactor of interest, consists of a packed-bed column through which there is continuous flow of liquid and pollutant laden gas stream [3]. The continuous liquid stream (trickling liquid) consists of an aqueous solution of nutrients to sustain micro-organisms immobilized on the inert packing material. The reactor is operated either co-currently or counter-currently with respect to the gas and liquid phases. A schematic diagram of the biotrickling trickling filter is shown in Fig. 1-1.

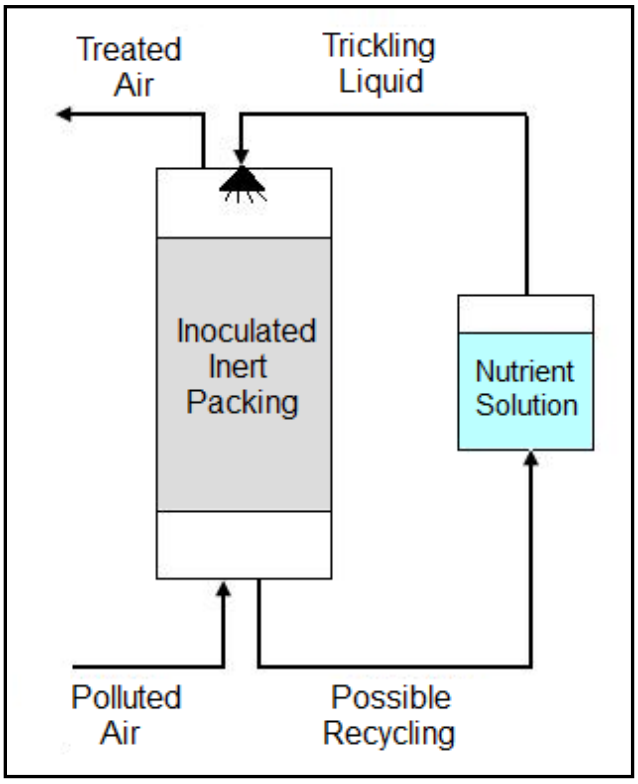

Figure 1-1. Schematic of a biotrickling filter [3]

The mechanism of a BTF consists of absorption of pollutant from the gas phase into the liquid phase and then into an aqueous biological layer known as biofilm. Once in the biofilm, the pollutant diffuses and gets biodegraded along the depth of the biofilm. Since the packing is inert, biotrickling filters need to be inoculated [3]. Some of the factors affecting the performance of a biotrickling filter are as follows:

– *Nutrient supply*

In general, continuous nutrient supply is needed to support the microbial community as well as control biological operating parameters such as pH, amount of nutrients, etc [1]. Moreover, the liquid supply may also reduce clogging problems by sloughing of biofilm [2]. However, excessive nutrient supply results in excessive biomass formation and clogging of filter bed, typically in case of VOC control [4]. On the other hand, in case of odor and H_2S control, clogging does not occur since thin biofilms are formed due to the inefficiency of the micro-organisms with respect to growth and biomass formation.

– *Mode of operation*

For VOC control, co-current operation is preferred. In case of counter current operation, stripping of the contaminant from the recycled liquid occurs at the gas outlet, resulting in lower removal efficiency. For H_2S and odor control, where such processes are mass transfer limited due to the low solubility of the contaminants in the liquid, counter current operation is preferred. [4]

– *Trickling rate*

The effect of trickling rate depends on the nature of process that limits the pollutant removal. For treatment of acid producing pollutants such as H_2S, pH control can be achieved with the trickling liquid. For a low trickling rate, the rate of removal of acid products will be low, causing inhibition of the process culture. However, high trickling rate results in the formation of a thick liquid layer over the biofilm. A thick layer will result in high mass transfer resistance, thereby reducing the removal efficiency.

– *Oxygen content*

Oxygen, needed by the micro-organisms, has a high value of Henry's law constant, implying that penetration depth of oxygen in biofilm will be lower than the pollutant. Hence, limitation of oxygen occurs that might result in the development of anaerobic zones. [4]

– *Inoculation*

As mentioned above, the inert packing requires inoculation since there are no microbial populations on the inert packing initially. Inoculation is usually done using activated sludge, compost extract, specialized enriched cultures, etc [4]. Initially, water supply and purge through the BTF is reduced to avoid possible wash out and facilitate attachment of micro-organisms onto the packing.

1.2 Overview of Biotrickling Filter Modeling and Control

To achieve an understanding and improvement of reactor performance, several mathematical models have been developed for BTFs [2]. As mentioned earlier, a BTF process consists of contaminants being transferred from gas phase to the trickling liquid and then into the biofilm, where diffusion and biodegradation of contaminants take place. Hence, the major concepts involved in the existing biotrickling filter models are: 1) mass transfer, 2) biodegradation, and 3) biomass growth. In the gas phase, most models assume plug flow conditions, neglecting axial dispersion effects [2]. However, there are few models that have considered axial dispersion effects in cases where axial gradients are significant. With regard to pollutant mass transfer through the liquid layer, the liquid phase is usually neglected due to the assumption that a thin liquid layer offers less resistance to mass flow [5]. However, there are some models that use Henry's law equilibrium at gas-liquid interface. In case of the biofilm phase, mass transfer has been described by Fick's law [2]. The most important process that limits the performance of any bioreactor considered is biodegradation [2]. Most of the models incorporate Monod type kinetics for biodegradation that considers contaminant as the only limiting substrate. More realistic models have considered oxygen limitations and also inhibition effects sometimes in addition to the substrate limitation by using the Michaelis-Menten relationships and Haldane type kinetics. However, the major challenge in using such kinetics is the accurate prediction of biokinetic parameters [2]. Finally, many models have incorporated the effect of biomass growth since it affects the formation of biofilm and hence, performance of the BTF. As biomass increases, biofilm gets thicker. In this case, deeper portions of the biofilm will be deprived of oxygen and nutrients, resulting in

the formation of inactive zones [2]. Moreover, thickening of biofilm causes reduction of pore size and increase in the pressure drop, thereby resulting in the clogging of the filter bed. While some models have considered changes in biofilm thickness due to biomass growth, other models usually assume constant biofilm thickness since there is constant sloughing of biofilm by the trickling liquid. Despite the achievements made in BTF modeling, there hasn't been a generally accepted BTF model because most of the models are specific to a particular application under study [2].

Apart from theoretical modeling, there are few studies that focused on using simpler data driven or *black-box* models to predict the performance of a BTF [6], [7], [8]. While there have been major improvements in the model prediction of BTF performance, there is a need to design an optimum control scheme for a BTF as well; a major field that has not been quite addressed yet. Only one such research could be found where an effective control system for a BTF treating hydrogen sulphide (H_2S) was designed [9].

1.3 Problem Statement

Based on the overview presented in the previous section, it can be deduced that there is a need to develop an appropriate BTF model for general acceptance and equally important to design an optimum control strategy before utilizing this technology on a large scale. Hence, this thesis aims to develop a representative dynamic model for the biotrickling filter based on the review of existing models, provide accurate analytical and numerical solution of the model under different conditions, and also select an optimum control strategy amongst the different control systems designed in this study.

1.4 Thesis Organization

Chapters 2 of this thesis pertains to screening of different biotrickling filter models available in the literature, and then modify the most appropriate model to be simulated and validated against literature experimental data. Next, simulation and sensitivity analysis was performed on the proposed model quantifying the effect of different operating conditions on process performance. Chapter 3 of the thesis will be

dedicated to control system design and system identification of the BTF process. *Black-box* reduced-order models for the BTF were fitted with the data generated from the rigorous model. The control system design was implemented on these identified models via classical and advanced control algorithms outlined in Chapter 3. Finally, major conclusions of this study and recommendations for future work are presented in Chapter 4.

Chapter 2. Modeling and Simulation of Biotrickling Filter

In general, developing a rigorous model for any given process is essential to achieve an accurate representation, prediction and understanding of its expected outcomes in real world situations. Likewise, there have been several models proposed to predict the performance of biotrickling filters. However, most of these models are only specific to the pollutants under consideration and hence, there is still a need for a generally accepted BTF model. This chapter focuses on the modeling aspect of the BTF where some existing theoretical models will be reviewed and an appropriate model will be selected, modified, and validated against process data. In addition, the developed model will be simulated and analyzed for its sensitivity towards different process parameters.

2.1 Review of Existing BTF Models

To select an appropriate BTF model, a review on existing literature models had been performed. Five such literature models had been reviewed and analyzed namely the models proposed by Kim & Deshusses [5], Alonso et al. [10], Liao et al. [11], Sharvelle et al. [12], and Lee & Heber [13]. Prior to summarizing the model assumptions made in these studies, a description of each model is provided in the following sections.

2.1.1 Model by Kim & Deshusses [5]. A transient model was developed for biodegradation of H_2S in a counter current biotrickling filter. Moreover, the model had been successfully validated with experimental data obtained from a differential BTF in batch mode. The dynamic model was developed from existing biotrickling filter models with some improvements, mainly in the area of mass transfer effects since it was pointed out that the biotrickling filtration of H_2S and other reduced compounds is often a mass transfer limited process. One of the main contributions made by this model was to account for the presence of both wetted and non-wetted biofilm as a result of incomplete biofilm wetting by the trickling liquid. This concept leads to removal of the pollutant by both direct transfer to the biofilm from the gas stream and indirect transfer to the biofilm

from the gas stream with liquid film as the intermediate layer. Biodegradation in the biofilm followed Michaelis-Menten relationship with H_2S as the only limiting substrate. The model also considered mass transfer resistances at gas-liquid, gas-biofilm, and liquid-biofilm interfaces (Fig. 2-1) while assuming plug flow conditions in the gas stream. Biodegradation of H_2S and other reduced compounds usually result in thin biofilms, thus the need to account for changes in biofilm thickness had been neglected [5]. The resulting model equations consist of mass balances in each of the phases considered (gas, liquid and biofilm layers). Mathematically, the equations contain finite difference approximations for concentration changes along the packed bed height and biofilm depth included in a system of ordinary differential equations for changes in concentration with time.

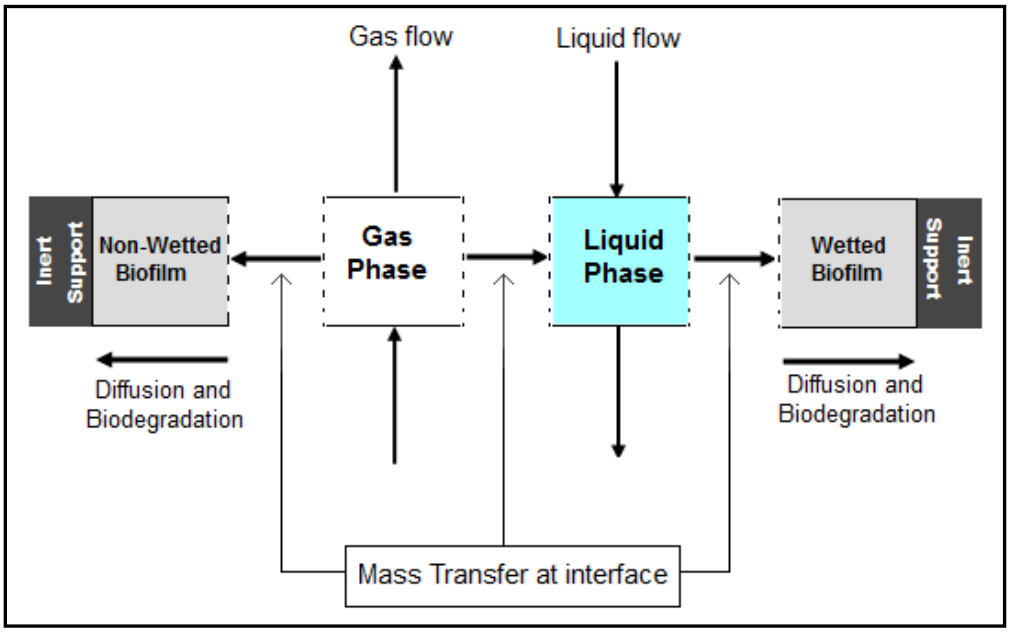

Figure 2-1. Schematic of the BTF model concept proposed by Kim and Deshusses [5]

2.1.2 Model by Alonso et al. [10]. A dynamic model was developed to describe physical and biological processes occurring in a co-current trickle-bed biofilter for volatile organic compound (VOC) removal, with the focus being mainly on analyzing the "relationship between biofilter performance, biomass accumulation in the reactor, and mathematical description of the porous media" [10]. Three models were proposed with respect to the description of the porous medium: (a) spheres based model, (b) parallel

pipes based model, and (c) parallel plates based model (Fig. 2-2). Each model was compared with experimental data and it was concluded that the sphere and parallel pipes models were in close agreement with experimental data.

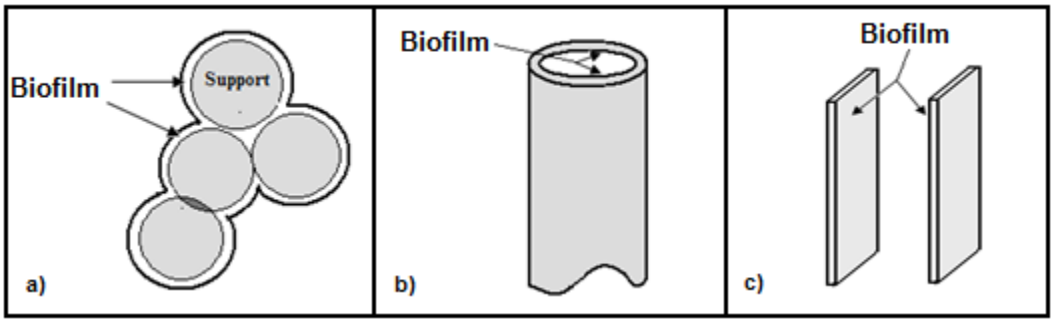

Figure 2-2. Proposed models by Alonso et al. [10]: a) spheres based, b) parallel pipes based, and c) parallel plates based

All the three proposed models assumed plug flow conditions in the gas phase whereas mass transfer resistance occurred in the liquid phase (Fig. 2-3). However, in addition to plug flow assumption, the parallel pipes based model considered a case where axial dispersion (in the gas phase) across the cross-section of the BTF existed. Biodegradation in the completely wetted biofilm followed Monod kinetics with VOC as the only limiting substrate. Moreover, the effect of biomass accumulation had been considered, thereby accounting for changes in biofilm thickness. The resulting equations consist of a system of partial differential equations for mass balances in the three phases and a dynamic model for biofilm thickness.

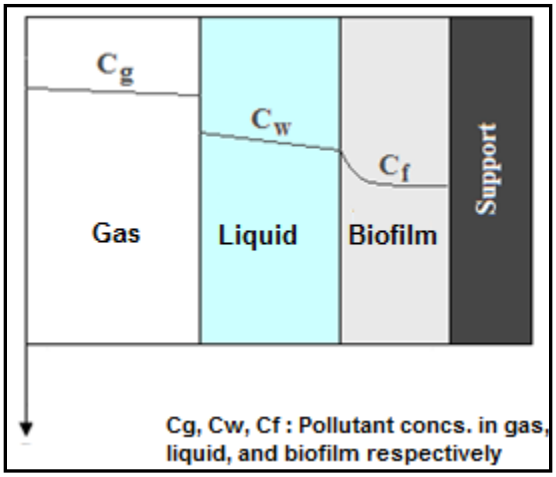

Figure 2-3. General model concept by Alonso et al. [10]

2.1.3 Model by Liao et al. [11]. A steady state model was developed describing biodegradation of a low concentration VOC in a BTF. The proposed *capillary tube* model considers packed bed as a series of straight capillary tubes with inner walls covered by the biofilm, and where the inner region consists of liquid flowing downward and the polluted gas flowing either co-currently or counter currently to the liquid flow (Fig. 2-4).

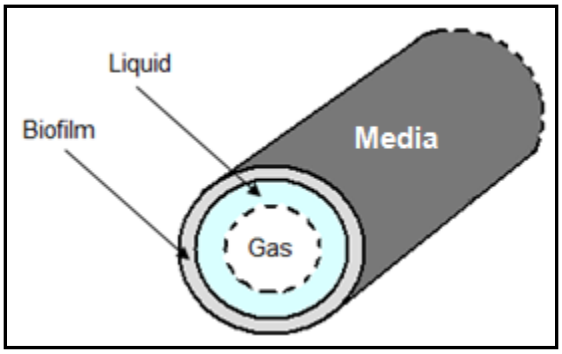

Figure 2-4. Schematic of the capillary tube model proposed by Liao et al. [11]

The model considers mass transfer effect at gas-liquid interface, mass transfer resistance in the liquid phase, variation of liquid film thickness, and velocity distribution in the liquid and gas regions (Fig. 2-5). Variation in liquid film thickness was considered in response to the significant effect of mass transfer in liquid layer on VOC removal. Although equations were derived for changes in liquid film thickness with the height of the packed bed, the liquid film thickness was eventually concluded to be constant on account of a fully developed gas flow. Over prediction was observed while comparing theoretical results with experimental data. It was then proposed that the packing material was not fully covered with the biofilm, implying that the original area of active biofilm needed to be modified through a correction factor. With the modified area, the experimental results were well predicted by the model. Biodegradation in the biofilm followed Monod and Andrews type kinetics that considers oxygen limitation and inhibition effects in addition to the substrate (VOC) limitation. The resulting equations consist of steady state mass balance equations for both VOC and oxygen in the three phases and momentum balance equations for derivation of the liquid film thickness profile.

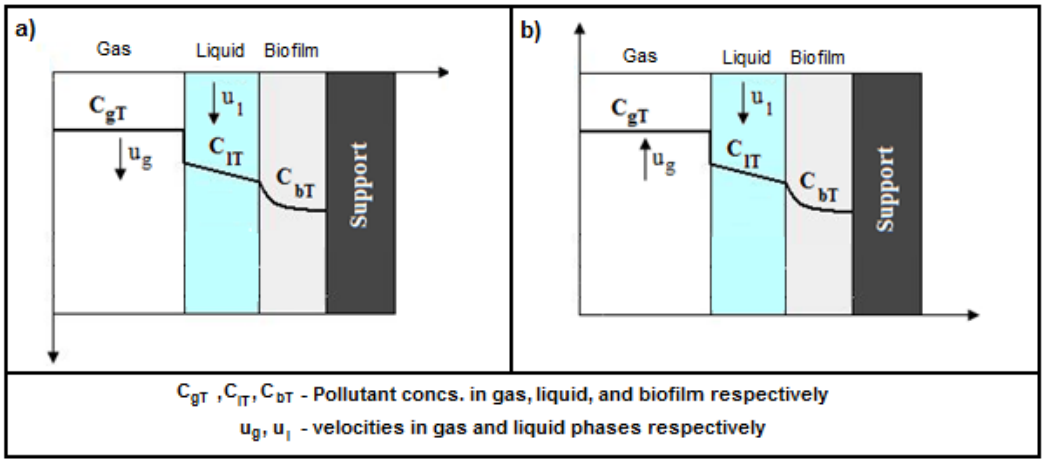

Figure 2-5. Schematic of the model structure proposed by Liao et. al [11] under a) co-current and b) counter-current flows

2.1.4 Model by Sharvelle et al. [12]. A simple model was developed for simultaneous treatment of graywater stimulant and waste gas containing ammonia and H_2S in a BTF under counter and co-current flow regimes. The model accounts for mass transfer effects at gas-liquid and liquid-biofilm interface. Theoretical predictions were compared with experimental data obtained from bench-scale reactors. The proposed model was based on the combination of models proposed by Diks and Ottengraf & Ockeleon et al. and had only considered process parameters with significant effect on reactor performance. In addition, the accuracy was improved by introducing the following modifications while maintaining the simplicity of the model at the same time: a) addition of correction factors to the fraction of wetted area, gas and liquid mass transfer coefficients b) accounting for pH effects on Henry's constants since the Henry's constants for pollutants under consideration are highly dependent on pH. In the biofilm (completely wetted), biodegradation of pollutants followed zero order Monod kinetics. The model equations consist of steady state mass balances in the gas and liquid phases resulting in a system of ordinary differential equations. The Henry's constant in the equations was modified to account for pH effects, and also correction factors were added to obtain accurate estimates of wetted area, gas and liquid mass transfer coefficients.

2.1.5 Model by Lee & Heber [13]. A genetic algorithm was implemented using a dynamic model to obtain accurate estimates of process parameters for the removal of ethylene in a co-current BTF. The model was based on the modified form of the model proposed by Alonso et al. [10]. Experimental data were used to get optimum values of the parameters that would result in the least mean square errors between model and experimental results. Although the pollutant in the gas diffuses into the liquid layer and then into the biofilm where biodegradation occurs, it was emphasized that the pollutant transfer through the aqueous layers is affected by its hydrophilicity. A hydrophilic compound has less resistance to mass flow through the liquid layer than a hydrophobic compound. Large mass transfer resistance through a thick liquid film prevents transfer of a hydrophobic compound to the biofilm, resulting in an inactive biofilm. Since the pollutant under consideration (ethylene) is a hydrophobic compound, it was proposed that the liquid film thickness could be minimized to the point of being almost non-existent and that the pollutant in the gas phase is directly transferred to the biofilm (Fig. 2-6). On the other hand, pollutant removal in the completely non-wetted biofilm is described by first order Monod kinetics and that there are dynamic changes in biofilm thickness as well.

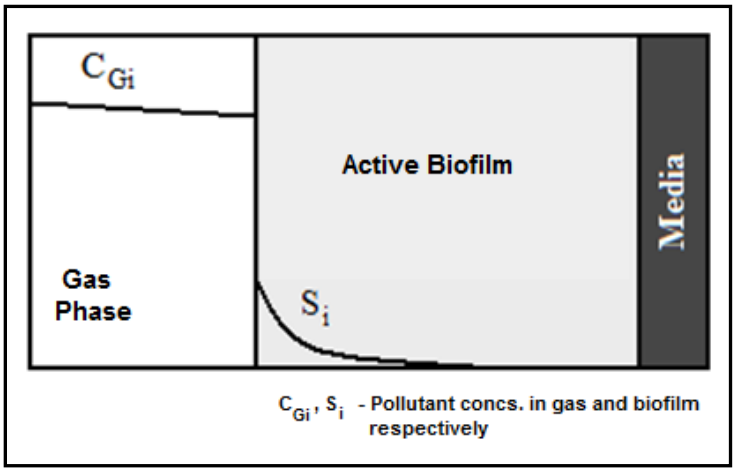

Figure 2-6. Concentration gradient of hydrophobic compound without liquid barrier in the model proposed by Lee and Heber [13]

The model equations consisted of partial differential equations (PDEs) describing dynamic changes of pollutant concentrations in the gas and biofilm phases. The gas phase concentration of pollutant varied with time and height of the BTF whereas the

concentration of pollutant in the biofilm varied with biofilm depth, height, and time. The PDEs also included an equation for describing dynamic change in the biofilm thickness.

2.1.6 Summary of models reviewed. A summary of the models reviewed above is shown in Table 2-1. As shown, there have been some remarkable achievements in the field of BTF modeling. Most of the models reviewed are similar to each other with respect to the processes occurring in each of the three phases. It has also been observed that in most of the VOC removal BTF models, biomass accumulation effect on biofilm thickness has been considered while for H_2S removal process the accumulation effects have been neglected. This observation has been supported by [5] as well, where it has been stated that VOC degrading BTFs produce thicker biofilms than H_2S degrading BTFs. Regarding the biodegradation of pollutant in the biofilm, there has been a variation in the type of kinetics used ranging from the simplest form of Monod kinetics to the more realistic Andrews type kinetics. The main limitation observed in these models is their specific applicability towards the pollutant being treated. Thus, there may be uncertainties in applying a model, specific to one pollutant, over another pollutant [5]. Although coming up with a general BTF model would be a great achievement, this task is quite challenging and would require considerable effort. One probable cause of facing such difficulties may be the “difference in process biology” observed between treating different types of pollutants [5].

Table 2-1
Summary of Reviewed Models

	Kim & Deshusses [5]	**Alonso et al.** [10]	**Liao et al.** [11]	**Sharvelle et al.** [12]	**Lee & Heber** [13]
Gas Pollutant (s)	H_2S	VOC	Low conc. VOC	Ammonia H_2S	Ethylene
Model Dynamics	Dynamic	Dynamic	Steady state	Steady state	Dynamic
Mode of Operation	Countercurrent	Co-current	Counter & Co-current	Counter & Co-current	Co-current
Phases Considered	Gas Liquid Wetted biofilm Non-wetted biofilm	Gas Liquid Wetted biofilm	Gas Liquid Wetted biofilm	Gas Liquid Wetted biofilm	Gas Non-wetted biofilm
Gas Phase Properties	Plug flow	Plug flow Additional case of axial dispersion for *parallel pipes based* model	Plug flow	Plug flow	Plug flow
Biofilm Phase Characteristics	Michelis-Menten kinetics Constant biofilm depth	Monod kinetics Variation in biofilm depth	Monod and Andrews type kinetics Constant biofilm depth	Zero order Monod kinetics Constant biofilm depth	First order Monod kinetics Variation in biofilm depth
Other Characteristics	Conc. varies along bed height and biofilm depth Interfacial mass transfer resistances	Conc. varies along bed height and biofilm depth Three models proposed w.r.t. to packing geometry	Conc. varies along bed height and biofilm depth Considers change in liquid film thickness & incomplete coverage of packing by biofilm	Conc. varies along bed height Added correction factors to mass transfer parameters pH effects considered	Conc. varies along bed height and biofilm depth Considers non-existent liquid layer due to min. trickling liq. rate & hydrophobic pollutant

2.2 BTF Model Selection

As mentioned earlier, selecting a BTF model is one of the main objectives of this study. The main aim here was to select a model that would be simple in terms of getting a mathematical solution while at the same time, it would account for most of the phenomena occurring in a BTF process. Therefore, the model proposed by Kim & Deshusses [5] met these objectives and was selected as the target model for performance prediction and analysis of the BTF process. While the modeling achievements made by other researchers are worth mentioning, the significant consideration of mass transfer resistances and additional phase for non-wetted biofilm in the model by [5] is remarkable. However, the only limitation lies in the type of pollutant being treated. As a result, hydrogen sulphide (H_2S), pollutant of interest in [5], is the target pollutant considered in this study.

2.3 BTF Model Formulation

This section focuses on listing the assumptions and equations used by [5] in model formulation of H_2S abatement in a BTF. Moreover, Kim & Deshusses' model [5] was modified to account for continuous and larger BTF system.

2.3.1 Model assumptions. The model had been developed based on the following assumptions [5]:

1) There is complete coverage of the packing material by the biofilm, which has uniform thickness. The assumption of a constant biofilm thickness has been supported by the observation that H_2S removing BTFs usually produce thin biofilms [5].
2) There is presence of both wetted and non-wetted biofilm due to partial wetting of the biofilm.
3) Dynamic changes in the wetting of the biofilm are not considered.
4) There is no adsorption of contaminant onto the support material

5) Plug flow conditions exist in the gas phase. There are no radial changes in concentration or axial dispersion.
6) Interfacial mass fluxes are expressed by mass transfer coefficients.
7) Gas to liquid and gas to non-wetted biofilm mass transfer coefficients are equal to each other
8) Gas-liquid, gas-biofilm, and liquid-biofilm interfaces are at equilibrium
9) Diffusion in the biofilm is described by Fick's law
10) Biodegradation kinetics in the biofilm follow a Michelis-Menten relationship and H_2S is the only rate limiting substrate. Hence, there are no oxygen and nutrient limitations. Moreover, the biokinetic parameters are same for the wetted and non-wetted biofilm.
11) No reaction in the liquid phase since there is negligible amount of biomass in the recycled trickling liquid used in [5].
12) pH effects are neglected since pH had been controlled in the experiment conducted by [5].
13) Physical properties like temperature, pressure etc. are assumed to be constant.

2.3.2 Model equations. The dynamic model equations consist of mass balances in each phase, where the height of the BTF and biofilm depth has been discretized into *j* (numbered from bottom of the packed bed) and *i* (numbered from biofilm interface) segments respectively. Hence, the equations contain finite difference approximations for changes along the height and biofilm depth, resulting in a system of ordinary differential equations. For finite differentiation, each subdivision is assumed to be ideally mixed. A schematic of the resulting model structure is shown in Fig. 2-7.

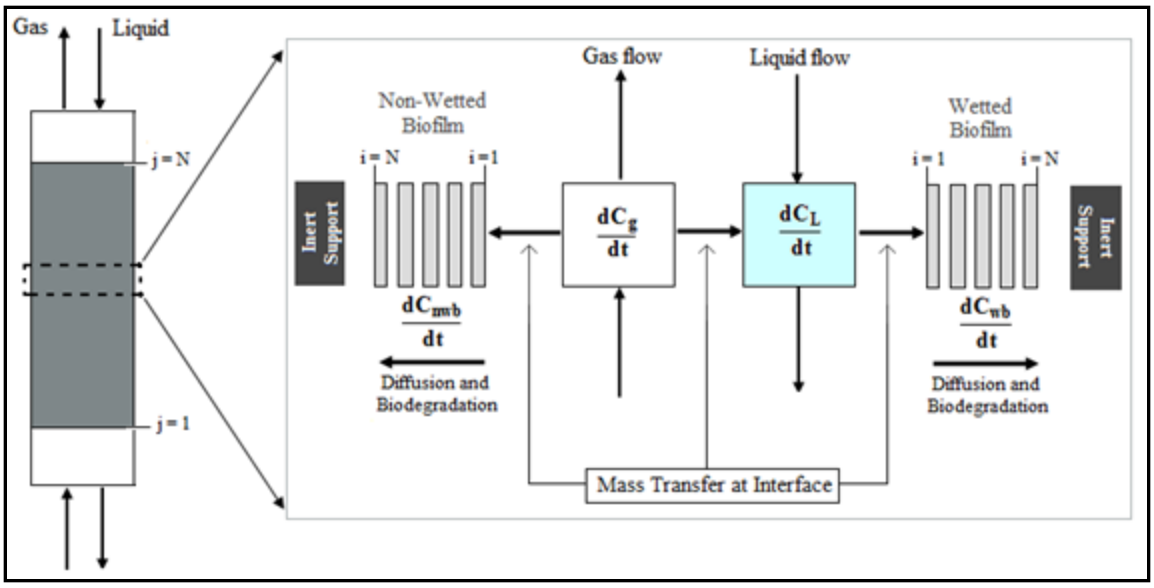

Figure 2-7. Model structure proposed by Kim and Deshusses [5].
Note: Notations given in *Nomenclature* section

Based on the assumptions, the equations developed by Kim and Deshusses [5] are as follows:

Gas phase

$$V_g \frac{dC_g[j]}{dt} = F_g\left(C_g[j-1] - C_g[j]\right) - k_{gl} A_w\left(C_g[j] - C_{gi1}[j]\right) - k_{g2} A_{nw}\left(C_g[j] - C_{gi2}[j]\right) \quad (2.1)$$

Liquid phase

$$V_L \frac{dC_L[j]}{dt} = F_L\left(C_L[j+1] - C_L[j]\right) + k_{gl} A_w\left(C_g[j] - C_{gi1}[j]\right) - k_L A_w\left(C_L[j] - C_{Li2}[j]\right) \quad (2.2)$$

Non-wetted biofilm phase

– For i =1 (biofilm interface),

$$\frac{dC_{wb}[1\,,j]}{dt} = \frac{D_L}{(FT^2)}\,(C_L[\,j\,] - 2C_{wb}[1\,,j] + C_{wb}[\,2\,,j]) - \frac{R_{max}\,C_{wb}[1\,,j]}{K_s + C_{wb}[1\,,j]} \qquad (2.3)$$

– For i = 2 to N -1,

$$\frac{dC_{wb}[i\,,j]}{dt} = \frac{D_L}{(FT^2)}\,(C_{wb}[\,i-1\,,j] - 2C_{wb}[i\,,j] + C_{wb}[\,i+1\,,j]) - \frac{R_{max}\,C_{wb}[i\,,j]}{K_s + C_{wb}[i\,,j]} \qquad (2.4)$$

– For $i = N$ (biofilm depth point),

$$\frac{dC_{wb}[N\,,j]}{dt} = \frac{D_L}{(\Delta FT)^2}\,(C_{wb}[\,N-1\,,j] - C_{wb}[N\,,j]) - \frac{R_{max}\,C_{wb}[N\,,j]}{K_s + C_{wb}[N\,,j]} \qquad (2.5)$$

Wetted biofilm phase

– For i =1 (biofilm interface),

$$\frac{dC_{nwb}[1\,,j]}{dt} = \frac{D_L}{(\Delta FT)^2}\left(\frac{C_g[\,j\,]}{H} - 2C_{nwb}[1\,,j] + C_{nwb}[\,2\,,j]\right) - \frac{R_{max}\,C_{nwb}[1\,,j]}{K_s + C_{nwb}[1\,,j]} \qquad (2.6)$$

– For i = 2 to N -1,

$$\frac{dC_{nwb}[i\,,j]}{dt} = \frac{D_L}{(\Delta FT)^2}\,(C_{nwb}[\,i\,\text{-}1\,,j] - 2C_{nwb}[i\,,j] + C_{nwb}[\,i\text{+}1\,,j]) \qquad (2.7)$$

$$- \frac{R_{max}\,C_{nwb}[i\,,j]}{K_s + C_{nwb}[i\,,j]}$$

– For $i = N$ (biofilm depth point),

$$\frac{dC_{nwb}[N\,,j]}{dt} = \frac{D_L}{(\Delta FT)^2}\,(C_{nwb}[\,N\text{-}1\,,j] - C_{nwb}[N\,,j]) - \frac{R_{max}\,C_{nwb}[N\,,j]}{K_s + C_{nwb}[N\,,j]} \qquad (2.8)$$

Note: Variable notations have been provided in the *Nomenclature* section.

Initial conditions

Gas and liquid phases

$C_g(1) = Cg0$

$C_L(1) = \frac{Cg0}{H}$ (Henry's law)

$C_g(j) = C_L(j) = 0$, where $j \neq 1$

Wetted and non-wetted biofilm phases

$C_{wb}(1,1) = \frac{Cg0}{H}$

$C_{wb}(i,j) = 0$, where $j \neq 1$

$C_{nwb}(i,j) = 0$, for all i and j

2.3.3 Modified BTF Model. In the modeling study conducted by [5], the proposed model was validated with a differential BTF operated in batch mode. This was done to ease the effort required in the determination of the biodegradation kinetics parameters and also to reduce the mass transfer resistance in the gas film by operating at higher gas flows than usual. The model equations for gas phase listed in the previous

section account for the gas outlet being continuously recycled to BTF column as the inlet. In this case, the inlet concentration decreases and depends on the outlet concentration whereas the inlet concentration to a continuous BTF is usually constant and independent of outlet concentration. For the purpose of modeling the BTF process in continuous mode, equation (2.1) was reconstructed as follows:

- For $j = 1$ (reactor inlet),

$$C_g(1) = Cg0 \tag{2.9}$$

- For $j = 2$ to N (reactor outlet point),

Refer to equation (2.1)

Another issue that needs discussion is the size of the experimental reactor and the estimated parameters used in the validation experiment conducted by [5]. A differential reactor had been used and some of the model parameters were experimental. In particular, the dynamic liquid hold-up (V_L) appearing in equation (2.2) was calculated based on an empirical equation and it is applicable only for the size of the packed bed considered and not valid for extrapolation [5]. For the control objectives considered in this study, using a differential BTF would be inappropriate. Moreover, if the BTF is scaled up, there would be uncertainties in using some of the experiment based model parameters provided in [5]. Also, determining these parameters using alternative methods is quite difficult and in some cases impossible without an experiment. To solve this problem, cascade of n-multistage batch reactors were proposed to represent the continuous process in the limit as the number of stages goes to a large number *n* as shown in Fig. 2-8.

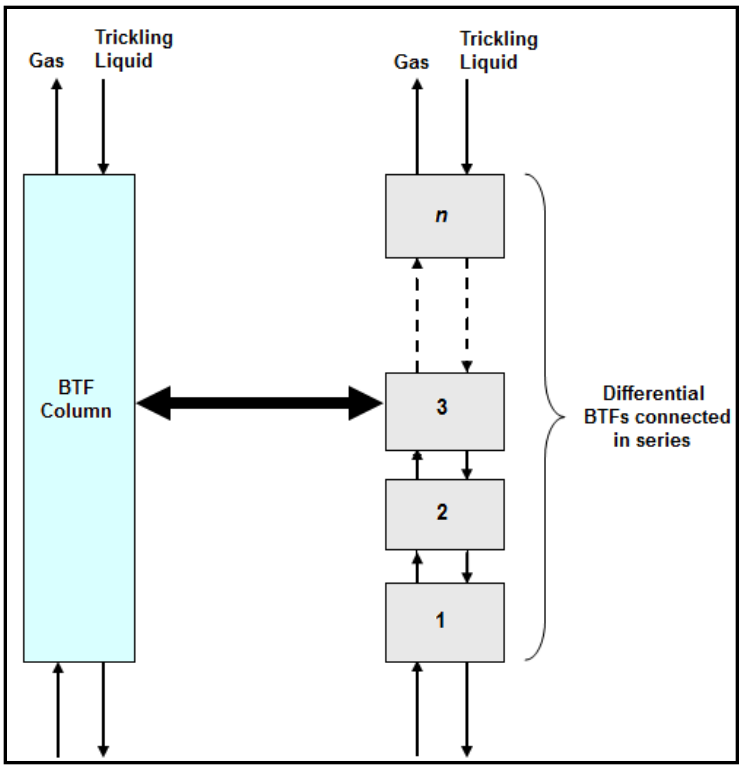

Figure 2-8. BTFs in series model structure

With the proposed *reactors in series* model and in addition to the assumptions listed earlier, it is assumed that the BTFs connected in series are identical to each other in terms of size and performance as predicted by Kim & Deshusses' [5] model. The required changes in the model equations for the proposed model are as follows:

- For the first reactor, equation (2.9) applies in addition to equations (2.1) – (2.8) since this represents the inlet point of the scaled-up reactor and has a constant H_2S feed concentration.

- For second to n^{th} reactor, only equations (2.1) to (2.8) apply since the inlet concentration to each of these reactors is changing. This is due to the fact that the outlet of one reactor serves as an input to the other reactor that follows it in series and the outlet concentration is changing with time.

2.4 Model Simulation

This section provides a dynamic analysis of the BTF performance through simulation of the model formulated in the previous sections. Both Kim and Deshusses' original model [5] and the modified model proposed in this work will be simulated. Sensitivity analysis of the important process parameters using steady state outlet concentration of H_2S as the BTF performance indicator has also been performed. However, the dynamic analysis will be based on simulation of the modified model only. Kim and Deshusses' model will be simulated only for the purpose of comparing the results with those obtained in [5] and also to verify its validity with experimental data. All the required simulations were carried out using MATLAB R2009b numerical solver for ODEs. MATLAB codes are given in the Appendix. Moreover, the simulations were run on an Intel Core 2 Duo T5800 2.00 GHz processor.

2.4.1 BTF process conditions and model parameters. In the validation experiment conducted by [5], the packed bed consisted of a single cube of open pore polyurethane foam (PUF) with the gas and the trickling liquid being continuously circulated through the differential BTF in batch mode. Further details about the experiment can be found in [5]. The BTF system properties and conditions used for model simulations and analyses are shown in Table 2-2. The height of the BTF required for scale-up was fixed and determined according to the removal efficiency of the original differential BTF in [5]. In other words, the height was adjusted until the removal efficiency in the scaled-up BTF was approximately the same as that observed in the differential BTF. Hence, according to the *BTFs in series* model, the resulting pilot scale BTF required forty differential BTFs in series.

Table 2-2
BTF process properties and conditions

Packing size (cubic shape)	0.04 m
Packed bed dimensions - Differential BTF	0.04 m x 0.04 m x 0.04 m [5]
Packed bed dimensions - Pilot scale BTF	1.6 m x 0.04 m x 0.04 m
Pollutant	Hydrogen sulphide (H_2S)
Pollutant Carrier	Air
Trickling Liquid	Water
Mode of Operation – Pilot scale BTF	Continuous Counter current flow
System Temperature (constant)	25^{o}C
System Pressure (constant)	1 atm
Inlet H_2S concentration	0.1 – 0.25 (g/m^3)
Gas Velocity	100 – 10 000 (m/h) 0.02778 – 2.778 (m/s)
Liquid - Gas Velocity Ratio	5 x 10^{-4} – 0.05

Some of the model parameters like the dynamic liquid hold up and the biokinetic parameters were obtained from experimentally based values given in [5], while others were estimated using the correlations. In particular, the mass transfer parameters were estimated using Onda's correlations although there is an uncertainty in extending the applicability of these correlations to PUF packing [5]. The correlations are given as follows [5], [14]:

$$k_L = 0.0051 \left(\frac{L}{a_w \mu_L}\right)^{\frac{2}{3}} \left(\frac{\mu_L}{\rho_L D_L}\right)^{-0.5} (aD_p)^{0.4} \left(\frac{\rho_L}{\mu_L g_c}\right)^{-0.5} \tag{2.10}$$

$$k_g = 5.23 \left(\frac{G}{a\,\mu_g}\right)^{0.7} \left(\frac{\mu_g}{\rho_g D_g}\right)^{\frac{1}{3}} (a\,D_p)^{-2}\, a\,D_g \tag{2.11}$$

$$\mathrm{WR} = \frac{A_w}{A} = 1 - \exp\left[-1.45 \left(\frac{\sigma_p}{\sigma}\right)^{0.75} Re^{0.1}\, Fr^{-0.05}\, We^{0.2}\right] \tag{2.12}$$

A summary of the model parameters used excluding the system conditions is shown in Table 2-3. Since the value of gas hold up had not been mentioned in [5], it was estimated using a simple expression (shown in Table 2-3) involving an approximated gas-liquid volume ratio and liquid hold up.

Table 2-3
BTF model parameters

Parameter	Value/Equation	Calculation Method/ Reference
k_g (gas-liq. mass transfer coefficient)	Equation (2.10)	Onda's correlation [5], [14]
k_L (liq. -biofilm mass transfer coefficient)	Equation (2.11)	Onda's correlation [5], [14]
FT (biofilm thickness)	23 μm	[5]
R_m (maximum reaction rate)	58 400 g/(m^3.h)	Experiment based value [5]
K_S (Michaelis-Menten constant)	0.0279 g/m^3	Experiment based value [5]
H (Henry's constant for H_2S)	0.387	[5]
D_L (diffusion coefficient of H_2S in liq.)	5.796×10^{-6} m^2/h	[5]
D_g (diffusion coefficient of H_2S in air)	1.6332×10^{-2} m^2/h	Fuller correlation [15]
a (specific interfacial area)	600 m^2/m^3	[5]
V_L (dynamic liquid holdup)	$(1 \times 10^{-5})F_L + (8 \times 10^{-6})$	Experimental correlation [5]
$V_{g/L}$ (gas-liquid volume ratio)	8.6×10^4	Approximation based on experimental conditions in [5]
V_g (gas volume/gas hold up)	$V_{g/L} * V_L$	Estimation
i,j (discretized segments along biofilm depth and BTF height respectively)	10	[5]

In [5], the model results were validated with experimental data at certain process conditions. These conditions (shown in Table 2-4) have been considered as the base conditions and the term will be used wherever the use of these conditions is required in the upcoming discussions.

Table 2-4
Base conditions for BTF process

Variable	Value
Inlet concentration of H_2S (g/m^3)	0.164
Gas velocity (m/h)	9 400
Liquid-gas velocity ratio	1.2553×10^{-3}

2.4.2 Solution Methodology. The simulation of the model required for analyses was performed using MATLAB R2009b. The original Kim and Deshusses' model [5] involving system of stiff ordinary differential equations (ODEs) was solved using the *ode15s* solver in MATLAB. The *ode15s* is a multistep solver based on numerical differentiation formulae (NDF) and is used for solving stiff initial value problems for ODEs [16]. In case of the proposed model, a different solution methodology was applied before solving the model equations in MATLAB. Solving the ODEs for each of the forty reactors in series in MATLAB would require tremendous computational effort and time, making this solution methodology an unfeasible technique for simulation of the proposed model. Hence, a *pseudo-steady state* assumption was applied while simulating the proposed model where all the reactors in series except the first are simulated at steady state. For the first reactor, the equations are solved using the ODE solver in MATLAB similar to the solution of the original model. This numerical solution generates H_2S concentrations at each of the discretized time elements. At each discretized time, the outlet concentrations are input as the inlet concentrations to the second reactor. In addition, the model equations are solved assuming steady state condition at each discretized time (Fig. 2-9). Finally, the steady state concentrations at all time elements are compiled together to obtain a time dependent concentration profile for the second reactor. This algorithm is repeated for all the remaining reactors to obtain the outlet concentration profile for the pilot scale BTF overall. Hence, a program was created in MATLAB to perform these computations for the proposed model scheme. In case of model sensitivity analysis, the model equations for all the reactors were solved at steady state conditions since the analyses had been performed based on the effect of process parameters on steady state outlet concentration. The system of non-linear equations resulting from the steady state assumption of the model equations was solved using the *fsolve* command in MATLAB that uses the trust-region dogleg method of solution for non-linear equations [17].

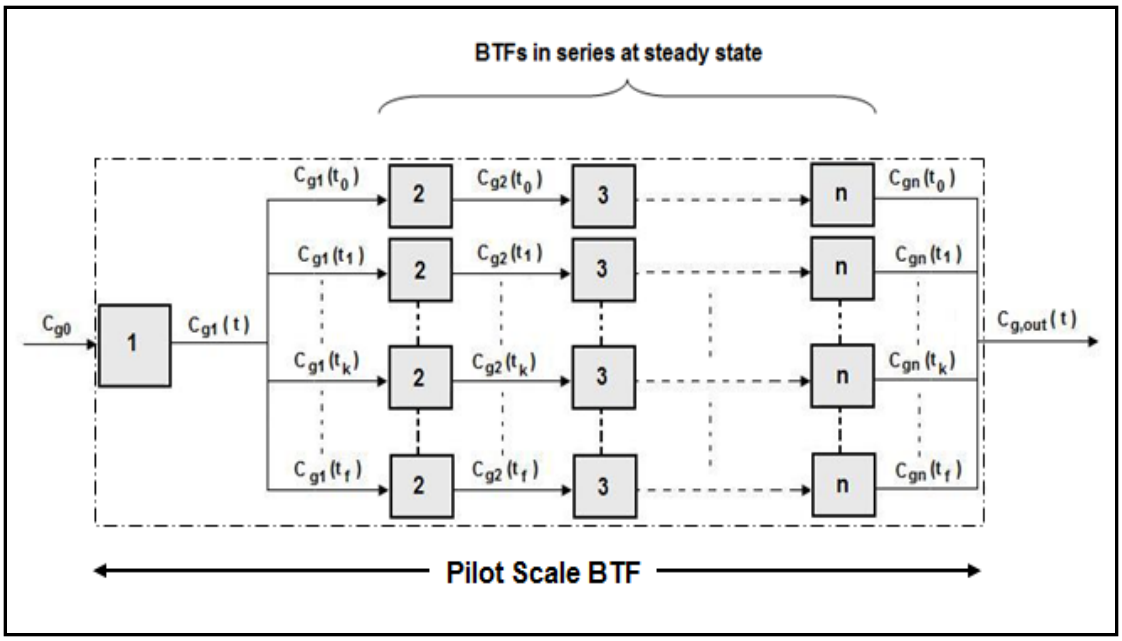

Figure 2-9. Solution scheme for BTFs in series model

2.4.3 Results and discussion

2.4.3.1 Simulation and validity of original model. The simulated concentration profiles at the inlet of the differential BTF including the experimental data obtained from [5] are shown in Fig. 2-10. The CPU time for this simulation was around 53 seconds. The original model was simulated at the base gas and liquid flows with concentration profiles obtained at both high and low initial inlet H_2S concentrations. As expected, both the profiles show a non-linear decrease in inlet H_2S concentration with time since the pollutant (H_2S) is continuously being removed by mass transfer and biodegraded by the micro-organisms during circulation of the gas through the batch reactor. At the end of the simulation time, approximately 94 percent H_2S removal efficiency had been achieved. The profiles in Fig. 2-10 also include the original model solution by Kim and Deshusses [5]. It can be clearly seen that the original model profiles from [5] have been successfully reproduced by the model solution in this work as both the profiles are mostly close to each other. Overall, it can be observed that the model agrees well with experimental data at high initial H_2S concentration whereas over prediction exists at lower concentration. Through sensitivity analysis of nine model parameters and examination of concentration profiles in the biofilm at low H_2S

concentration, [5] deduced that there had been mass transfer limitation in the biofilm resulting in the formation of inactive biofilm zones. It was also observed that the accuracy of model prediction at lower concentration improved after changing the value of H_2S diffusivity in liquid [5]. The exact justification for this behavior could not be figured out, but was explained to be probably related to inaccuracies in model parameters [5]. Nevertheless, changes to the H_2S diffusivity were unnecessary for this study since the inlet H_2S concentrations considered for simulations ranged from intermediate to high levels. Hence, the model proves to be sufficiently reliable for the range of the inlet concentrations considered without the need of modification to H_2S diffusivity.

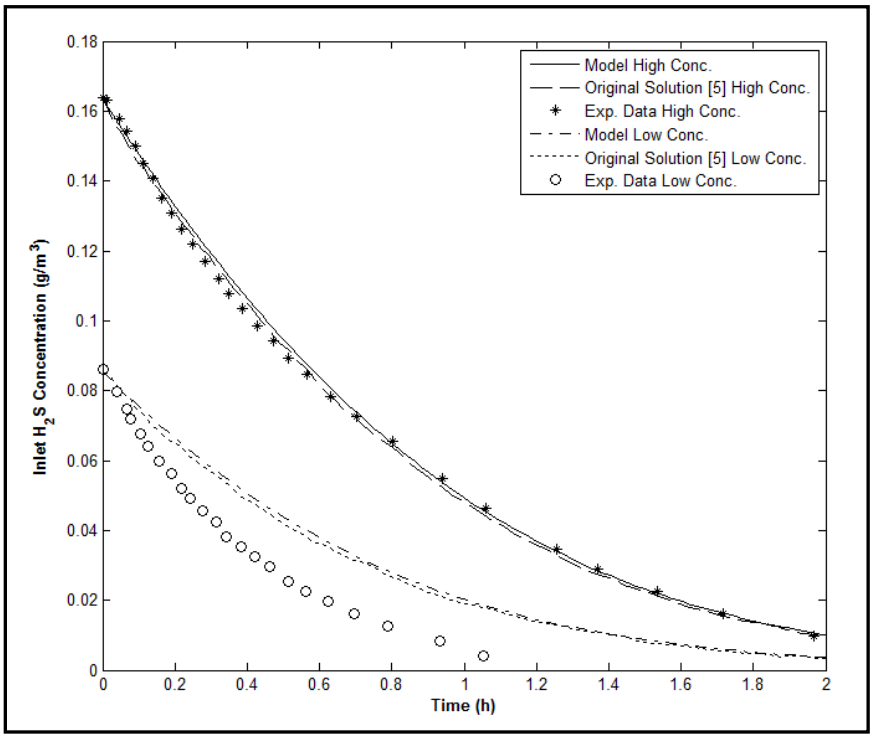

Figure 2-10. Comparisons between original model predictions and experimental data.

2.4.3.2 Simulation of the modified model. Analogous to the dynamic batch concentration profiles in Fig. 2-10, the steady state concentration profile at the base conditions along the length (or number of differential BTFs) of the continuous pilot scale BTF is shown in Fig. 2-11. A similar non-linear behavior is observed where the steady state H_2S concentration continuously decreases as the gas flows through the length of the BTF column. It can also be deduced that more H_2S could be treated by increasing the height of packed bed. Since the size of pilot scale BTF had been adjusted according to the

performance of the batch BTF in [5] at the base conditions, overall H_2S removal efficiency of approximately 94 % had been observed with the modified model simulation.

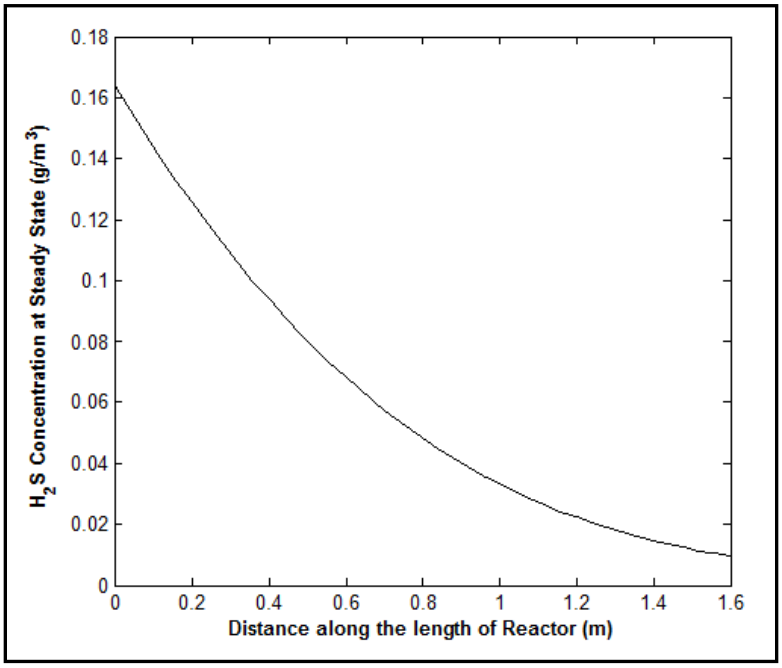

Figure 2-11. Simulation of the proposed BTFs in series model at steady state

A dynamic concentration profile of H_2S at the BTF outlet had also been simulated and is shown in Fig. 2-12 at the base conditions. Initially, the H_2S concentration is zero since the system has not yet "felt" the presence of H_2S at the outlet. After a while, there is a quasi-linear increase in the outlet concentration before reaching a steady state value in approximately 9 minutes (0.15 h). This behavior is analogous to the reaction rate sigmoid curve observed in the Michaelis-Menten biodegradation kinetics. It is also observed that the continuous BTF column reaches the steady state outlet concentration faster since a large BTF indicates faster and efficient removal of the pollutant. Although the proposed solution methodology for the modified model had been successfully implemented, the simulation of the dynamic response in Fig. 2-12 required CPU time of around 1 hour and 28 minutes with the Intel Core 2 Duo processor. While the modified model solution is computationally challenging in terms of effort, the computational time could be reduced with a faster processor. Overall, the modified model simulation has produced reliable results in representing the process dynamics of the scaled up BTF.

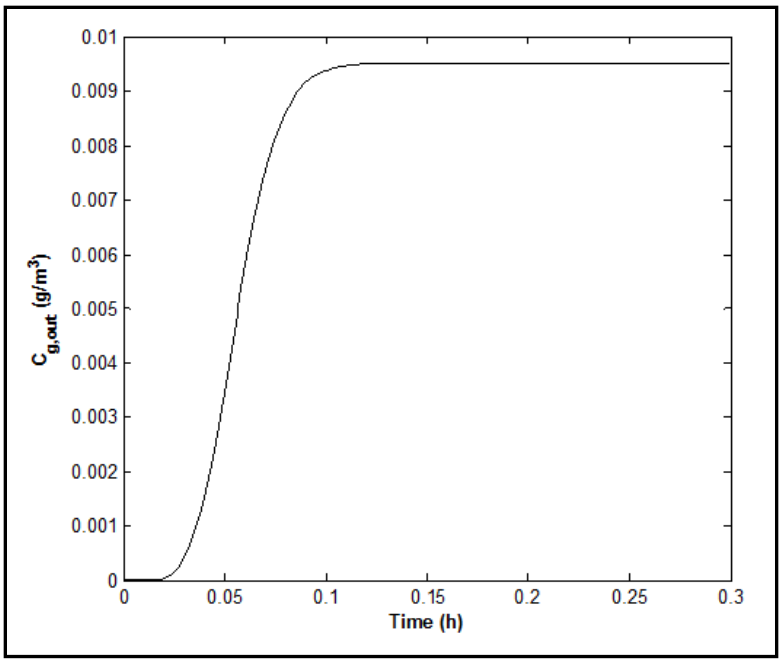

Figure 2-12. Dynamic simulation of the proposed BTFs in series model

2.4.3.3 Sensitivity analysis of the modified model. Using the modified model predictions, sensitivity of the system specific parameters towards the process performance had been performed to determine the parameters that significantly affect the BTF performance. Moreover, this analysis is a prerequisite to determine the process variables that could be effectively used in BTF control. For the sensitivity analysis, the effects of gas velocity, liquid-gas velocity ratio (LGVR), and inlet H_2S concentration on the steady state outlet concentration of H_2S had been analyzed. The sensitivity of the model specific parameters such as the diffusion coefficient, liquid mass transfer coefficient and the biodegradation parameters has not been analyzed in this study. Since the modified model is based on Kim and Deshusses' model [5] and is similar in prediction to the original model, the parametric sensitivity analyses have been provided in [5] where the maximum elimination capacity has been used as the performance variable. To analyze the effects of parameters considered in this study, the modified model had been simulated by varying one of the parameters while maintaining the others at constant values. Moreover, the simulations were performed at the base conditions wherever possible.

Fig. 2-13 shows the effect of inlet concentration of H_2S on the steady state outlet concentration. It is observed that the outlet concentration is proportional to the inlet

concentration and that the relationship is non-linear. Alternatively, it could also be said that the H_2S removal efficiency decreases with the increase in inlet concentration. The observed behavior can be accounted to the performance limitation of the BTF since at higher pollutant loadings, the extent of effective pollutant treatment by the BTF is decreased. However, with the BTF being operated at the base gas and liquid flows, high removal efficiencies were observed ranging from 92 to 96 percent overall.

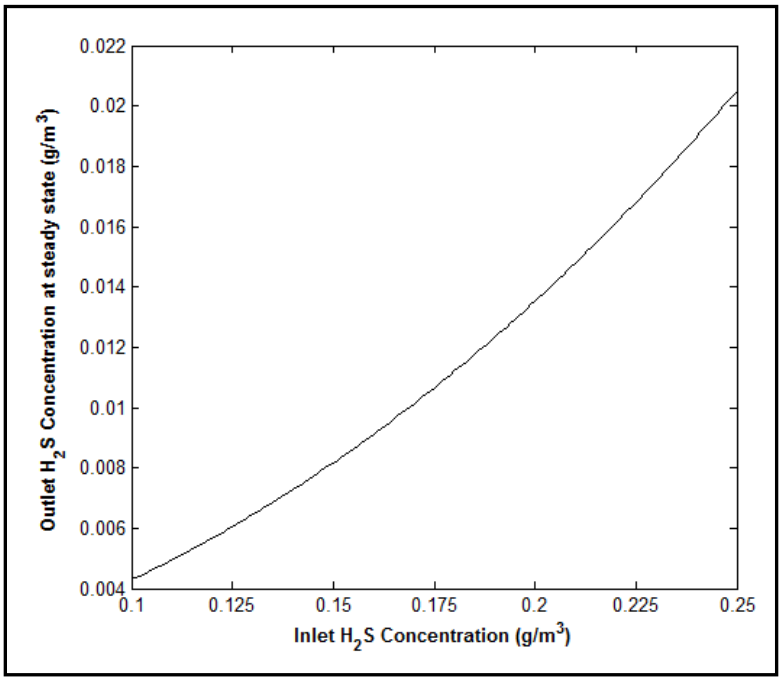

Figure 2-13. Effect of inlet concentration on BTF performance

The effect of gas velocity on the outlet concentration of H_2S is shown in Fig. 2-14. Except for the lower values of gas velocity, there is a linear increase in the outlet concentration with the gas velocity. Change in gas velocity results in variation of the empty bed residence time (EBRT); the time spent by the chemical species in the reactor. High EBRT increases the removal efficiency of the pollutant since there is enough time for the process to effectively treat the pollutant whereas lower EBRTs decrease the removal efficiency due to insufficient time for effective biodegradation. As a result, there is an increase in the outlet concentration or a decrease in the removal efficiency with an increase in the gas flow through the BTF. At lower gas flows (~100 m/h – 2000 m/h), the concentration profile is non-linear with complete pollutant removal

observed at very low gas flows (~ 100m/h – 500 m/h). Hence, the pollutant removal efficiency of a BTF could be improved by decreasing the gas velocity, but only to a certain extent since gas phase mass transfer resistances increase at lower gas flows.

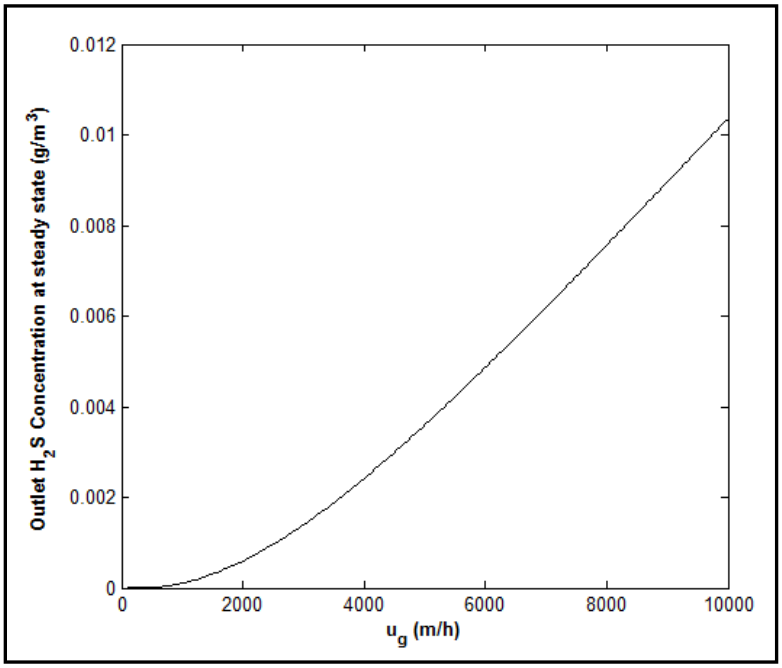

Figure 2-14. Effect of gas velocity on BTF performance

Finally, the effect of liquid-gas velocity ratio (or the liquid velocity in other words) at the base inlet concentration and gas velocity is shown in Fig. 2-15. Interestingly, a parabolic relationship is observed between the steady state outlet concentration and liquid-gas velocity ratio (LGVR) where the outlet concentration initially increases with the LGVR until reaching a maximum value and decreasing with further increase in LGVR. It can be observed that apart from the maximum point, two LGVR values exist for the same outlet concentration. This behavior is indicative of the mass transfer limitations in the liquid phase since a change in LGVR causes a change in the liquid velocity which in turn affects the thickness of the liquid layer surrounding the wetted biofilm. At very low values of LGVR (low liquid velocity), the removal efficiency is high (low outlet concentration) since the hydrodynamic layer is almost non-existent and offers very less resistance to mass flow of the pollutant to the biofilm. As the LGVR increases, the addition of a liquid layer increases the mass transfer resistance resulting in the increase of outlet concentration or decrease in removal efficiency. In fact, while

performing a trial simulation of the original model with the assumption of a completely wetted biofilm, it had been observed that the removal efficiency at the end of the simulation time (2 hours) was very low. The increase in the removal efficiency beyond the minimum point (maximum point in case of outlet concentration) can be related to the decrease in the hydrodynamic layer at higher LGVR values. In other words, the liquid velocity is now sufficiently large to cause a decrease in the hydrodynamic layer and also a decrease in the mass transfer resistance as a result. Looking at the trend of the concentration profile, it is expected that beyond the maximum limit of the LGVR considered in this study, the outlet concentration would eventually reach a constant value, implying that the removal process is now limited to diffusion and biodegradation in the biofilm and that the outlet concentration is no longer affected by higher values of LGVR. In general, it can be deduced that BTFs can be operated at lower trickling liquid rates and also, that the performance of a BTF is not strongly affected by the trickling liquid.

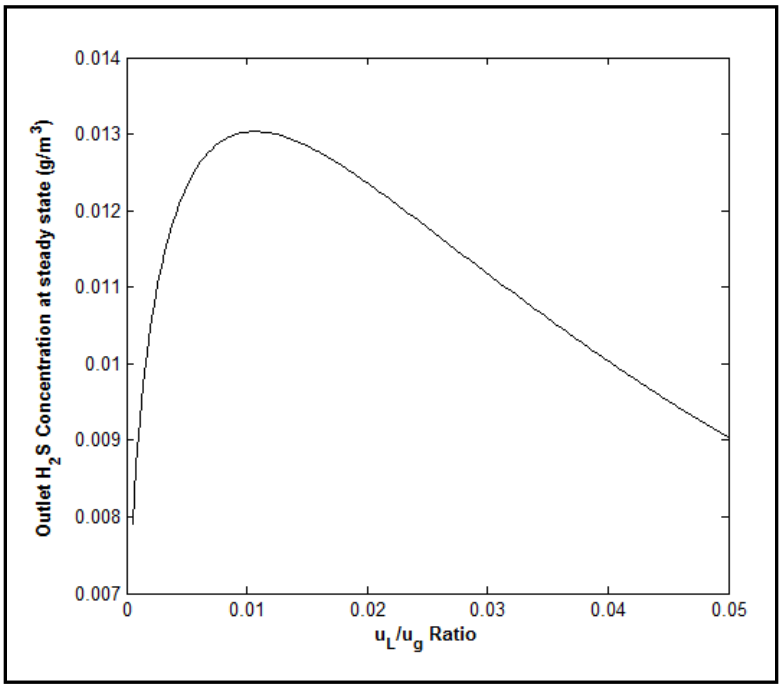

Figure 2-15. Effect of liquid-gas velocity ratio on BTF performance

Based on the sensitivity analysis of the physical process parameters, it can be concluded that the inlet concentration of H_2S and the gas velocity are the most significant variables affecting the performance of the BTF and that the performance is only affected

at very small range of LGVR. Hence, the LGVR can be considered as a constant and optimized to achieve an efficient performance overall. These conclusions would be helpful in designing and implementing an efficient control strategy for the BTF; a major part of this study that will discussed in the next chapter.

Chapter 3. Biotrickling Filter System Identification and Control

Designing an optimum control system is one of the most essential phases during the implementation of any pollutant treatment process. Complying with environmental regulations and meeting the legal pollutant release limits are the primary reasons of designing efficient control systems for such processes. However, without accurate understanding of the process dynamics, designing and effectively implementing control strategies is impossible. Hence, it is essential that accurate and reliable model identification of the process dynamics is obtained before implementing any control strategy. Moreover, it is also important that simulation of the identified model requires less computational effort and time. This chapter focuses on identifying the BTF process with simpler and reliable data-driven models followed by proposition of some classical and advanced control strategies. Through analyses of alternative control strategies developed in this work, an optimum control strategy will also be determined. Although the modified model proposed in section 2.3.3 could successfully represent the BTF process, simulation still requires some computational effort and time. Hence, control strategies have been based on data-driven models of the BTF. Nevertheless, these *black box* models have been fitted with data generated from simulation of the modified model. Two empirical models have been obtained for the BTF process: 1) step response model and 2) neural network model.

3.1 BTF System Identification

In general, models developed for identification of process dynamics can be classified into the following types [18]:

1) *Theoretical models*: these are first-principles models built upon fundamental laws of science and simplifying assumptions [19]. Although they provide "physical insight into process behavior", they are time-consuming and require parameters that may not be readily available [18].
2) *Empirical or black-box models*: these are experimentally-fitted models and are more easily developed than theoretical models. Moreover, they require less

computational effort and time when compared to theoretical models. However, they have higher certainties of being unreliable for extrapolation [18].

3) *Semi-empirical models*: these widely used models are combination of theoretical and empirical models. They offer combined advantages of incorporating theory, being safe in terms of their use for extrapolation, and requiring less development effort [18].

In case of designing efficient control systems for complex processes, acquiring empirical models is more feasible than theoretical models [18]. Several techniques for experimental identification of process dynamics exist in literature ranging from simplest models like linear and nonlinear autoregressive exogenous (ARX) models, step response models to more advanced models like state space models, state estimators or *soft sensors*, and the widely known artificial neural network (ANN) models [18], [19], [20]. While the models are usually developed in continuous form, some of these models have been developed in discrete form and are applied in cases when the sampling data exist in discrete form.

Besides the presence of several theoretical BTF models in literature, some studies have successfully developed empirical models specific to the experimental BTFs under consideration. In a study conducted by [6], a simple second-order empirical model was developed for an experimental anoxic BTF treating H_2S in biogas. The model had been successfully developed to predict BTF performance parameters namely H_2S removal efficiency and loading rate using H_2S inlet concentration and biogas flow rate as the inputs. In another study [8], ANN models were developed for three different fungal bioreactors treating gas phase styrene. The models were developed for three different bioreactor configurations: 1) biofilter, 2) continuous stirred tank reactor, and 3) monolith bioreactor also commonly known as BTF [8]. In case of the monolith bioreactor, the ANN model was used to predict styrene removal efficiency (performance parameter) using inlet concentration of styrene, gas-liquid flow rate ratio, and pressure drop as the inputs. Moreover, the ANN parameters were optimized to obtain an optimum value of the regression coefficient (R^2) between experimental and predicted results. Finally, ANN has also been used in another study [7], where a back-propagation neural network (NN) model had been successfully developed to predict the performance (elimination capacity

and removal efficiency) of a laboratory-scale BTF treating benzene, toluene, and xylene compounds.

In this work, two data-driven BTF models have been developed prior to the design and analyses of different control systems: 1) dynamic step response or transfer function model and 2) steady state NN model. The models are based on data generated from simulation of the modified model and will predict the outlet concentration of H_2S, selected as the BTF performance criterion, using the inputs discussed in the next section.

3.1.1 BTF input-output structure. In section 2.4.3.3, it had been concluded that the inlet concentration of H_2S and gas velocity were the most influential parameters affecting BTF performance while LGVR effects were significant only for a small range. These observations are necessary to list the sufficient number of inputs and outputs for system identification of the process. In addition, these observations would aid in proposing a control structure for the BTF process. Hence, the set of input-output variables used in developing data-driven BTF models is shown in Fig. 3-1. For more accurate identification of the BTF process with the NN model, LGVR and liquid velocity have also been used as the inputs. It should also be noted that the liquid velocity input depends on LGVR and gas velocity by the following relationship:

$$u_L = U_{L/g} \cdot u_g \tag{3.1}$$

On the other hand, transfer function models of the BTF process will be based only on the first two inputs shown in Fig. 3-1 while maintaining the LGVR at the base values.

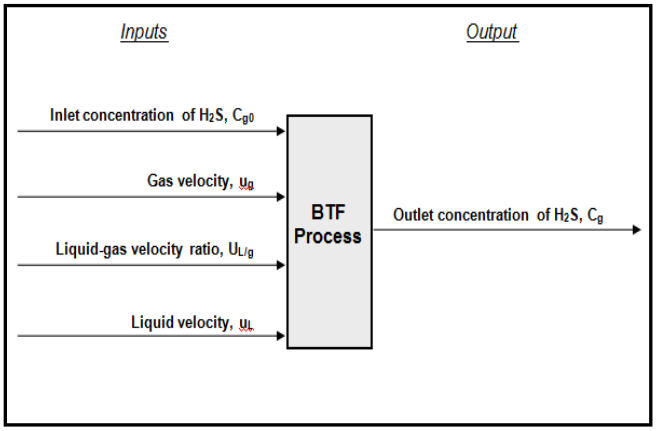

Figure 3-1. Input/output structure for system identification of the BTF process

3.1.2 Open loop step response models. Fitting a model to step response data is the most direct method of system identification of a process [20]. This method involves creating a step change in one of the desired inputs and recording the corresponding output behavior as a function of time [20]. Once the data has been collected, an appropriate transfer function (TF) is fitted. Besides step function, the input change could also be in the form of a pulse signal, sine wave, *saw-toothed* signal or any arbitrary shaped signal [18]. Depending on the degree of accurate process representation, the fitted functions, in Laplace domain, can be either first- or higher-order models. These models are mainly represented by gain (K), time constant or lag time (τ), and sometimes time delay (θ) parameters. Process gain represents ratio of steady state change in the output over the step change in input whereas time constant provides an insight to the time taken by the process to reach steady state [20]. Finally, some processes exhibit delays in changes to output when disturbed by input changes. Hence, this behavior can be represented in the TF models with time delay terms. Most of the chemical engineering open loop processes are modeled with first order transfer function models having the following general form [20]:

$$G(s) = \frac{Y(s)}{U(s)} = \frac{K e^{-\theta s}}{\tau s + 1} \tag{3.2}$$

The parameters required for the TF models can be easily determined by graphical or non-linear regression methods [18]. For the BTF process considered in this work, first order TF models were obtained to predict the relationship between outlet concentration of H_2S and the two inputs: 1) inlet concentration of H_2S, C_{g0} and 2) gas velocity, u_g. The input-output dynamic data obtained from simulation of the modified model consisted of two sets. First, the modified model was simulated to obtain dynamic response of the outlet concentration at varying gas velocities while maintaining the other input (inlet concentration) at the base condition. The simulation was repeated with the inlet concentration being varied at the constant base gas velocity. The input changes were in step form and were within the operating ranges shown in Table 2-2. While fitting the TF models, the LGVR was maintained at the base value for the entire simulations. The

overall equation for predicting outlet concentration consists of two TF models that are added together by the superposition principle stated as follows:

$$Y(s) = \sum_{K=1}^{2} G_K(s)\, U_K(s) \tag{3.3}$$

Each of the two terms in the overall equation represents relationship between output (outlet concentration) and one of the inputs with no change in the other input. To develop this equation, it was necessary to transform the data into deviation form given as follows:

$$\Delta X = X - X_{nm} \tag{3.4}$$

This transformation ensures that while fitting the model between output and one of the inputs, the other input has a numeric value of zero. The required nominal values in equation (3.4) for the inputs were defined at the base conditions whereas the nominal value of the output was defined to be the steady state output resulting from modified model simulation at the base conditions. The required parameters for fitting the two TF models were obtained from the *Design Tools* Module in Loop Pro Trainer 5.1 software [21]. Each of the two sets of input-output data was entered in this software, a suitable fitting model from the available models was selected and the final results were obtained that includes plots, fitted parameters, and the resulting R^2 values. The fitted TF model output results from Loop Pro software were recorded and compared with the modified model simulation using MATLAB.

3.1.3 Neural network model. Artificial neural network (ANN) models are non-linear empirical models that have increasingly become important nowadays for modeling environmental systems [22]. The ANN concept was based on the operation of the human brain where substantial parallel computations are performed using “structural constituents called *neurons* and the synaptic interconnections between them”, thereby creating a neural network [18]. Likewise, NN computation structure consists of a network of interconnected *neurons* organized in layers [18] and it involves using a series of equations that “stimulate learning and memorization process” [8]. Fitting a neural

network model consists of two phases: 1) training phase where the model normally requires large data sets to estimate the unknown fitting parameters 2) validation and testing phase where the model uses another set of data to validate and test the *trained* network [18]. NN models are useful in modeling non-linear complex processes and also in replacing models that require significant computational effort and time [18]. Moreover, ANNs have the advantages of being simple, noise and fault tolerant, and versatile to process changes [8]. However, ANNs have some disadvantages as well: 1) they require large data sets for process identification, 2) there is a possibility of over-fitness of the model with the data, 3) determining network topology for the model by trial and error can be an intensive task, and 5) the model needs to be re-trained whenever data set is updated [8].

Depending on the nature of signal transmission between the neurons, NN models are categorized into two types: 1) feed-forward neural network (FNN) and 2) recurrent neural network (RNN) models [23]. RNN models consist of networks with both forward and backward or feedback connections and they are particularly useful in modeling dynamic systems [23]. FNNs or multilayer perceptrons (MLPs) [23], the model of interest in this paper, is the commonly used model where signal is transmitted in the forward direction. In this model, *neurons*, also known as processing elements (PEs), are organized into three main layers: 1) an input layer, 2) one or more hidden layers, and 3) an output layer [22]. At each PE in the hidden layer, inputs (x_i) from the preceding layer are weighted with adjustable connection weights (w_{ij}) , added to a threshold value (θ_j), combined into an input signal (I_j) and finally converted to the output neurons through an activation function ($f(I_j)$), as shown in Fig. 3-2. For optimization of the connection weights, there are many training algorithms available in literature some of which include the widely known back-propagation techniques like Levenberg-Marquardt, Shanno and conjugate gradient algorithms and global techniques like annealing and genetic algorithms [22]. In back-propagation FNN, input signals are transmitted in the forward direction while the error (between measured and predicted values) signals are transmitted backwards to re-adjust the connection weights accordingly [23]. This process continues until a best fit NN model is obtained. The most common activation function used in the FNNs is the logistic sigmoid function that has minimum and maximum values of 0 and 1

respectively [8]. Other activation functions include hyperbolic tangent, polynomial, rational functions and Fourier series [8]. Due to the nature of the activation functions, the measured data set needs to be normalized to fall within the range of these functions. Finally, determining the network topology, i.e. the optimum number of neurons in each layer, is the most important task that determines how well the model fits to the process data. The number of neurons in the input and output layers is equal to the number of process inputs and outputs. Although there are some heuristics that help in estimating the number neurons in the hidden layer, this task is usually accomplished by trial and error.

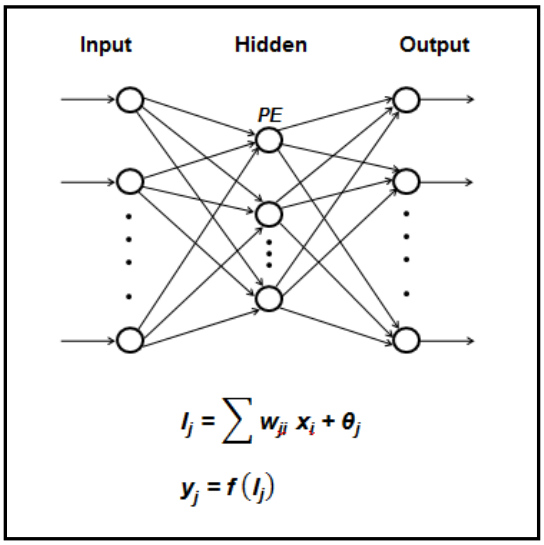

Figure 3-2. General FNN structure [22]

For modeling the BTF process with NNs, four inputs and one output, shown in Fig. 3-1, were used. A steady state NN model was obtained using the data from simulation of the modified model at steady state. The NN model was obtained using the *Neural Network Fitting Tool* in MATLAB R2009b. This tool uses two-layer FNN with log sigmoid function for the hidden layer neurons and a linear function for the output layer neurons. Moreover, this tool trains the network using Levenberg-Marquardt back-propagation algorithm. Due to the limits of the activation function, the input data was normalized using the following expression [8]:

$$X^n = \frac{X - X_{min}}{X_{max} - X_{min}} \tag{3.5}$$

Since the output data fall within the limits of the activation function, the output data was not normalized. Moreover, the percentages of overall data used for training, validating, and testing the NN model were 70, 20, and 10 respectively. The transformed steady state input-output data from the modified model simulation were entered into the NN fitting tool, an optimum network topology was determined through trial-and-error and the resulting best fitted NN model was finally obtained. The overall results included comparisons, error and R^2 value between NN model predictions and data. As a final step, the fitted NN model was simulated to analyze the output response with a step change in gas velocity and inlet concentration. Moreover, the output results were compared with those obtained from the modified model. The NN model obtained from the NN Fitting Tool was embedded and simulated in Simulink; an add-on software in MATLAB used to model, simulate, and analyze dynamic systems. The simulation results from Simulink were recorded and compared with the modified model using MATLAB. The Simulink block diagram for the NN model simulation is provided in the Appendix.

3.1.4 Results and discussion

3.1.4.1 Identified transfer function BTF models. The fitted TF model predictions of outlet concentration in response to step changes in gas velocity are compared with the modified model simulations and shown in Fig. 3-3. The input and output values represent deviation from the nominal values i.e. the base conditions. Since the values of the input and output in deviation form are considered to be zero at the base conditions, the negative and positive values represent negative and positive deviations from the base conditions respectively. In case of the output (outlet concentration), the base value represents the outlet concentration resulting from modified model simulation at the base conditions. Hence, the negative output values in Fig. 3-3 denote that the outlet concentration has decreased relative to the base value meaning that the removal efficiency has increased relative to the base removal efficiency (94%). Before commenting on the TF model representation of the BTF, some observations can be made on dynamic response of the output (outlet concentration) with respect to step changes in gas velocity. Almost all of the step changes in gas velocity cause similar step changes in the output. This implies that

the dynamic outlet concentration and gas velocity are linearly related to each other. Moreover, change in gas velocity causes immediate change in the output, implying that there is no time delay between output responses and input changes (gas velocity). Looking at Fig. 3-3, it can be seen that the TF model predictions agree well with the data except at some input changes where over and under predictions of TF model output results.

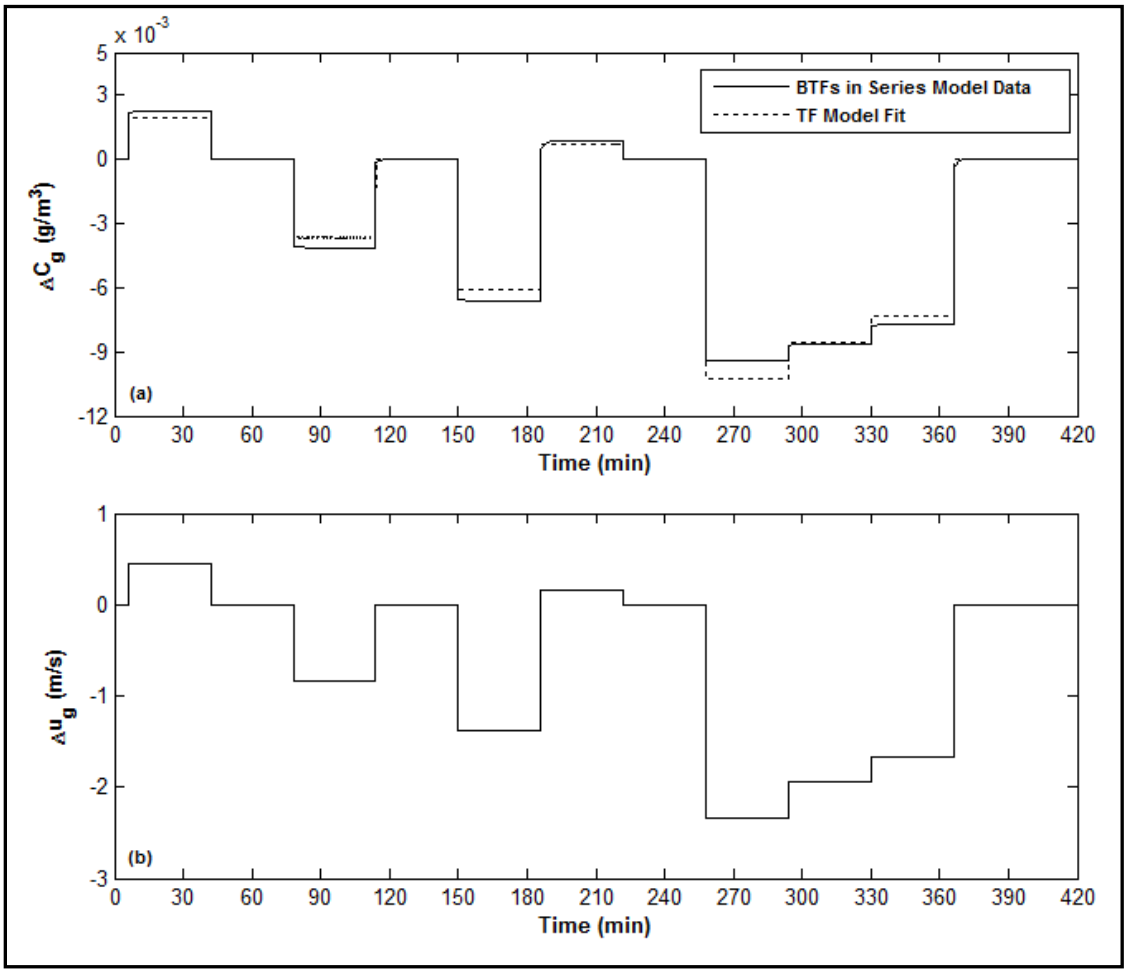

Figure 3-3. (a) Output comparison between modified model data and fitted TF model for (b) step changes in gas velocity (input 1) at base inlet concentration ($\mathbf{\Delta}C_{g0} = 0$)

On the other hand, Fig. 3-4 shows output comparisons between the second TF model and modified model data for step changes in inlet concentration in deviation form. Analyzing the dynamic response, it can be observed that there is non-linear change in output in response to step change in the second input (C_{g0}). Moreover, it can also be

deduced that there is a time delay between inlet (second input) and outlet concentrations (output). This behavior can be clearly seen at the initial time of simulation in Fig. 3-4. The TF model predictions for this input-output relationship agree quite well with the data and hence, give satisfactory results. However, it is observed that the TF model predicts linear change in outlet concentration in response to a step change in inlet concentration. These disparities are insignificant since the actual non-linear change occurs over a small time interval and can be safely modeled with a linear approximation.

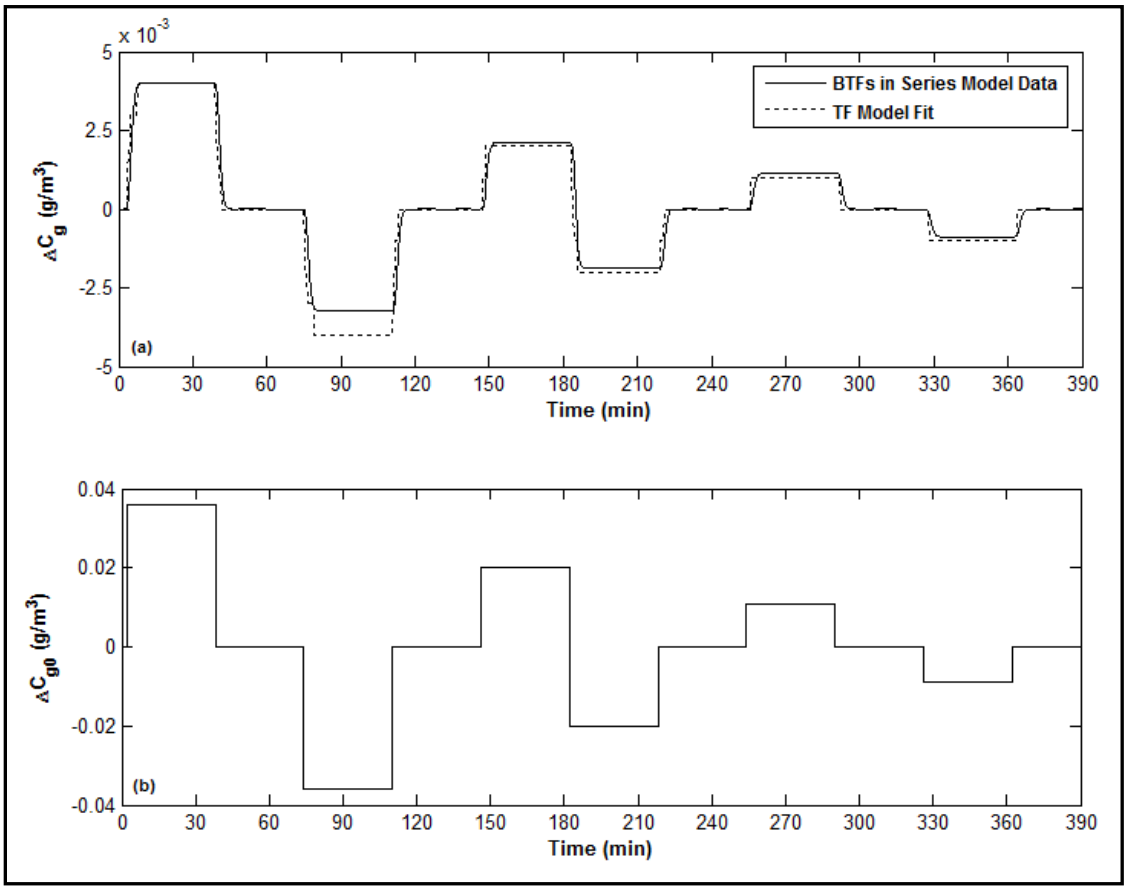

Figure 3-4. (a) Output comparison between modified model data and fitted TF model for (b) step changes in inlet concentration (input 2) at base gas velocity ($\Delta u_g = 0$)

The overall results of the two TF model fits obtained from Loop Pro software are shown in Table 3-1. Comparing the time constants of the two TF models, the time constant for the first TF model is about forty times smaller than that of the second model. This indicates that the response between outlet concentration and gas velocity is faster than the response between outlet concentration and inlet concentration. Hence, the output

(outlet concentration) will reach a new steady state much faster with change in gas velocity than the inlet concentration. Looking at the time delays, there is also an approximately 1 minute time delay between output and input changes for the second model whereas the first model has no time delay. These results indicate that the dynamic behavior of the output in response to inlet concentration is quite slow and that changes in inlet concentration will have a major effect on optimization of BTF process performance and control. Finally, the values of R^2 and sum of squares for error (SSE) prove that both the TF models are collectively reliable in predicting the BTF performance overall. The overall transfer function BTF model for predicting the outlet concentration can now be formulated in deviation form as follows:

$$\Delta C_g\ (s) = \frac{4.388 \text{ x } 10^{-3}}{(1.8s + 1)}\ \Delta u_g\ (s) + \frac{0.1007\ e^{-54s}}{(72.57s + 1)}\ \Delta C_{g0}\ (s) \qquad (3.6)$$

Table 3-1
Results summary of fitted BTF transfer function models

	TF Model 1 G_1 (s)	**TF Model 2 G_2 (s)**
Input	Δu_g (m/s)	ΔC_{g0} (g/m^3)
Output	ΔC_g (g/m^3)	ΔC_g (g/m^3)
Gain, K	4.388 x 10^{-3} $\left(\frac{\text{g/m}^3}{\text{m/s}}\right)$	0.1007 (-)
Time constant, τ	1.8 s	72.57 s
Time delay, θ	0	54 s
R^2 value	0.9824	0.9701
SSE	4.11 x 10^{-4}	1.28 x 10^{-4}

3.1.4.2 BTF neural network model identification and simulation. Table 3-2 shows the overall summary of the fitted NN model obtained from *NN Fitting Tool*. The optimum network topology was found to be 4 - 7 - 1. In other words, while the number of neurons in the input and output layers were equal to the number of inputs and output used for the BTF process, the optimum number of neurons in the hidden layer was found to be seven through trial and error. As evident from the R^2 and mean squared error (MSE) values, perfect NN model fit of the BTF process had been obtained. Hence, the NN model proves to be very reliable in predicting steady sate BTF performance. The ability of the NN model to accurately represent the BTF process can also be attributed to uncomplicated nature of the process itself where the simple relationships between inputs and the output can be easily modeled.

Table 3-2
Summary of fitted BTF neural network model

Properties	
Inputs	u_g^n C_{g0}^n $U_{L/g}^n$ u_L^n
Output	C_g (g/m^3)
Total number of data samples	483
Number of training samples	338
Number of validation samples	97
Number of test samples	48
Results	
Network topology (Input - hidden - output)	4 - 7 - 1
MSEs	
Training	1.12 x 10^{-11}
Validation	1.24 x 10^{-11}
Test	6.14 x 10^{-12}
R^2 values	
Training	1
Validation	1
Test	1

The dynamic response of the NN and modified models for a 32 % step decrease in gas velocity from base value is shown in Fig. 3-5. Although NN model is based on steady state data, it is observed that the NN model predictions almost perfectly agree with the modified model dynamic results. The NN model predictions are accurate because according to the dynamic response shown in Fig. 3-3 earlier, the output (outlet concentration) immediately reaches steady state value in response to a change in gas velocity.

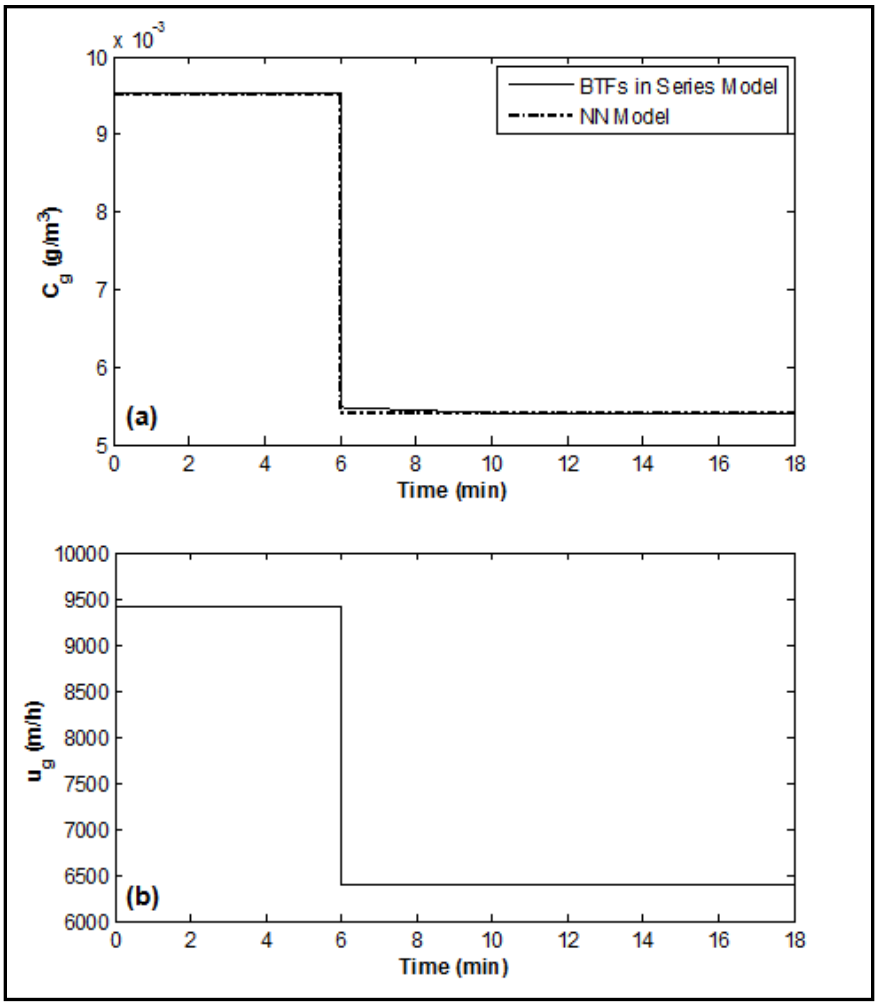

Figure 3-5. (a) Output comparison between modified model data and NN model for (b) step change in gas velocity at base inlet concentration

In response to a 12 % step increase in the inlet concentration from the base value, the dynamic output comparisons between the NN model and the modified model are shown in Fig. 3-6. Since the steady state NN model does not account for time delay between output and inlet concentration, a time delay term was included in the Simulink block diagram. Comparing the predictions between the two models, it is clearly observed that NN model does not capture the dynamic response observed in the modified model output observed between 10 and 15 minutes. This discrepancy between the two models is due to the fact that NN model was derived based on the steady state data. However, the NN model was able to accurately capture the final steady state values of the modified model responses.

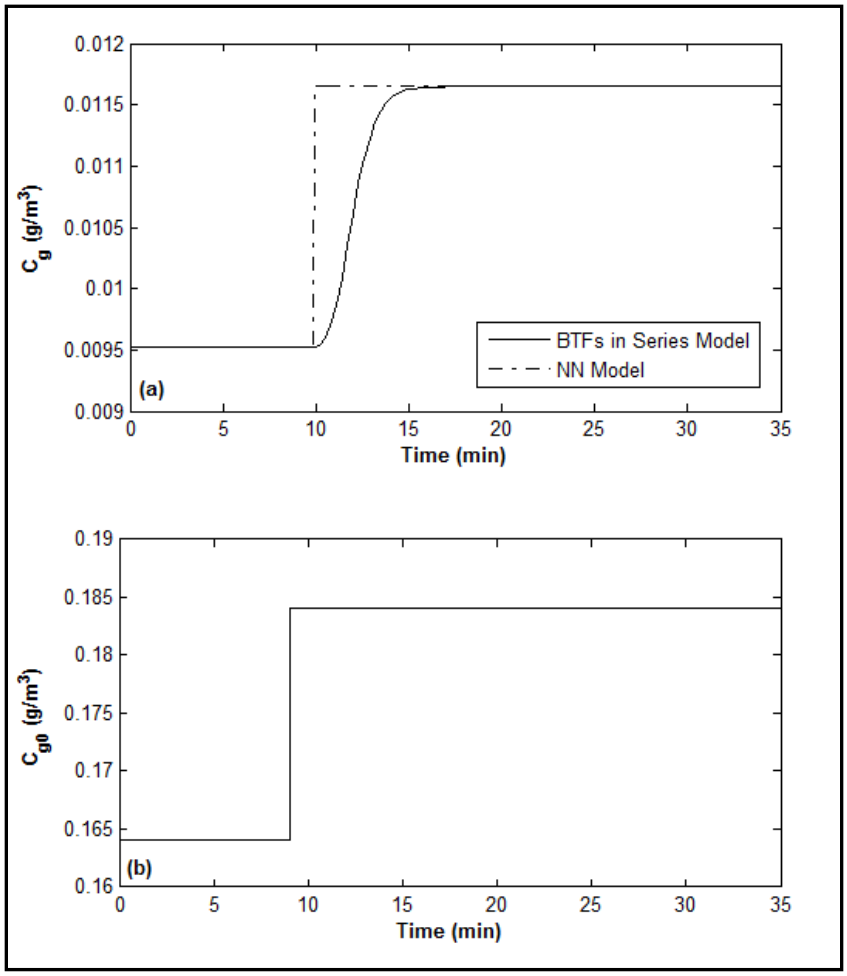

Figure 3-6. (a) Output comparison between modified model data and NN model for (b) step change in inlet concentration at base gas velocity

To sum up the discussion on system identification of the BTF process, TF and NN model representations of the BTF were successfully obtained. Overall, the agreement of dynamic responses from both the fitted models with the modified model data was satisfactory. With the BTF system being adequately described using simpler identification models obtained in this section, different control strategies based on these models will be proposed and implemented in the upcoming sections.

3.2 BTF Process Control

With process control, the goal of safely and efficiently maintaining a process at the desired conditions can be achieved [18]. For treatment processes, designing efficient control systems is necessary to comply with environmental regulations. To develop an effective control system, it is essential that the following characteristic process variables are specified first [18]:

1) *Controlled variables (CVs)*: these are the variables that require to be maintained at the desired values or *set points* [18]. In chemical processes, typical control variables include compositions, flow rates, levels, pressures and temperatures [20].

2) *Manipulated variables (MVs)*: these are the variables adjusted to maintain the control variables at their set points. Flow rates of entering or leaving streams are the most common manipulated variables [20].

3) *Disturbance variables (DVs)*: these variables affect the controlled variables and cannot be freely manipulated [18] since they are usually dependent on the upstream or downstream conditions of the plant [20]. An efficient control system must be robust towards preventing process disturbances as much as possible.

In general, control system design has either traditional or model-based approach [18]. In traditional approach, the control system is implemented only after major part of the plant design has been completed [18]. The second approach involves developing a process model first that would be helpful in: 1) forming a basis for model-based control strategies, 2) being directly integrated into the control law, and 3) being used in computer simulations for analyzing different control strategies and also in determining preliminary controller settings, an activity more commonly known as controller *tuning* [18]. For simple processes, traditional approach is adequate while the control system design must be model-based in case of complex processes [18]. Finally, several control strategies exist ranging from conventional to advanced control systems. Conventional techniques are the widely implemented control systems and include feedback controllers such as *on-off*, *proportional* (P), *integral* (I), *derivative* (D), or more

commonly combined PID controllers [18]. Other well known strategies include feedforward and the hybrid feedback-feedforward control systems. More advanced single-loop (single input-single output) strategies include cascade, inferential, selective and override, adaptive and non-linear control systems like non-linear PID control and fuzzy logic control [18]. Another important and widely known advanced control technique that has been advantageous in multivariable control is the model predictive control (MPC) [18]. Depending on the characteristic of data signal transmission, the controllers could be either *analog* (for continuous signals) or *digital* (discontinuous signals) [20].

Several achievements have been made in the field of BTF modeling, but research in the design and analysis of control systems for BTF has not been performed much and requires major focus to make the BTF technology viable for widespread application. Only one research could be found that focused on the design of an automated control system for the removal of H_2S in a BTF [9]. A multi-loop control system was implemented where five process variables were controlled: temperature of BTF bed, pH of nutrient in circulation tank, concentration of accumulated sulphate ions, liquid level, and outlet concentration of H_2S. Using an advanced integrated controller and a two-dimensional fuzzy PID controller, it was observed that the implemented control strategy gave satisfactory results [9].

As a major contribution to the field of BTF control system design and analysis, this work attempted to devise some control strategies and provide theoretical analysis on the performance of different control strategies proposed in this work. Moreover, these control systems were based on the data driven BTF models developed in section 3.1. The control strategies considered include both conventional and advanced control systems and are listed as follows:

1) Proportional-Integral (PI) feedback control
2) Hybrid feedback-feedforward control
3) Model predictive control (MPC) using TF models
4) Neural network model predictive control (NNMPC)
5) NNMPC with feedback integral control

3.2.1 General BTF control structure. As mentioned earlier in the previous section, the process variables need to be identified before designing any control system. For the BTF considered in this work, outlet concentration of H_2S is clearly the controlled variable since it is a performance variable that needs to be maintained at the desired value for effective degradation of the pollutant to permissible concentration levels. The outlet concentration will be maintained at the set point by manipulating the flow of the inlet gas stream. The choice of gas velocity as the manipulated variable is an obvious choice since it has direct and immediate effect on the outlet concentration, as observed from the dynamic responses in Fig. 3-3. Usually, the concentration of H_2S in the inlet gas stream is dependent on the upstream conditions especially in case of treating waste gases from municipal sewage treatment plants where the level of gas pollutants can fluctuate. There have been some full-scale BTFs where the pollutant concentration levels in waste gases generated from wastewater and solid waste treatment plants fluctuated during period of operation and testing [24], [25]. Hence, inlet concentration of H_2S can be considered as a disturbance variable in BTF control systems. The general feedback control structure for the BTF process is shown in Fig. 3-7. The proposed structure is a single-loop control system which consists of a concentration sensor, controller and control valve as the *final control element*. In general, the sensor measures the outlet concentration of H_2S and transmits this information in the form of an electric signal to the controller. Based on the concentration measurement and the desired set point, the controller determines the required change in the value of gas velocity and sends this information to the control valve to adjust the gas flow. This structure has been applied to all the control strategies proposed in this work except the feedback-feedforward (FB-FF) control. In FB-FF control, an additional sensor will be used for the measurement of the inlet concentration as well, more details of which will be given in section 3.2.2.2.

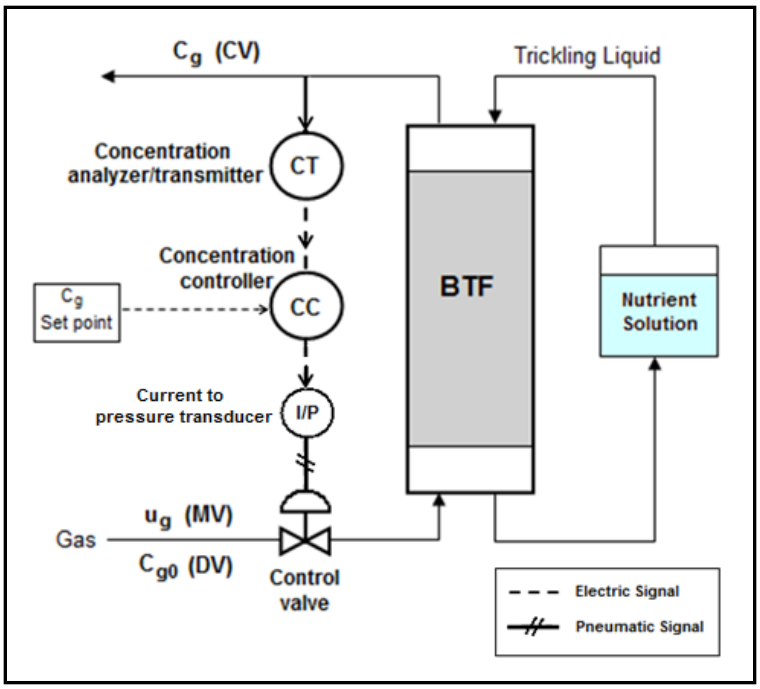

Figure 3-7. Feedback structure for BTF process control

3.2.2 Conventional control strategies

3.2.2.1 Feedback PI control. In general, feedback (FB) control systems are classical strategies where the controlled variable is measured, compared with the set point and the error between the two being fed to the controller which adjusts the manipulated variable, forcing the controlled variable back towards the set point [20]. A basic FB control loop consists of: 1) process under control, 2) sensor-transmitter device for measuring the controlled variable and transmitting this information to the controller, 3) feedback controller, 4) current-to-pressure transducer (I/P) that converts electric signal from the controller to pneumatic signal in case of adjusting the manipulated variable through a control valve, 5) final control element, most commonly a control valve, and 6) signal transmission lines, electric and pneumatic, that connect the instruments with each other [18]. The general block flow diagram of FB control system for a process with some known disturbance and control valve as the final control element is shown in Fig. 3-8. The blocks denote transfer function representations of different instruments and process, being connected together with signal transmission lines. As shown, the process output

(Y) is a combination of the process TF (G_p) and disturbance TF (G_d) with the rest of the TF blocks constituting control action elements.

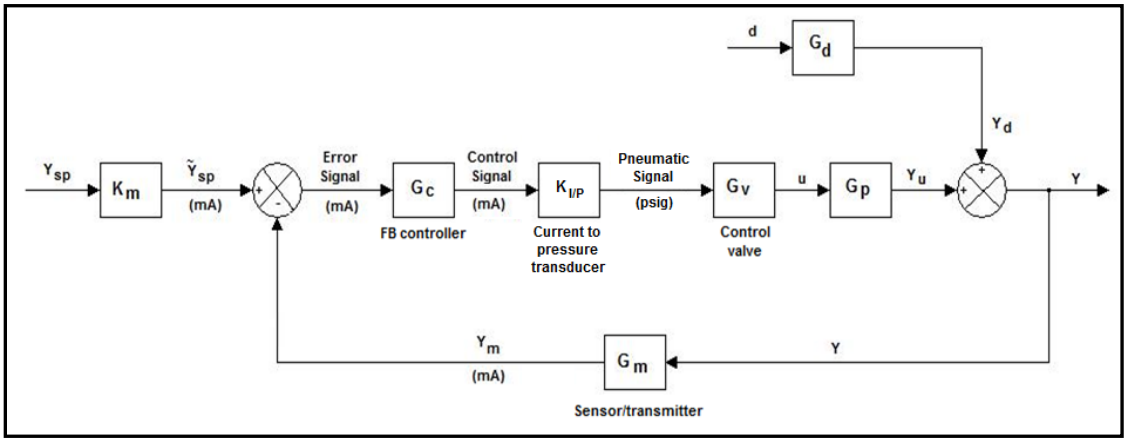

Figure 3-8. Block flow diagram of a FB control system [18].

FB controllers initiate control action as soon as the controlled variable deviates from the set point regardless of any disturbances [18]. Moreover, FB controllers do not necessarily require a process model and are robust in case of PID controllers [18]. However, these controllers initiate control action only when the controlled variable has deviated from its set point, and they cannot project control action for disturbance compensation [18]. Also, FB controllers are unfeasible for processes with large time delays or time constants and in situations where the controlled variable cannot be measured [18]. The main objective of FB controller is to reduce the error between measured control variable and set point. Basically, there are three modes of FB control [18]:

1) *Proportional control*: this is the simplest control mode where the controller output is proportionally adjusted according to the error using adjustable controller gain (K_c). The main disadvantage of this control is that there is a steady state *offset* after a set point change or disturbance. [18]
2) *Integral control*: in this mode, controller output is adjusted according to the integral of the error over time with integral time (τ_I) as a tunable parameter. It offers a great advantage of eliminating offset errors, but it usually gives oscillatory responses and may affect the stability of the control system. [18]

3) *Derivative control*: it predicts future behavior of the error signal by determining rate of change of the error and hence, manipulate the controller output accordingly using adjustable derivative time (τ_D). While it improves the stability of the controlled process, it can cause noise amplification in case of noisy measurement signals. [18]

Practically, most FB controllers exist as a combination of these control modes with PI and PID being the widely used controllers [18]. Likewise, a feedback control system was designed for the BTF in this work using a PI controller. Although several forms of PID controllers exist, parallel form of the PI controller was used which is defined by the following TF:

$$G_c(s) = K_c + \frac{K_c}{\tau_I s} \tag{3.7}$$

Following the FB block diagram in Fig. 3-8, the process and disturbance TFs are defined by the first and second TF expressions in equation (3.6) respectively. On the other hand, it has been assumed that control valve and concentration sensor have negligible dynamics and that the TFs for these instruments are pure gains. The range or *span* of electric signal, pneumatic signal, gas velocity, and H_2S concentration required for the calculation of control valve, current to pressure transducer, and concentration sensor/transmitter gains is shown in Table 3-3 including the TF representations. It should be noted that the concentration span is based on maximum and minimum concentrations observed overall during the simulation of the modified model. Hence, the value of the sensor gain (K_m) is just an approximation and that the accurate value of this gain will depend on characteristics of the actual measurement instrument. As a final note, the PI control system uses controlled, manipulated, and disturbance variables in deviation form.

Table 3-3
Control valve and sensor/transmitter properties for PI control system

Electric signal range	4 – 20 mA
Pneumatic signal range	3 – 15 psig
Gas velocity span	0.278 – 3.056 m/s (1000 – 11000 m/h)
Concentration span	0 – 0.2 g/m^3
$\mathbf{K_m}^*$	351 $\left(\frac{mA}{g/m^3}\right)$
$\mathbf{K_{I/P}}$	0.75 $\left(\frac{psig}{mA}\right)$
$\mathbf{K_v}^*$	0.231 $\left(\frac{m/s}{psig}\right)$
$\mathbf{G_m}^*$	351 $\left(\frac{mA}{g/m^3}\right)$
$\mathbf{G_v}^*$	0.231 $\left(\frac{m/s}{psig}\right)$

* Calculations were performed based on deviation values of H_2S concentration and gas velocity

The feedback PI control system was simulated using Simulink in MATLAB. Although several methods exist for controller tuning, a built-in tuning feature of the PID controller in Simulink was used to determine controller parameters. After tuning, the system performance was analyzed by observing the ability of the controller to deal with step changes in set point and disturbance separately. The resulting responses in deviation form were converted back to the actual values and these conversions are included in the Simulink simulation. The Simulink block diagram for this control system has been provided in the Appendix.

3.2.2.2 Feedback-feedforward hybrid control. This control configuration involves using a feedback control loop with a feedforward control loop. In a feedforward (FF) control system, disturbances are measured and control action is initiated accordingly to avoid process upsets [20]. Hence, FF control offers the advantage of reducing the effects of measurable disturbances by initiating the control action as soon as any disturbance is detected [18], [20]. However, FF control system requires a process model and is unfeasible if online measurement of disturbances is not possible [18]. Moreover,

designing ideal FF controller for perfect control may be “physically unrealizable” [18]. Consequently, FF control is not used alone and is practically used in conjunction with a FB control loop [18]. With the FB-FF control system, there are combined advantages of dealing with model uncertainties, measurement errors, and measured and unmeasured disturbances [18]. The block flow diagram of a FF-FB control is similar to a FB control system configuration except for the addition of a FF control loop as shown in Fig. 3-9. As shown, there is an addition of a FF controller and sensor for measuring disturbance. In this configuration, the manipulated variable is adjusted by the combined efforts of FB and FF controllers. Any change in controlled variable (Y) will be rectified by the FB controller while changes in the measured disturbance (d_m) will be identified and compensated by the FF controller. For perfect control i.e. in situation where the controlled variable is to be exactly maintained at the set point regardless of disturbance changes, the TF for an ideal FF controller can be determined as follows [18]:

$$G_f(s) = -\frac{G_d}{G_t K_{I/P} G_v G_p} \tag{3.8}$$

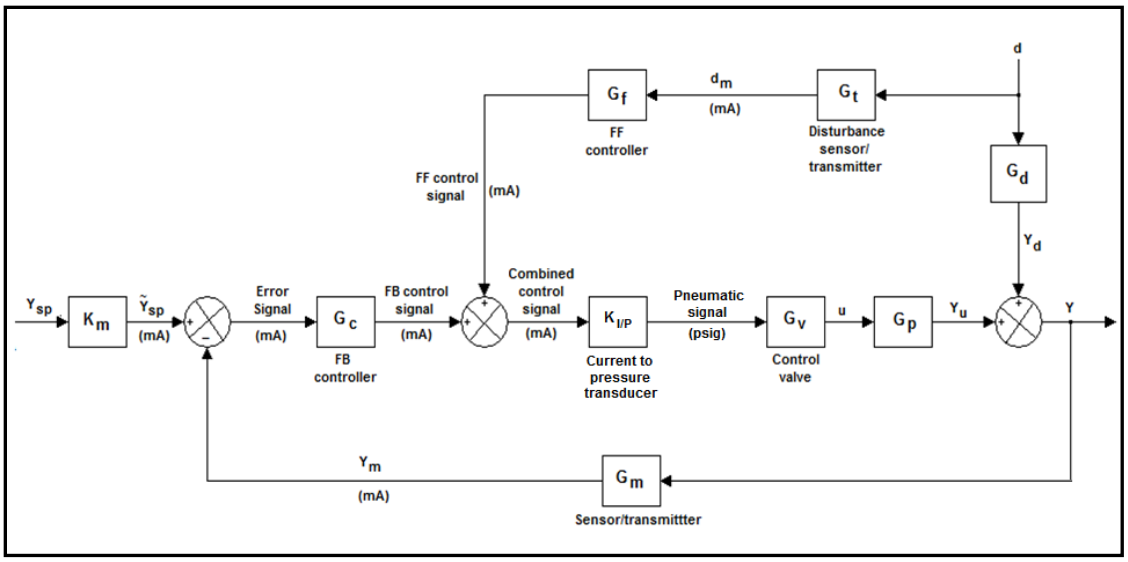

Figure 3-9. Block flow diagram of a FB-FF control system [18]

The FB-FF control system is the second control strategy that had been implemented for the BTF process in this work. For this control configuration, the PI controller developed in section 3.2.2.2 and an ideal FF controller were used as FB and FF

controllers respectively. The basic BTF control structure in Fig. 3-7 needs to be modified for the proposed FB-FF control system and is shown in Fig. 3-10. The control structure now consists of an additional sensor that measures inlet concentration of H_2S and relays this information to the FF controller. The FF control signal is combined with the FB control signal and the resulting signal is sent to the control valve for adjusting the gas velocity. The TFs and gains developed in section 3.2.2.2 apply to the FB-FF control system as well. The disturbance sensor/transmitter (G_t) has the same TF as the sensor/transmitter for output measurement (G_m) since the disturbance and controlled variables are both concentrations. Using equation (3.8), the resulting ideal FF controller TF is given as follows:

$$G_f(s) = -0.376\,\frac{(1.8s+1)\,e^{-54s}}{(72.57s+1)} \tag{3.9}$$

As evident from equation (3.9), the ideal FF controller is physically realizable. Finally, simulation and analysis of the FB-FF control system was performed using Simulink.

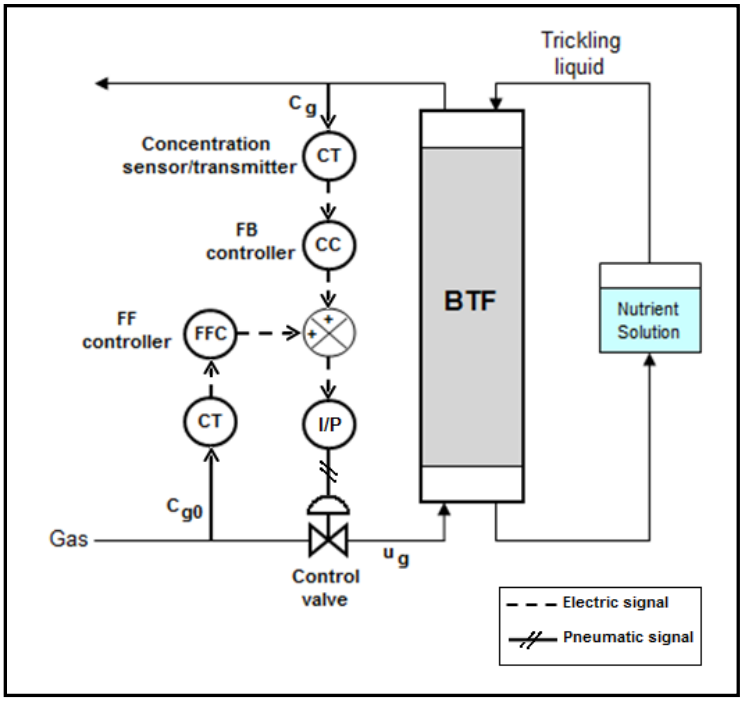

Figure 3-10. FB-FF control structure for BTF process

3.2.3 Advanced control strategies

3.2.3.1 Model predictive control. In short, model predictive control (MPC) represents a class of advanced control methods that explicitly use a process model to determine the control signal through minimization of an objective function [26]. The various forms of MPC differ from each other with respect to the type of process model used and the form of cost function (objective function) minimized [26]. For simple processes that could be approximated with a linear model, linear MPC is employed whereas for highly nonlinear processes, nonlinear MPC should be employed [18]. MPC has received widespread application in academics and industrial processes [26]. In addition to applications in medical field, MPC has been applied in several processing industries like the cement production industry, drying towers, distillation columns, PVC plants, and steam generators [26]. MPC offers several advantages, some of which include: 1) it can be applied to several types of processes; from simple to complex processes, processes with large time delays, and unstable processes 2) it can offer multivariable control 3) its features have a natural feedforward control element to deal with measured disturbances 4) its control law can be easily implemented 5) it can systematically consider input and output constraints [18], [26]. Nevertheless, MPC has drawbacks like complex control law derivation and requirement of high computational effort when considering constraints [26]. The most serious drawback of using MPC is its requirement of a reliable process model that would provide accurate input-output predictions while being easy to implement at the same time [26].

The basic concept of MPC is shown in Fig. 3-11. The methodology involves predicting future outputs within a prediction horizon (P) at each sampling time instant using the process model [26]. Moreover, the output prediction calculations are dependent on past inputs, past actual outputs and future control signals (u) [26]. Next, the set of future control moves is optimally obtained within a certain control horizon (M) through minimization of the objective function so that the process is maintained at the desired set point [26]. The objective function includes a term for errors between the predicted output and set point. Usually, the objective function also includes control effort term [26]. Finally, from the set of M control moves, only the first control move is implemented while the rest are rejected; the approach commonly known as *receding horizon*

concept [26]. These procedures are repeated until the predicted output reaches the set point value. The block flow diagram for the implementation of these procedures is shown in Fig. 3-12.

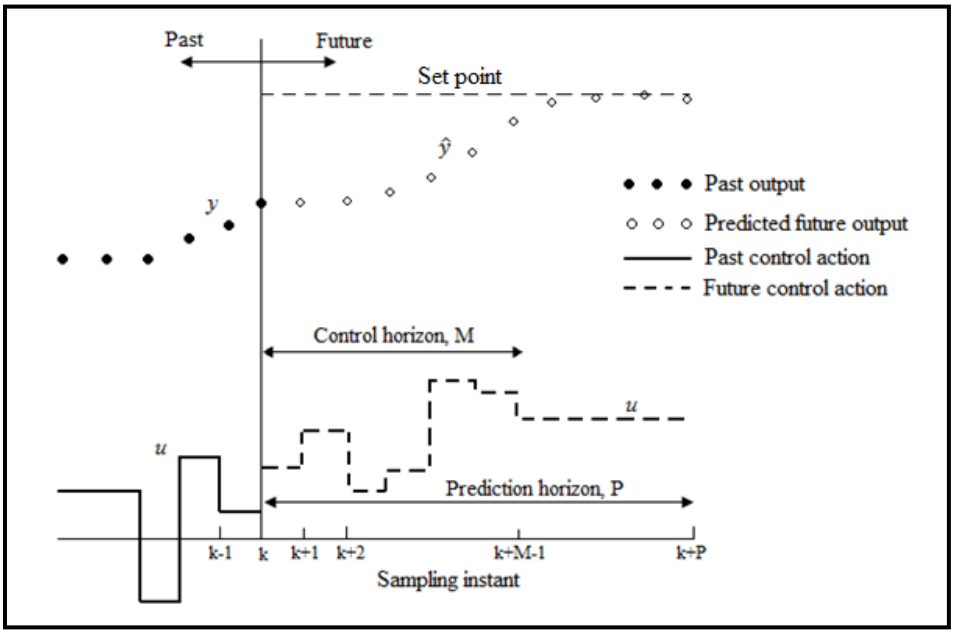

Figure 3-11. Basic concept of MPC [18]

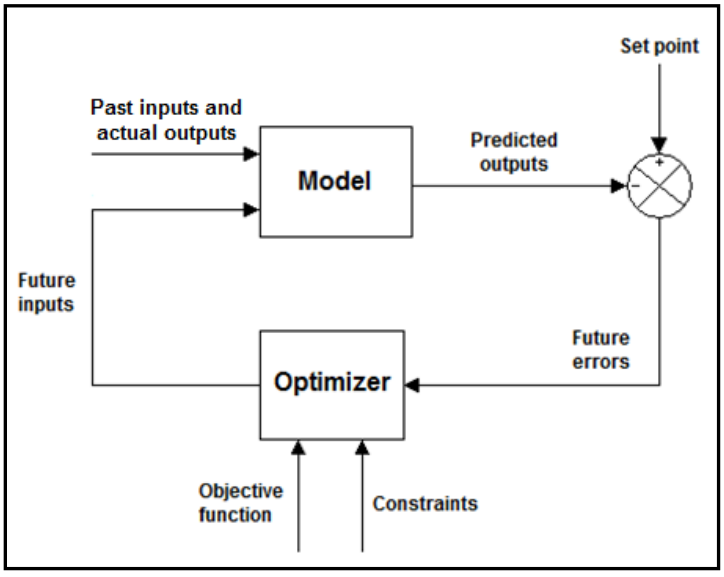

Figure 3-12. Basic MPC structure [26]

As an important consideration in deriving MPC control law, objective or cost functions have various forms. The objective function (J) should be formulated such that the predicted future output ($\hat{y}$) within the prediction horizon (P) follows the set point signal (w) while avoiding excessive control action (Δu) at the same time [26]. The objective function with such properties is generally expressed as follows [26]:

$$J\ (N_1, N_2, N_u) = \sum_{k=N_1}^{N_2} q(k)[\hat{y}(t+k) - w(t+k)]^2 \qquad (3.10)$$

$$+ \sum_{k=1}^{M} r(k)\,[\Delta u(t+k-1)]^2$$

Parameters N_1, N_2 are the minimum and maximum cost horizons while $q(k)$ and $r(k)$ represent output and input change weighing coefficients respectively [26]. The MPC optimization algorithm will determine the set of control actions (Δu) that would minimize the cost function given in equation (3.10). Overall, for MPC design and tuning, following parameters are required [18]:

1) *Sampling time*
2) *Control horizon* (M)*:* increasing the control horizon results in aggressive control but it increases the computational effort as well [18].
3) *Prediction horizon* (P): the prediction horizon should be selected such that adequate time is given for the required input changes to reach steady state values. While increasing the value of P results in aggressive controller, it is theoretically advantageous to use larger values. [18]
4) *Output and input weighing coefficients:* input weighing coefficient determines the degree of control move suppression. Increasing this coefficient results in smooth input changes but can cause large deviation of the output response from the set point. On the other hand, increasing output weighing coefficient results in tight control. [18]

For the BTF in this work, two MPC systems were implemented:

1) *Transfer function model predictive control.* As the name suggests, this linear control system involves using TF model as the prediction model for MPC. For the BTF process, this control scheme was implemented using BTF transfer function model defined in equation (3.6) as the prediction and plant model. The control system was simulated in Simulink using MPC Toolbox in MATLAB for designing the controller. The tuning parameters required by the toolbox to design the MPC controller were obtained by trial and error. Moreover, constraints were defined in the toolbox so that the input (gas velocity) and the output (outlet concentration) would not have negative values. The toolbox also has an input port for measured disturbances where the inlet concentration signal was connected. The resulting system was then analyzed for its performance towards set point and disturbance changes. The Simulink block diagram for this system has been provided in the Appendix. The results occurring in deviation form due to the TF model were converted back to the actual values. These conversions have been shown in the Simulink block diagram.

2) *Neural network model predictive control (NNMPC).* This is a nonlinear model predictive control technique where NN is used as the nonlinear model. Generally, the nonlinear MPC determines output predictions from solution of the analytical model [27]. The main drawback of this control strategy is that optimization of the objective function requires repeated solution of the analytical model which may require immense computational effort and time [27]. The controller may even be unfeasible for complicated models. However, this scenario can be avoided by using NN as the nonlinear model because of its advantages listed earlier in section 3.1.3. The NNMPC control strategy was implemented on the BTF process and simulated in Simulink where the controller was designed using the NN Predictive control block. Before controller tuning, this control block requires NN training of the plant dynamics and it can only model single input-single output relationship. In other words, multivariable control is not possible with NNMPC. For the BTF plant model, modified model could not be used since it requires considerable amount of computational effort and time. Hence, the steady state NN model developed in section 3.1 was used as the BTF plant model. The NN Predictive controller

in Simulink offers the choice of training the NN model from input-output data or from the plant model. The latter case was used to train the NN in the NNMPC controller. In this case, the controller first obtains input-output training data automatically through simulation of the plant model at random step changes of input and then fits a NN model to these simulated data. After successful training of the NN model, the controller was tuned by trial and error. Finally, the performance of the control system was analyzed through set point and disturbance step changes. It should be noted that control was based on normalized values of input and output since the BTF NN plant model was fitted with normalized data. However, the results were converted back to the actual values and are shown in the Simulink block diagram. Since there is single control loop, the LGVR input to the BTF NN model was held constant while the inlet concentration was considered as a disturbance.

3.2.3.2 NNMPC with FB integral control. An attempt was made to propose a control strategy based on the combination of conventional FB and advanced model predictive control. Hence, in this work, an NNMPC controller was used in conjunction with an integral FB controller. The block diagram for this control system is shown in Fig. 3-13. In this system, the set point and measured output signals are transmitted to both the controllers, the corrective actions from the two controllers are combined and finally transmitted to the process to maintain the output at the set point. The proposed control system was simulated in Simulink and procedures for designing the two controllers are same as the ones mentioned in the previous sections. Moreover, NN model developed in section 3.1 was used as the process model with LGVR and inlet concentration being constant and disturbance inputs respectively.

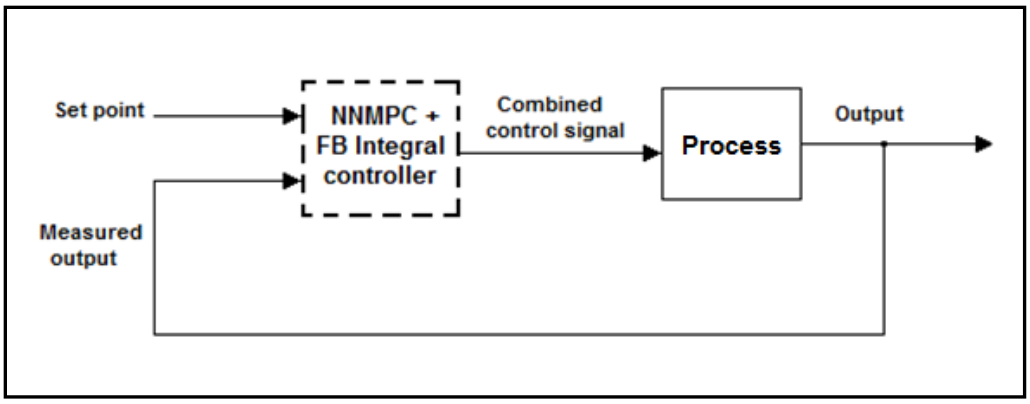

Figure 3-13. Block flow diagram of NNMPC - FB integral control system

3.2.4 Results and discussion. For all the proposed control strategies, the initial outlet concentration set point was set at the value that represented base removal efficiency of 94% (outlet concentration of 9.52 x 10^{-3} g/m^3). Moreover, during the analysis of the controller performance towards set point changes, the changes ranged from values representing 94 – 99% (outlet concentration of 1.64 x 10^{-3} g/m^3) removal efficiency with respect to the base inlet concentration. For all the control systems that had been analyzed with a single step change in set-point, the set-point was changed from 9.52 x 10^{-3} g/m^3 to 3.28 x 10^{-3} g/m^3. Moreover, single step change in the disturbance was made that consisted of changing the inlet concentration from 0.164 g/m^3 to 0.184 g/m^3 at the initial time (t = 0). The input-output responses obtained from the simulations were recorded and plotted using MATLAB.

3.2.4.1 Analysis of feedback PI controller. The tuning parameters determined from the PID controller block in Simulink are as follows:

K_c **= 3.89**

τ_I **= 0.6 s**

Set-point change

Fig. 3-14 shows the output and input responses for a step change in set-point at the base inlet concentration (no disturbance). It can be observed that within ten seconds

from the step change time instant, the PI controller has successfully driven the output to the new set point value. The observed overshoot and slightly oscillatory response signify characteristic behavior of proportional and integral control respectively. Due to aggressive control, the output response results in an overshoot. However, the error tracking ability of the integral action quickly forces the output to the set point. As expected, the input response is proportional to the output response and shows a similar pattern. This is evident from the fact that to decrease the outlet concentration of H_2S, the gas velocity has to be decreased so that enough time is available for higher biodegradation of H_2S by the micro-organisms.

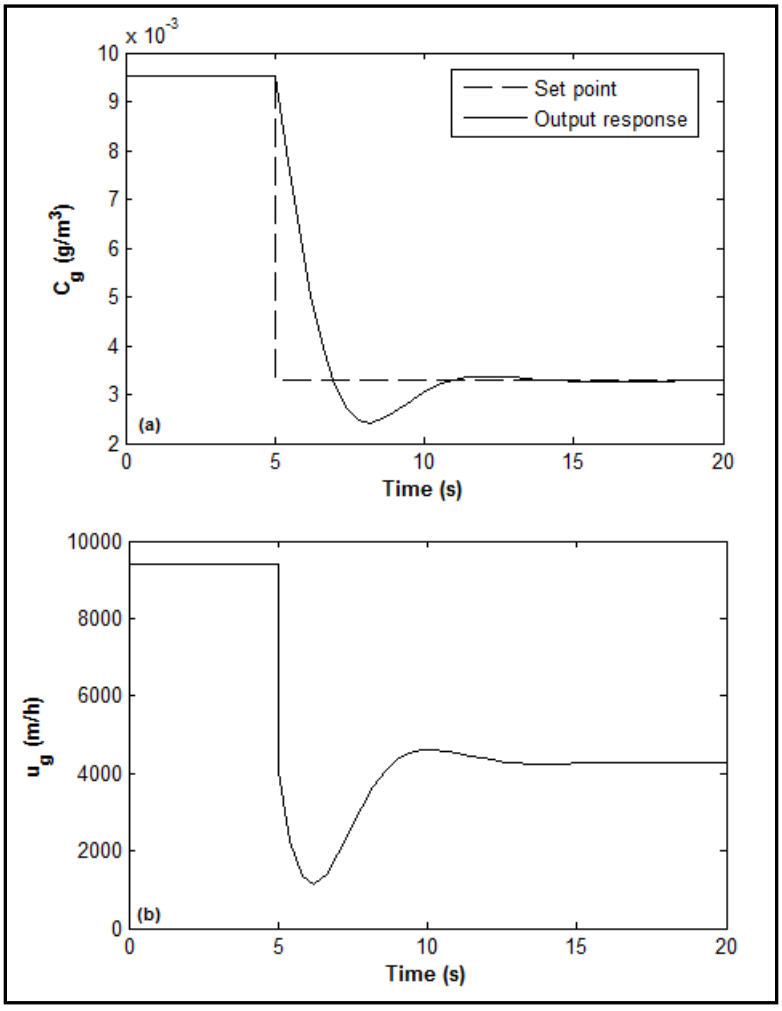

Figure 3-14. (a) Output and (b) input responses for set-point change in case of PI control

Disturbance change

The output response for step change in disturbance (inlet concentration) is shown in Fig. 3-15. Due to the time delay in case of disturbance, the process starts feeling the effect of the disturbance only after 54s. As the outlet concentration deviates from the set-point due to the disturbance change, the integral action of the PI control forces the output towards the set-point to minimize the errors. However, the output response is quite slow and is continuously oscillating. These behaviors are observed due to the slow dynamics of the process itself with respect to the disturbance variable and due to a low value of the integral time respectively. In general, the output response becomes more oscillatory at higher values of proportional gain (K_c) or lower values of integral time (τ_I). Nevertheless, it can be observed that output deviations from the set point are very small and become almost non-existent with time. Hence, it can be said that the PI controller has effectively rejected the disturbance. The control input is overall smooth and eventually reaches a steady state value with time.

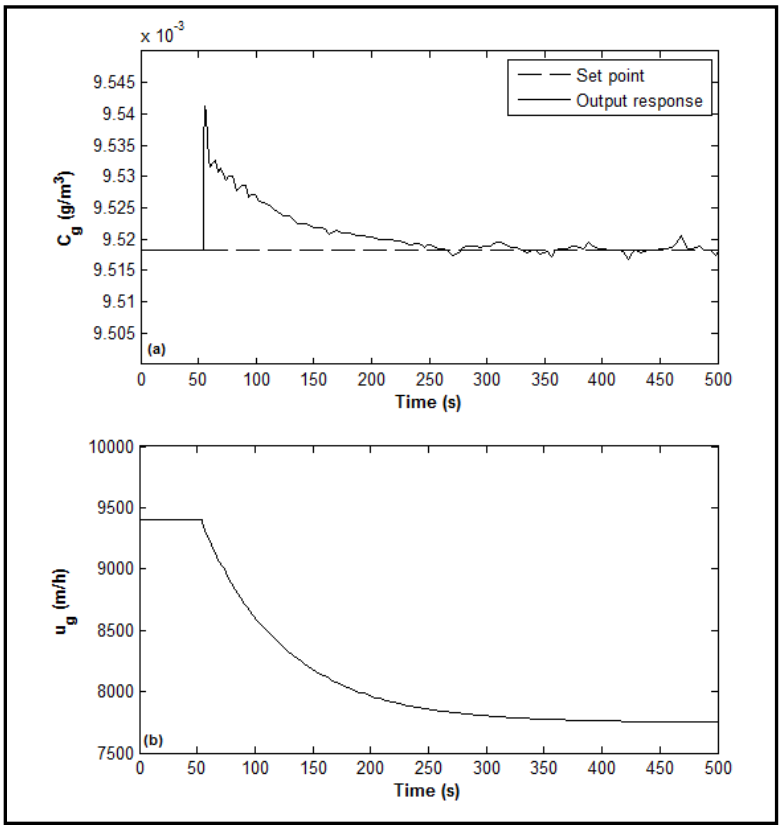

Figure 3-15. (a) Output and (b) input responses for disturbance change in case of PI control

3.2.4.2 Analysis of FB-FF control system. The tuning parameters for the FB controller are equal to parameter values listed in section 3.2.4.1 since adding a FF controller has no effect on the performance of the PI controller. The transfer function for the FF controller had already been determined in section 3.2.2.2.

Set-point change

The output response was the same as in Fig. 3-14 since the same PI controller was used and the set-point change was made with no disturbance change. The behavior is similar because the PI feedback controller deals with output deviations from the set-point whereas the FF controller deals with the disturbance. Hence, when there are only set-point changes (*servo* problem), the combined FB-FF corrective action has the entire contribution from the PI controller.

Disturbance change

The output response for the step change in disturbance is shown in Fig. 3-16. It can be clearly observed that the ideal FF controller has achieved almost perfect disturbance rejection since the output is nearly close to the set-point throughout the simulation time. Despite the oscillatory response, the controller performance is still superior. The combined input response shows a smooth control action and is expected to reach steady state condition eventually.

Overall, it had been observed that the FB-FF control system provided both good set point tracking and nearly perfect disturbance rejection. Based on these responses, it can be deduced that FB-FF control strategy offers superior performance when compared with the conventional FB controller.

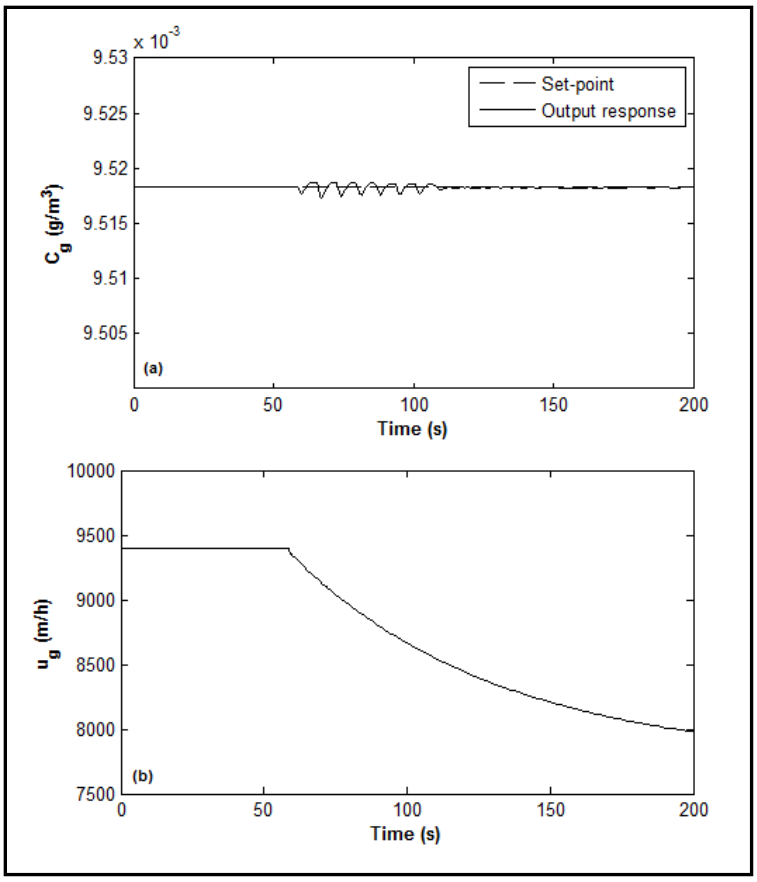

Figure 3-16. (a) Output and (b) input responses for disturbance change in case of FB-FF control

3.2.4.3 Analysis of transfer function MPC controller. The controller settings obtained after trial and error are shown in Table 3.4. The value of sampling time is an approximation since actual value will depend on the sampling time of the concentration sensor used in the actual process. Having a higher output weight implies that the output deviation from set-point is more penalized i.e. there will be tight control of output in response to set-point changes.

Table 3-4
Transfer function MPC controller settings

Sampling time	2s
Prediction horizon	80
Control horizon	2
Input change rate weight	0.008
Output weight	7.389

Set-point change

The output behavior in response to a set-point step change is shown in Fig. 3-17. Looking at the output and input responses, the tuned MPC controller has successfully achieved good set-point tracking with minimal amount of control moves. In addition, the response was fast with negligible overshoot. It should be noted that the input response is in the form of a discrete signal since the MPC controller collects the data at discrete times and calculates the set of control moves at each of these time instants. Overall, good set-point tracking was observed due to the heavy weighting of the output shown in Table 3-4.

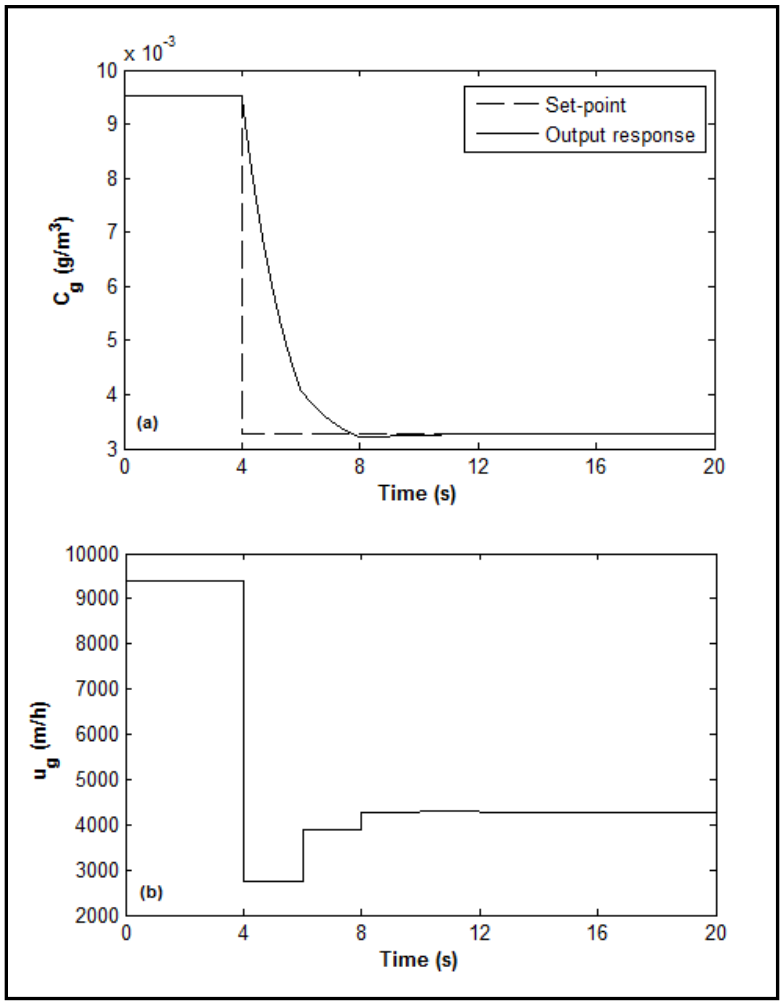

Figure 3-17. (a) Output and (b) input responses for set-point change in case of transfer function MPC

Disturbance change

In case of step change in disturbance, the output response with MPC controller in Fig. 3-18 is similar to the one with the FB controller in Fig. 3-15 except that the response is smoother and less oscillatory. In response to the disturbance, a maximum output deviation of 0.7% from the set-point is observed with the MPC controller. Although the output response takes long time to reach the set-point value, the deviation errors are very small. Hence, the MPC controller has successfully dealt with the disturbance effects. Looking at the input response, the profile is continuous indicating excessive implementation of control moves. This is because the deviation in the output response is very small and to force the output back to the set-point very small changes in input are required. Hence, the controller provides smooth and slow control action at the expense of the control moves.

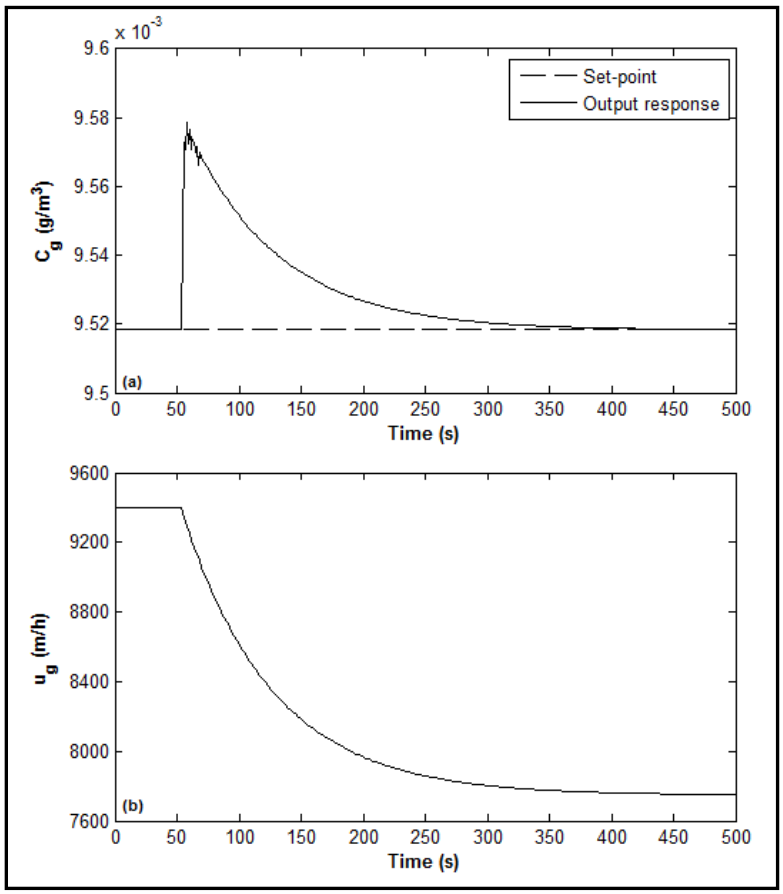

Figure 3-18. (a) Output and (b) input responses for disturbance change in case of transfer function MPC

3.2.4.4 Analysis of neural network MPC controller. The trained NN results and the controller settings determined by trial-and-error are shown in Table 3-5. The MSE and R^2 values suggest that the NN model had been successfully trained. It can be seen that the NNMPC controller requires a search parameter. This parameter is used for controlling optimization performance of the controller [28].

Table 3-5
Trained NN and NNMPC controller setting results

NN Plant Identification results	
Total simulated data samples	1000
Sampling interval	2 s
Size of hidden layer	5
Validation MSE	2.81×10^{-8}
Overall R^2 value	0.998
Controller settings	
Maximum cost horizon (N_2)	100
Control horizon	2
Control (input) weighting factor	1×10^{-4}
Search parameter	5×10^{-3}

Set-point change

The output response for set-point change is shown in Fig. 3-19. It is observed that the NNMPC controller provides excellent set-point tracking using less control moves. However, there are time delays in the control actions of the controller. While training the NN model in the NNMPC controller, the NNMPC control block in Simulink required non-zero entry values for input and output delays so that the time variation of variables could be accounted in the system. Hence, two delays on input and output were defined for the NNMPC controller training that resulted in the response delays observed in Fig. 3-19. Towards the end of the simulation time, it can be observed that there is a small offset error between the new set-point value and the output response. Nevertheless, this small discrepancy is eventually eliminated in the limit as time goes to infinity.

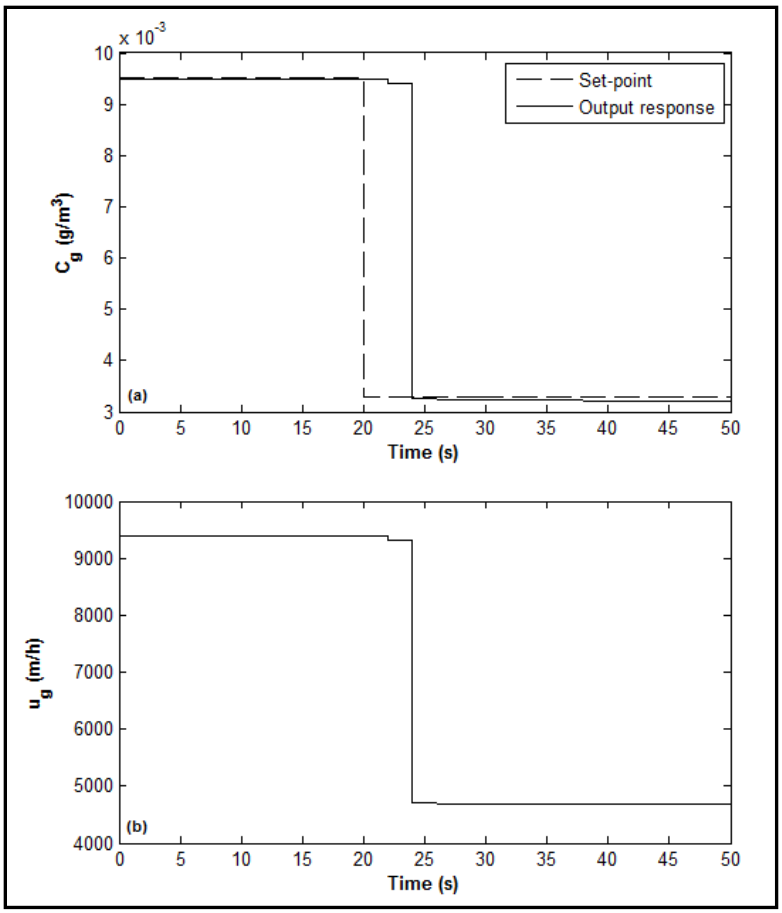

Figure 3-19. (a) Output and (b) input responses for set-point change in case of NNMPC

Disturbance change

The output response in Fig. 3-20 shows no disturbance rejection by the controller. Keeping in mind that there is a time delay between disturbance and output variables, it is observed that the process never reaches the set-point after being disturbed i.e. an offset occurs. This implies the serious limitation of using a NN based MPC. This behavior had also been observed and proven by Chu et al. [29] through experimental implementation of feedforward neural network (FNN) MPC and external recurrent network (ERN) MPC controllers on pilot-scale distillation column. In [29], it had been experimentally proven that FNN based MPC results in an offset error in presence of disturbance while using ERN based MPC eliminates the offset. It was also justified analytically that the output prediction characteristics of the FNNs have an inherent disadvantage of being unable to

deal with model mismatch when the process is upset by a disturbance [29]. Based on the justifications, Chu et al. claimed that using a FNN based MPC is unfeasible for practical applications and that ERN based MPC should be used instead [29]. Since the NNMPC controller in MATLAB uses a FNN model, it is clear that there will be an offset in case of disturbance. Hence, based on the output responses observed towards set-point and disturbance changes, it can be said that the NNMPC controller behaves like a *proportional* only controller.

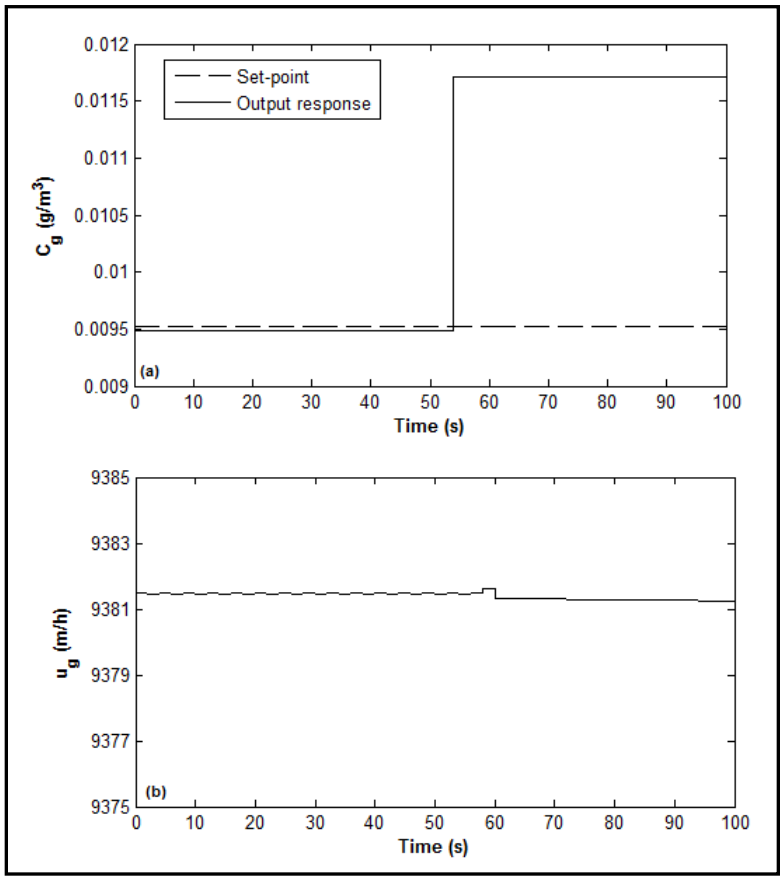

Figure 3-20. (a) Output and (b) input responses for disturbance change in case of NNMPC

3.2.4.5 Analysis of combined NNMPC and integral control. The design properties of the controllers are shown in Table 3-6.

Table 3-6
NNMPC and integral controller properties

NNMPC Plant Identification results	
Total simulated data samples	1000
Sampling interval	2 s
Size of hidden layer	5
Validation MSE	3.48×10^{-10}
Overall R^2 value	0.999
Controller settings	
Maximum cost horizon (N_2)	150
Control horizon	2
Control (input) weighting factor	1×10^{-4}
Search parameter	5×10^{-3}
Integral gain (for integral controller)	8

Set-point change

The output response resulting from set-point change is shown in Fig. 3-21. It can be seen that with the addition of an integral controller, the time delay that had been observed for the NNMPC in Fig. 3-19 has been eliminated. Although, the combined NNMPC-integral controller shows good set-point tracking, the output response has overshoots. The overshoot occurs due to the combined control action of the two controllers. In other words, the control signals from both the controllers add together, resulting in a higher input value than the desired which causes the output to exceed the set-point.

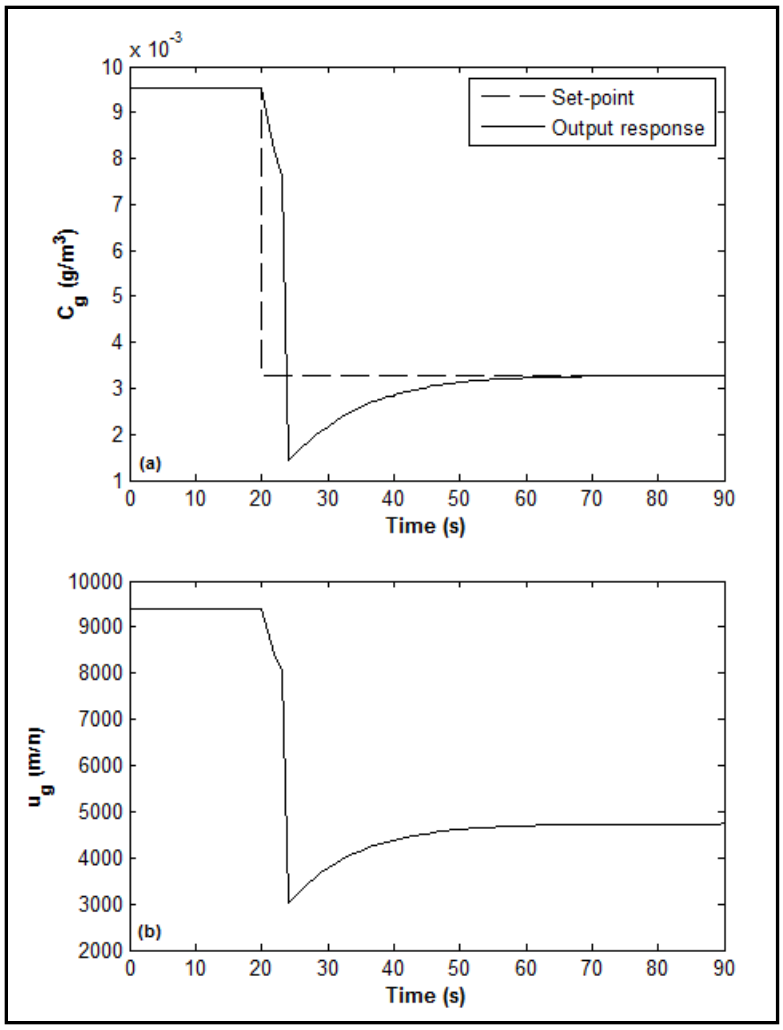

Figure 3-21. (a) Output and (b) input responses for set-point change in case of NNMPC-integral control

Disturbance change

It can be observed in Fig. 3-22 that the controller has managed to deal with disturbance that had been initiated at the initial time. During the process upset (after the time delay) by the disturbance, corrective action is initiated only by the integral controller while the NNMPC becomes ineffective due to the reasons explained earlier in section 3.2.4.4. Despite the disturbance rejection, there is a large overshoot where there is 141% deviation of the output from the desired set-point. The disadvantage of the additive control action from the two controllers is the reason for the resulting overshoot. This large overshoot is highly unacceptable in practical application since the outlet

concentration (output) must be maintained below the legal limit. Hence, this control strategy is unfeasible in this case.

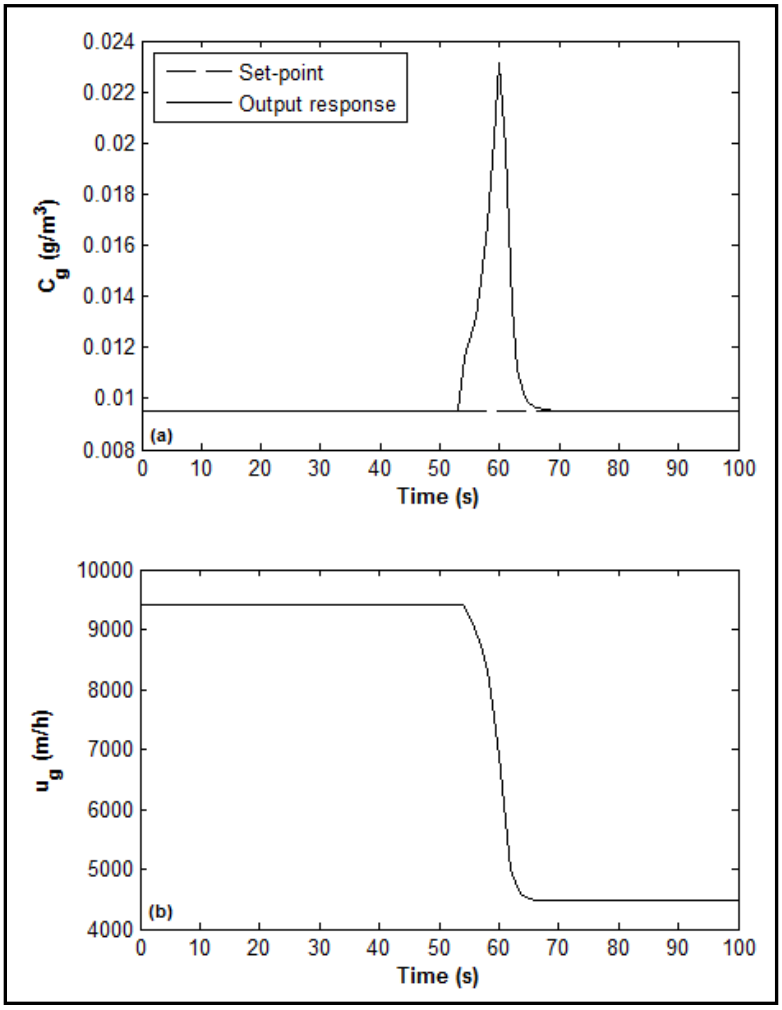

Figure 3-22. (a) Output and (b) input responses for disturbance change in case of NNMPC-integral control

3.2.4.6 Comparison of BTF control strategies. Based on the analysis of the control strategies in the previous sections, it can be deduced that three BTF control strategies provided best control performance: 1) PI, 2) PI – FF, and 3) TF MPC based control systems. To determine the optimum control strategy, these TF model based control systems were qualitatively compared against each other for their performance towards set-point and disturbance changes separately. The set-point changes consisted of a set of random step changes ranging from 1.64 x 10^{-3} g/m^3 (99% removal efficiency with respect to base inlet concentration) to 9.518 x 10^{-3} g/m^3 (base removal efficiency of 94%). For analysis of disturbance rejection, a single disturbance step change from base inlet concentration (0.164 g/m^3) to a higher concentration (0.2 g/m^3) at the initial time was used. The results from all the controllers were compiled and plotted in the same graph. The Simulink block diagram is provided in the Appendix.

Set-point changes

The output responses of the selected control strategies are shown in Fig. 3-23. Overall, all the controllers showed excellent set-point tracking with TF MPC controller showing the best control since there are no overshoots. In case of PI and PI-FF controllers, there are overshoots which may be disadvantageous in situations where strict control is needed. In case of a BTF process or any other environmental treatment technology, this may be a serious consideration where safe pollutant release must be below the legal limits. However, overshoots could be avoided by either decreasing proportional gain or increasing the integral time at the expense of a sluggish response.

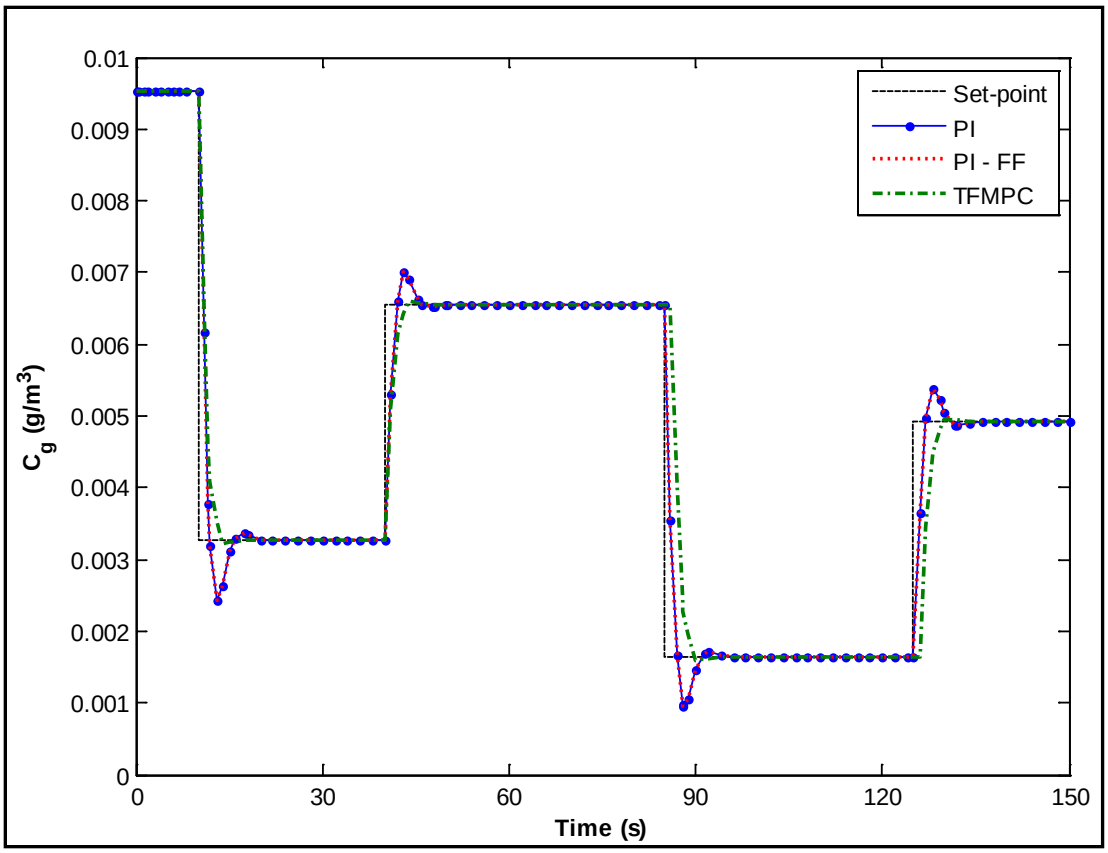

Figure 3-23. Output responses of TF based controllers in case of step changes

Disturbance change

In case of disturbance change, varied responses are observed in Fig. 3-24. Looking at the output deviations from the set-point, the hybrid PI-FF controller offers superior performance amongst the controllers with perfect disturbance rejection while the TF MPC offers the least since it produces largest output deviation from the set-point. For the TF MPC controller, the deviations due to inlet concentration disturbance could be reduced by reducing the sampling period. The reason for this justification is that the sooner the controller detects process upsets the better the control action. Practically, however, the sampling period could not be optimized as it would depend on the sampling time of the measurement device. Nevertheless, for the PI and TF MPC controllers, maximum output deviations of 0.4 % and 1.1 % from the set-point were observed respectively. These deviations are quite small and hence, the performances from these two controllers are satisfactory. In case of BTF, there could be fluctuations in inlet

concentrations and it would be therefore essential to have an efficient control system for disturbance rejections. In this situation, using a PI-FF controller would be ideal.

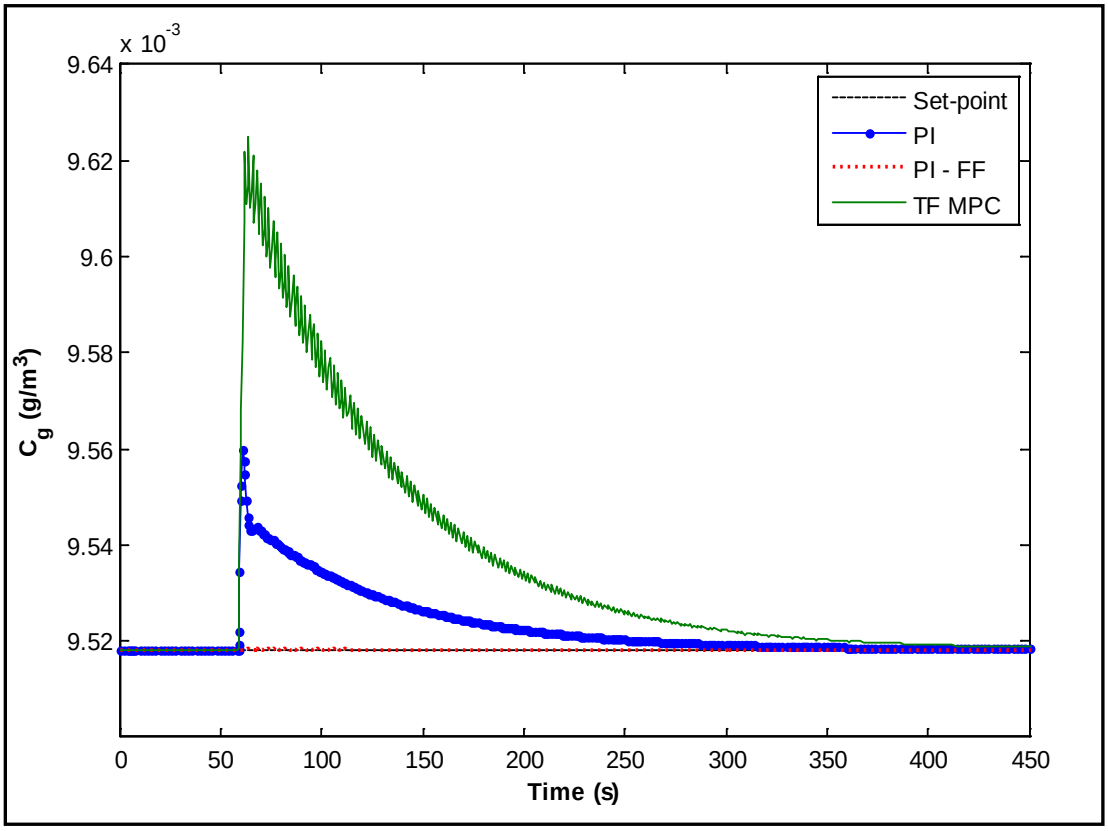

Figure 3-24. Output responses of TF based controllers in case of disturbance change

Chapter 4. Conclusion

This work aimed to provide a theoretical aspect on the modeling and control of a BTF for making it a viable air pollution treatment technology on a large-scale. The work was focused on selecting an appropriate theoretical model from literature first that would provide adequate insight into the dynamics and performance of a BTF in general. From the review of five literature BTF models, it had been observed that the models were mostly specific to the type of pollutants being treated. Although several achievements were observed in these BTF models, there is still a need for an appropriate model that could be universally used for practical applications. However, developing such model may require a great deal of effort and time. Likewise, the theoretical analyses performed in this work were based on a specific pollutant due to the specific nature of the selected BTF model. Amongst the models reviewed, Kim and Deshusses' model [5] was selected as the target model with H_2S being the target pollutant treated. The choice of the target model selection was based on the simplicity of the mathematical model formulation while at the same time capturing significant phenomena as well. Kim and Deshusses' model [5] had a simple model formulation which could be easily solved and also the model captured many phenomena occurring in the BTF process. The most striking feature of the model was its ability to simultaneously account for wetted and non-wetted biofilm due to incomplete wetting of biofilm by the trickling liquid. However, the model was developed for a differential BTF in batch mode and most of the model parameters were experimental. For practical situations, a continuous operation of the BTF is required. Moreover, there is also an issue on implementing and analyzing the performance of BTF with the control strategies proposed in this work. Since the model parameters listed by Kim and Deshusses [5] could not be used in case of a large continuous BTF, an alternative strategy was used by considering cascaded *n*-batch BTFs in series. In this configuration, the large BTF could be considered as a combination of differential BTFs connected in series with each other. With the proposed configuration and some modifications to the original model equations, the BTF reactor was scaled-up with continuous mode of operation. Moreover, the need to determine new set of model parameters for the large BTF was avoided. The original BTF model had been

successfully validated by Kim and Deshusses [5] with experimental data. Hence, it was assumed that each of the differential BTFs in the proposed model structure behaved exactly like the differential BTF in [5]. There could be an uncertainty in the reliability of the proposed model to accurately represent the BTF dynamics in this case. Nevertheless, the modified model was successfully simulated and analyzed for performance evaluation. To solve the modified model where equations need to be solved for each reactor, a pseudo steady state assumption was used. This strategy reduced the computational effort and time required to solve the model. The performance was determined by analyzing the effect of inlet concentration of H_2S, gas velocity, and LGVR on the steady state outlet concentration. The outlet concentration was directly related to inlet concentration and gas velocity while a parabolic profile was observed in case of LGVR. This parabolic profile indicated mass transfer effects occurring in the trickling liquid phase that affected the removal efficiency of the pollutant. It had been observed that the inlet concentration and gas velocity had strong affect on system performance while LGVR had effect only for a small range.

For the implementation of control strategies on the BTF process, simple data driven models were used. The modified model could not be used since it was still computationally challenging in terms of effort and time. Moreover, controlling BTF process based on the modified model would require continuous solution of the model which is unfeasible. Hence, transfer function and neural network based models were selected for identification of the BTF process. Assuming that the modified model represents the actual BTF process, the TF and NN models were fitted with data from simulation of the modified model. Gas velocity and inlet concentration were considered as the main process inputs while outlet concentration was selected as the BTF performance variable (output). The TF and NN models had been successfully obtained with R^2 values above 0.97 overall. For the NN model, the optimum size of the hidden layer was 7 and the resulting NN model had a nearly perfect fit. However, the NN model had been based on steady state data while the TF was fitted with dynamic step response data. Hence, a TF model representation would be more accurate at this stage.

Finally, five control strategies were implemented namely PI, FB PI-FF, TF MPC, NNMPC and NNMPC with integral control. The first three controllers were based on TF

model representation of BTF while the rest used NN model. For the control structure, gas velocity, inlet concentration, and outlet concentration were selected as manipulated, disturbance and controlled variables respectively. Through set-point and disturbance step testing, it was found that the first three controllers provided satisfactory control responses. While the NNMPC controller showed excellent set-point tracking, the presence of a constant offset error in response to disturbance change was the main limitation. The offset errors resulting from the use of NNMPC controller prove that using FNN based model for MPC control is unfeasible and as suggested by [29], the use of recurrent neural based models is recommended. Although the addition of an integral controller to the NNMPC eliminated the offset error due to disturbance change, large overshoots had been observed in response to set-point and disturbance changes. Since a steady state NN model was used as the BTF plant model for the last two controllers (NNMPC and NNMPC with integral controllers), it would be unjust to comment on the performance of these controllers.

With regard to the theoretical model used for the BTF system, the modified Kim and Deshusses' model [5] could be more realistic by considering a change in biofilm thickness due to biomass growth although it had been justified that H_2S treating BTF produce thin biofilms [5]. The effects of biomass growth can be easily implemented by repeating the solution of the modified model with the pseudo steady state assumption at different biofilm thickness. On the other hand, for practical implementation of the BTF process, it would be essential to analyze the extent of BTF performance by considering shock loading effects. For the BTF process, shock loading would refer to sudden large change in the inlet concentration of the pollutant. It would be important to consider the maximum shock loading as well to analyze the ability of the micro-organisms to effectively remove the pollutant under extreme conditions and hence, investigate the robustness of the BTF system. It is therefore recommended to consider shock loading effects through experimental testing and model predictions. Finally, since the discussions in this work are all based on theoretical analyses, it would be recommended to validate the findings in this work with experimental testing.

References

[1] S. Mudlier et al., "Bioreactors for VOCs and odours - A review," *Journal of Environmental Management,* vol. 91, pp. 1039-1054, 2010.

[2] J. S. Devinny and J. Ramesh, "A phenomenological review of biofilter models," *Chemical Engineering Journal,* vol. 113, pp. 187-196, 2005.

[3] M. C. Delhomenie and M. Heitz, "Biofiltration of Air: A Review," *Critical Reviews in Biotechnology,* vol. 25, pp. 53-72, 2005.

[4] M. A. Deshusses and D. Gabriel, "Biotrickling Filter Technology," in *Biotechnology for Odor and Air Pollution Control,* Z. Shareefdeen and A. Singh, Eds., New York, Springer, 2005, pp. 147-166.

[5] S. Kim and M. A. Deshusses, "Development and Experimental Validation of a Conceptual Model for Biotrickling Filtration of H2S," *Environmental Progress,* vol. 22, no. 2, pp. 119-128, 2003.

[6] G. Soreanu et al., "Empirical modelling and dual-performance optimisation of a hydrogen sulphide removal process for biogas treatment," *Bioresource Technology,* vol. 101, pp. 9387-9390, 2010.

[7] E. R. Rene et al., "Back-propagation neural network for performance prediction in trickling bed air biofilter," *International Journal of Environment and Pollution,* vol. 28, no. 3-4, pp. 382-401, 2006. [Abstract].

[8] E. R. Rene et al., "Neural network models for biological waste-gas treatment systems," *New Biotechnology,* vol. 29, no. 1, pp. 56-73, December 2011.

[9] J. M. Yu et al., "Automatic control system for purifcation of H2S-contained waste gas with biotrickling filter," *Journal of PLA University of Science and Technology (Natural Science Edition),* vol. 9, no. 3, pp. 228-231, June 2008. [Abstract].

[10] C. Alonso et al., "Dynamic mathematical model for the Biodegradation of VOCs in a Biofilter: Biomass accumulation study," *Environment Science & Technology,* vol. 32, no. 20, pp. 3118-3123, 1998.

[11] Q. Liao et al., "Mathematical model for gas-liquid two-phase flow and biodegradation of a low concentration volatile organic (VOC) in a trickling biofilter," *International Journal of Heat and Mass Transfer,* vol. 51, pp. 1780-1792, 2008.

[12] S. Sharvelle et al., "Model Development for Biotrickling Filter Treatment of Graywater Simulant and Waste Gas. I," *Journal of Environmental Engineering,* vol. 134, no. 10, pp. 813-825, October 2008.

[13] S. Lee and A. J. Heber, "Ethylene removal using biotrickling filters: part II. Parameter estimation and mathematical simulation," *Chemical Engineering Journal,* vol. 158, pp. 89-99, 2010.

[14] B. I. Dvorak et al., "Evaluation of the Onda Correlations for Mass Transfer with Large Random Packings," *Environmental Science & Technology,* vol. 30, no. 3, pp. 945-953, 1996.

[15] J. R. Welty et al., Fundamentals of Momentum, Heat, and Mass Transfer, 5th ed., New Jersey: John Wiley & Sons, Inc., 2008.

[16] Matlab R2009b Help Files, "ode23, ode45, ode113, ode15s, ode23s, ode23t, ode23tb," The Mathworks, Inc., 2009.

[17] MATLAB R2009b Help Files, "fsolve," The Mathworks, Inc., 2009.

[18] D. E. Seborg et al., Process Dynamics and Control, 3rd ed., New Jersey: John Wiley & Sons, Inc., 2011.

[19] R. K. Pearson, "Nonlinear empirical modeling techniques," *Computers and Chemical Engineering,* vol. 30, p. 1514–1528, July 2006.

[20] W. L. Luyben, Process Modeling, Simulation, and Control for Chemical Engineers, 2nd ed., Boston: McGraw Hill, Inc., 1990.

[21] Loop-Pro TRAINER version 5.1, Tolland, Connecticut: Control Station, Inc., 2008.

[22] H. R. Maier and G. C. Dandy, "Neural Network Based Modelling of Environmental Variables: A Systematic Approach," *Mathematical and Computer Modelling,* vol. 33, pp. 669-682, 2001.

[23] H. Tang et al., Neural Networks: Computational Models and Applications, New York: Springer, 2007.

[24] O. J. Prado et al., "Retrofitting of an Industrial Chemical Scrubber into a Biotrickling Filter: Performance at a Gas Contact Time below 1 s," *Journal of Environmental Engineering,* vol. 135, no. 5, p. 359–366, May 2009.

[25] D. Gabriel et al., "Conversion of Full-Scale Wet Scrubbers to Biotrickling Filters for H2S Control at Publicly Owned Treatment Works," *Journal of Environmental Engineering,* vol. 130, no. 10, p. 1110–1117, October 2004.

[26] E. F. Camacho and C. Bordons, Model Predictive Control, London: Springer, 1999.

[27] Z. K. Nagy, "Model based control of a yeast fermentation bioreactor using optimally designed artificial neural networks," *Chemical Engineering Journal*, vol. 127, p. 95–109, 2007.

[28] B. ZareNezhad and A. Aminian, "Application of the Neural Network-Based Model Predictive Controllers In Nonlinear Industrial Systems. Case Study," *Journal of the University of Chemical Technology and Metallurgy*, vol. 46, no. 1, pp. 67-74, 2011.

[29] J. Chu et al., "Multistep Model Predictive Control Based on Artificial Neural Networks," *Ind. Eng. Chem. Res.*, vol. 42, no. 21, pp. 5215-5228, 2003.

Appendix

MATLAB Codes for Biotrickling Filter Model Solutions

1. Kim & Deshusses' [5] model solution

Function file for ODEs

```
function
dC=gLbio_conc_profiles_lat(t,C,D,H,FT,N,kg,kL,r,A,Fg,FL,Vg,VL,Rm,Ks)
a1=Fg/Vg;
Aw=r*A;
a2=(kg*Aw)/Vg;
a3=(kg*Aw*((1-r)/r))/Vg;
a4=FL/VL;
a5=(kg*Aw)/VL;
a6=(kL*Aw)/VL;
a7=D/(FT^2);

dCg(1)=-a2*(C(1)-H*C(N+1))-a3*(C(1)-H*C(12*N+1));
dCL(1)=a4*(C(2+N)-C(1+N))+a5*(C(1)-H*C(1+N))-a6*(C(1+N)-C(1+2*N));
for j=2:N-1
    dCg(j)=a1*(C(j-1)-C(j))-a2*(C(j)-H*C(j+N))-a3*(C(j)-H*C(j+12*N));
    dCL(j)=a4*(C(j+1+N)-C(j+N))+a5*(C(j)-H*C(j+N))-a6*(C(j+N)-
C(j+2*N));
end
dCg(N)=a1*(C(N-1)-C(N))-a2*(C(N)-H*C(N+N))-a3*(C(N)-H*C(N+12*N));
dCL(N)=a5*(C(N)-H*C(N+N))-a6*(C(N+N)-C(N+2*N));

for j=1:N
    dCwb_interface(j)=a7*(C(j+N)-2*C(j+2*N)+C(j+3*N))-
((Rm*C(j+2*N))/(Ks+C(j+2*N)));
    dCnwb_interface(j)=a7*((C(j)/H)-2*C(j+12*N)+C(j+13*N))-
((Rm*C(j+12*N))/(Ks+C(j+12*N)));
    dCwb_iN(j)=a7*(C(j+10*N)-C(j+11*N))-
((Rm*C(j+11*N))/(Ks+C(j+11*N)));
    dCnwb_iN(j)=a7*(C(j+20*N)-C(j+21*N))-
((Rm*C(j+21*N))/(Ks+C(j+21*N)));
end

for j=1:N
    dCwbi2(j)=a7*(C(2*N+j)-2*C((2+1)*N+j)+C((2+2)*N+j))-
((Rm*C((2+1)*N+j))/(Ks+C((2+1)*N+j)));
    dCwbi3(j)=a7*(C(3*N+j)-2*C((3+1)*N+j)+C((3+2)*N+j))-
((Rm*C((3+1)*N+j))/(Ks+C((3+1)*N+j)));
    dCwbi4(j)=a7*(C(4*N+j)-2*C((4+1)*N+j)+C((4+2)*N+j))-
((Rm*C((4+1)*N+j))/(Ks+C((4+1)*N+j)));
    dCwbi5(j)=a7*(C(5*N+j)-2*C((5+1)*N+j)+C((5+2)*N+j))-
((Rm*C((5+1)*N+j))/(Ks+C((5+1)*N+j)));
    dCwbi6(j)=a7*(C(6*N+j)-2*C((6+1)*N+j)+C((6+2)*N+j))-
((Rm*C((6+1)*N+j))/(Ks+C((6+1)*N+j)));
    dCwbi7(j)=a7*(C(7*N+j)-2*C((7+1)*N+j)+C((7+2)*N+j))-
((Rm*C((7+1)*N+j))/(Ks+C((7+1)*N+j)));
```

```
    dCwbi8(j)=a7*(C(8*N+j)-2*C((8+1)*N+j)+C((8+2)*N+j))-
((Rm*C((8+1)*N+j))/(Ks+C((8+1)*N+j)));
    dCwbi9(j)=a7*(C(9*N+j)-2*C((9+1)*N+j)+C((9+2)*N+j))-
((Rm*C((9+1)*N+j))/(Ks+C((9+1)*N+j)));
    dCnwbi2(j)=a7*(C((2+10)*N+j)-2*C((2+1+10)*N+j)+C((2+2+10)*N+j))-
((Rm*C((2+1+10)*N+j))/(Ks+C((2+1+10)*N+j)));
    dCnwbi3(j)=a7*(C((3+10)*N+j)-2*C((3+1+10)*N+j)+C((3+2+10)*N+j))-
((Rm*C((3+1+10)*N+j))/(Ks+C((3+1+10)*N+j)));
    dCnwbi4(j)=a7*(C((4+10)*N+j)-2*C((4+1+10)*N+j)+C((4+2+10)*N+j))-
((Rm*C((4+1+10)*N+j))/(Ks+C((4+1+10)*N+j)));
    dCnwbi5(j)=a7*(C((5+10)*N+j)-2*C((5+1+10)*N+j)+C((5+2+10)*N+j))-
((Rm*C((5+1+10)*N+j))/(Ks+C((5+1+10)*N+j)));
    dCnwbi6(j)=a7*(C((6+10)*N+j)-2*C((6+1+10)*N+j)+C((6+2+10)*N+j))-
((Rm*C((6+1+10)*N+j))/(Ks+C((6+1+10)*N+j)));
    dCnwbi7(j)=a7*(C((7+10)*N+j)-2*C((7+1+10)*N+j)+C((7+2+10)*N+j))-
((Rm*C((7+1+10)*N+j))/(Ks+C((7+1+10)*N+j)));
    dCnwbi8(j)=a7*(C((8+10)*N+j)-2*C((8+1+10)*N+j)+C((8+2+10)*N+j))-
((Rm*C((8+1+10)*N+j))/(Ks+C((8+1+10)*N+j)));
    dCnwbi9(j)=a7*(C((9+10)*N+j)-2*C((9+1+10)*N+j)+C((9+2+10)*N+j))-
((Rm*C((9+1+10)*N+j))/(Ks+C((9+1+10)*N+j)));
end
dC=[dCg';
    dCL';
    dCwb_interface';
    dCwbi2';
    dCwbi3';
    dCwbi4';
    dCwbi5';
    dCwbi6';
    dCwbi7';
    dCwbi8';
    dCwbi9';
    dCwb_iN';
    dCnwb_interface';
    dCnwbi2';
    dCnwbi3';
    dCnwbi4';
    dCnwbi5';
    dCnwbi6';
    dCnwbi7';
    dCnwbi8';
    dCnwbi9';
    dCnwb_iN'];
```

M-file for solution

```
% Kim & Deshusses' Original Model Simulation (2003)

uL=11.8;                        % Trickling rate (m3/m2.h)
ug=9400;                        % Gas flow rate (m3/m2.h)
N=10;                 % No of segments along the height of BTF/biofilm
FT=(23e-6)/N;                   % Biofilm thickness (m)
Rm=58400;                       % Max reaction rate (g.m3/h)
Ks=0.0279;                      % Michaelis-Menten constant (g/m3)
```

```
H=0.387;                        % Henry's constant
D=5.796e-6;                     % H2S Diffusion coefficient (m2/h)
Dg=0.016332;                    % H2S diffusion in gas using Fuller
correlation at 25C and 1 atm (m2/h)
a=600;                          % Specific interfacial area (m2/m3)
Dp=0.04;                        % Size of packing (m)
rhoL=1007;                      % Density of water (trickling liquid)
(kg/m3)
rhog=1.1845;                    % Density of gas (kg/m3)
mL=3600*0.0008904;              % Viscosity of water at 25C (kg/m.h)
mg=0.0678;                      % Viscosity of gas from HYSYS (kg/m.h)
gc=1.271376e8;                  % Acc. due to gravity (m/h2)
stw=933120;                     % Surface tension of water at room
temperature (kg/h2)

ab=Dp^2;                        % Cross-sectional area of bed (m2)
FL=uL*ab;                       % Volumetric flow rate of liquid (m3/h)
Fg=ug*ab;                       % Volumetric flow rate of gas (m3/h)
L=uL*rhoL;                      % Superficial liq. mass velocity(kg/m2.h)
G=ug*rhog;                      % Superficial gas mass velocity (kg/m2.h)
V=Dp^3;                         % Volume of bed (m3)
A=a*V;                          % Interfacial Area (m2)

% Finding surface tension term in equation 13

rr=0.2298;                       % Wetting ratio at FL=0.01888 m3/h
uLL=11.8;                        % Trickling rate (m3/m2.h)
FLL=uLL*ab;                      % Volumetric flow rate of liquid (m3/h)
LL=uLL*rhoL;                    % Superficial liq. mass velocity (kg/m2.h)
Ree=LL/a/mL;                     % Reynolds number
Frr=(a*LL^2)/gc/(rhoL^2);        % Froude number
Wee=(LL^2)/rhoL/stw/a;           % Weber number
STR=-log(1-rr)/(1.45*(Ree^0.1)*(Frr^(-0.05))*(Wee^0.2));     % Surface
tension ratio term in equation 13

% Finding wetting ratio, wetted area and specific wetted area

Re=L/a/mL;                                                  % Reynolds number
Fr=(a*L^2)/gc/(rhoL^2);                                       % Froude number
We=(L^2)/rhoL/stw/a;                                          % Weber number
r=1-exp(-1.45*STR*(Re^0.1)*(Fr^(-0.05))*(We^0.2));          % Wetting ratio
Aw=r*A;                                                    % Wetted area (m2)
aw=Aw/V;                                             % Specific wetted area
(m2/m3)

% Finding mass transfer coefficients
kg=5.23*((G/(a*mg))^0.7)*((mg/(rhog*Dg))^(1/3))*((a*Dp)^(-2))*a*Dg;
% Gas-Liq mass transfer coefficient (m/h)
kL=0.0051*((L/(aw*mL))^(2/3))*((mL/(rhoL*D))^(-
0.5))*((a*Dp)^0.4)*((rhoL/(mL*gc))^(-1/3));   % Liq-biofilm mass
transfer coefficient (m/h)


% Finding Gas and Liquid Volumes
VL=(0.00001*FL)+0.0000008;    % Dynamic holdup/liq. phase volume (m3)
```

```
Vol_ratio=8.6e4;              % Gas/liquid Volume ratio
Vg=Vol_ratio*VL;              % Gas phase volume (m3)


% Solution

tspan=[0 2];
Cg0=0.164;                    % Initial concentration of H2S (g/m3)
C0=zeros(22*N,1);
C0(1,1)=Cg0;
C0(N+1,1)=Cg0/H;
C0(12*N+1,1)=Cg0/H;

[t,C]=ode23s(@gLbio_conc_profiles_lat,tspan,C0,[],D,H,FT,N,kg,kL,r,A,Fg
,FL,Vg,VL,Rm,Ks)
Time1=[0 0.0132 0.046 0.0658 0.0921 0.112 0.138 0.164 0.1908 0.2171
0.25 0.283 0.322 0.349 0.388 0.428 0.474 0.513 0.566 0.632 0.704 0.803
0.941 1.059 1.257 1.368 1.533 1.717 1.967];
High_Conc_Exp=[0.1640 0.1633 0.1577 0.1542 0.15 0.1451 0.1408 0.1352
0.131 0.1261 0.1218 0.1169 0.112 0.1077 0.1035 0.0986 0.0944 0.0894
0.0845 0.0782 0.0725 0.0655 0.0549 0.0465 0.0345 0.0289 0.0225 0.0162
0.00986];
plot(t,C(:,1),Time1,High_Conc_Exp,'*')
hold on

%  ------------- Low Inlet Concentration -----------------------------

Cg0=0.08592;                    % Initial concentration of H2S (g/m3)
C0=zeros(22*N,1);
C0(1,1)=Cg0;
C0(N+1,1)=Cg0/H;
C0(12*N+1,1)=Cg0/H;

kL=0.0051*((L/(aw*mL))^(2/3))*((mL/(rhoL*D))^(-
0.5))*((a*Dp)^0.4)*((rhoL/(mL*gc))^(-1/3));   % Liq-biofilm mass
transfer coefficient (m/h)
[tlow,C_low]=ode23s(@gLbio_conc_profiles_lat,tspan,C0,[],D,H,FT,N,kg,kL
,r,A,Fg,FL,Vg,VL,Rm,Ks)
Time2=[0 0.0395 0.0658 0.0789 0.1053 0.125 0.1579 0.1908 0.2171 0.2434
0.2763 0.3158 0.3421 0.3816 0.4211 0.4605 0.5132 0.5632 0.625 0.6974
0.7895 0.9342 1.0526];
Low_Conc_Exp=[0.08592 0.07958 0.07465 0.07183 0.06761 0.06408 0.05986
0.05634 0.05211 0.04930 0.04577 0.04225 0.03803 0.03521 0.03239 0.02958
0.02535 0.02254 0.01972 0.01620 0.01268 0.00845 0.00423];
plot(tlow,C_low(:,1),'-.',Time2,Low_Conc_Exp,'o')
xlabel('\bfTime (h)')
ylabel('\bfInlet H_2S Concentration (g/m^3)')
legend('Model High Conc.','Exp. Data High Conc.','Model Low
Conc.','Exp. Data Low Conc.')
axis([-inf inf 0 0.18])
hold off
```

2. Modified model solution

Function file for 1st reactor

```
% Concentration profiles for Reactor in Series Model for 1st Reactor

function
dC=gLbio_conc_profiles_continuos_RIS_R1(t,C,D,H,FT,N,kg,kL,r,A,Fg,FL,Vg
,VL,Rm,Ks)
a1=Fg/Vg;
Aw=r*A;
a2=(kg*Aw)/Vg;
a3=(kg*Aw*((1-r)/r))/Vg;
a4=FL/VL;
a5=(kg*Aw)/VL;
a6=(kL*Aw)/VL;
a7=D/(FT^2);

dCg(1)=0;
dCL(1)=a4*(C(2+N)-C(1+N))+a5*(C(1)-H*C(1+N))-a6*(C(1+N)-C(1+2*N));
for j=2:N-1
    dCg(j)=a1*(C(j-1)-C(j))-a2*(C(j)-H*C(j+N))-a3*(C(j)-H*C(j+12*N));
    dCL(j)=a4*(C(j+1+N)-C(j+N))+a5*(C(j)-H*C(j+N))-a6*(C(j+N)-
C(j+2*N));
end
dCg(N)=a1*(C(N-1)-C(N))-a2*(C(N)-H*C(N+N))-a3*(C(N)-H*C(N+12*N));
dCL(N)=a5*(C(N)-H*C(N+N))-a6*(C(N+N)-C(N+2*N));

for j=1:N
    dCwb_interface(j)=a7*(C(j+N)-2*C(j+2*N)+C(j+3*N))-
((Rm*C(j+2*N))/(Ks+C(j+2*N)));
    dCnwb_interface(j)=a7*((C(j)/H)-2*C(j+12*N)+C(j+13*N))-
((Rm*C(j+12*N))/(Ks+C(j+12*N)));
    dCwb_iN(j)=a7*(C(j+10*N)-C(j+11*N))-
((Rm*C(j+11*N))/(Ks+C(j+11*N)));
    dCnwb_iN(j)=a7*(C(j+20*N)-C(j+21*N))-
((Rm*C(j+21*N))/(Ks+C(j+21*N)));
end

for j=1:N
    dCwbi2(j)=a7*(C(2*N+j)-2*C((2+1)*N+j)+C((2+2)*N+j))-
((Rm*C((2+1)*N+j))/(Ks+C((2+1)*N+j)));
    dCwbi3(j)=a7*(C(3*N+j)-2*C((3+1)*N+j)+C((3+2)*N+j))-
((Rm*C((3+1)*N+j))/(Ks+C((3+1)*N+j)));
    dCwbi4(j)=a7*(C(4*N+j)-2*C((4+1)*N+j)+C((4+2)*N+j))-
((Rm*C((4+1)*N+j))/(Ks+C((4+1)*N+j)));
    dCwbi5(j)=a7*(C(5*N+j)-2*C((5+1)*N+j)+C((5+2)*N+j))-
((Rm*C((5+1)*N+j))/(Ks+C((5+1)*N+j)));
    dCwbi6(j)=a7*(C(6*N+j)-2*C((6+1)*N+j)+C((6+2)*N+j))-
((Rm*C((6+1)*N+j))/(Ks+C((6+1)*N+j)));
    dCwbi7(j)=a7*(C(7*N+j)-2*C((7+1)*N+j)+C((7+2)*N+j))-
((Rm*C((7+1)*N+j))/(Ks+C((7+1)*N+j)));
    dCwbi8(j)=a7*(C(8*N+j)-2*C((8+1)*N+j)+C((8+2)*N+j))-
((Rm*C((8+1)*N+j))/(Ks+C((8+1)*N+j)));
```

```
    dCwbi9(j)=a7*(C(9*N+j)-2*C((9+1)*N+j)+C((9+2)*N+j))-
((Rm*C((9+1)*N+j))/(Ks+C((9+1)*N+j)));
    dCnwbi2(j)=a7*(C((2+10)*N+j)-2*C((2+1+10)*N+j)+C((2+2+10)*N+j))-
((Rm*C((2+1+10)*N+j))/(Ks+C((2+1+10)*N+j)));
    dCnwbi3(j)=a7*(C((3+10)*N+j)-2*C((3+1+10)*N+j)+C((3+2+10)*N+j))-
((Rm*C((3+1+10)*N+j))/(Ks+C((3+1+10)*N+j)));
    dCnwbi4(j)=a7*(C((4+10)*N+j)-2*C((4+1+10)*N+j)+C((4+2+10)*N+j))-
((Rm*C((4+1+10)*N+j))/(Ks+C((4+1+10)*N+j)));
    dCnwbi5(j)=a7*(C((5+10)*N+j)-2*C((5+1+10)*N+j)+C((5+2+10)*N+j))-
((Rm*C((5+1+10)*N+j))/(Ks+C((5+1+10)*N+j)));
    dCnwbi6(j)=a7*(C((6+10)*N+j)-2*C((6+1+10)*N+j)+C((6+2+10)*N+j))-
((Rm*C((6+1+10)*N+j))/(Ks+C((6+1+10)*N+j)));
    dCnwbi7(j)=a7*(C((7+10)*N+j)-2*C((7+1+10)*N+j)+C((7+2+10)*N+j))-
((Rm*C((7+1+10)*N+j))/(Ks+C((7+1+10)*N+j)));
    dCnwbi8(j)=a7*(C((8+10)*N+j)-2*C((8+1+10)*N+j)+C((8+2+10)*N+j))-
((Rm*C((8+1+10)*N+j))/(Ks+C((8+1+10)*N+j)));
    dCnwbi9(j)=a7*(C((9+10)*N+j)-2*C((9+1+10)*N+j)+C((9+2+10)*N+j))-
((Rm*C((9+1+10)*N+j))/(Ks+C((9+1+10)*N+j)));
end

dCnwb_interface(1)=0;
dC=[dCg';
    dCL';
    dCwb_interface';
    dCwbi2';
    dCwbi3';
    dCwbi4';
    dCwbi5';
    dCwbi6';
    dCwbi7';
    dCwbi8';
    dCwbi9';
    dCwb_iN';
    dCnwb_interface';
    dCnwbi2';
    dCnwbi3';
    dCnwbi4';
    dCnwbi5';
    dCnwbi6';
    dCnwbi7';
    dCnwbi8';
    dCnwbi9';
    dCnwb_iN'];
```

Function file for 2nd to nth reactor

```
% Concentration profiles for Reactor in Series Model for 2nd, 3rd ,
% 4th,...., nth Reactor at Steady state

function
F_C=gLbio_conc_profiles_continuos_RIS_Ri(C,M,D,H,FT,N,kg,kL,r,A,Fg,FL,V
g,VL,Rm,Ks)
a1=Fg/Vg;
Aw=r*A;
a2=(kg*Aw)/Vg;
a3=(kg*Aw*((1-r)/r))/Vg;
a4=FL/VL;
a5=(kg*Aw)/VL;
a6=(kL*Aw)/VL;
a7=D/(FT^2);

F_Cg(1)=a1*(M-C(1))-a2*(C(1)-H*C(1+N))-a3*(C(1)-H*C(1+12*N));
F_CL(1)=a4*(C(1+N)-C(1+N-1))+a5*(M-H*C(1+N))-a6*(C(1+N-1)-C(1+2*N-1));
for j=2:N-1
    F_Cg(j)=a1*(C(j-1)-C(j))-a2*(C(j)-H*C(j+N))-a3*(C(j)-H*C(j+12*N));
    F_CL(j)=a4*(C(j+1+N-1)-C(j+N-1))+a5*(C(j-1)-H*C(j+N-1))-a6*(C(j+N-
1)-C(j+2*N-1));
end
F_CL(N)=a5*(C(N-1)-H*C(N+N-1))-a6*(C(N+N-1)-C(N+2*N-1));

F_Cwb_interface(1)=a7*(C(1+N-1)-2*C(1+2*N-1)+C(1+3*N-1))-((Rm*C(1+2*N-
1))/(Ks+C(1+2*N-1)));
F_Cnwb_interface(1)=a7*((M/H)-2*C(1+12*N-1)+C(1+13*N-1))-((Rm*C(1+12*N-
1))/(Ks+C(1+12*N-1)));
F_Cwb_iN(1)=a7*(C(1+10*N-1)-C(1+11*N-1))-((Rm*C(1+11*N-
1))/(Ks+C(1+11*N-1)));
F_Cnwb_iN(1)=a7*(C(1+20*N-1)-C(1+21*N-1))-((Rm*C(1+21*N-
1))/(Ks+C(1+21*N-1)));

for j=2:N
    F_Cwb_interface(j)=a7*(C(j+N-1)-2*C(j+2*N-1)+C(j+3*N-1))-
((Rm*C(j+2*N-1))/(Ks+C(j+2*N-1)));
    F_Cnwb_interface(j)=a7*((C(j-1)/H)-2*C(j+12*N-1)+C(j+13*N-1))-
((Rm*C(j+12*N-1))/(Ks+C(j+12*N-1)));
    F_Cwb_iN(j)=a7*(C(j+10*N-1)-C(j+11*N-1))-((Rm*C(j+11*N-
1))/(Ks+C(j+11*N-1)));
    F_Cnwb_iN(j)=a7*(C(j+20*N-1)-C(j+21*N-1))-((Rm*C(j+21*N-
1))/(Ks+C(j+21*N-1)));
end


for j=1:N
    F_Cwbi2(j)=a7*(C(2*N+j-1)-2*C((2+1)*N+j-1)+C((2+2)*N+j-1))-
((Rm*C((2+1)*N+j-1))/(Ks+C((2+1)*N+j-1)));
    F_Cwbi3(j)=a7*(C(3*N+j-1)-2*C((3+1)*N+j-1)+C((3+2)*N+j-1))-
((Rm*C((3+1)*N+j-1))/(Ks+C((3+1)*N+j-1)));
    F_Cwbi4(j)=a7*(C(4*N+j-1)-2*C((4+1)*N+j-1)+C((4+2)*N+j-1))-
((Rm*C((4+1)*N+j-1))/(Ks+C((4+1)*N+j-1)));
```

```
    F_Cwbi5(j)=a7*(C(5*N+j-1)-2*C((5+1)*N+j-1)+C((5+2)*N+j-1))-
((Rm*C((5+1)*N+j-1))/(Ks+C((5+1)*N+j-1)));
    F_Cwbi6(j)=a7*(C(6*N+j-1)-2*C((6+1)*N+j-1)+C((6+2)*N+j-1))-
((Rm*C((6+1)*N+j-1))/(Ks+C((6+1)*N+j-1)));
    F_Cwbi7(j)=a7*(C(7*N+j-1)-2*C((7+1)*N+j-1)+C((7+2)*N+j-1))-
((Rm*C((7+1)*N+j-1))/(Ks+C((7+1)*N+j-1)));
    F_Cwbi8(j)=a7*(C(8*N+j-1)-2*C((8+1)*N+j-1)+C((8+2)*N+j-1))-
((Rm*C((8+1)*N+j-1))/(Ks+C((8+1)*N+j-1)));
    F_Cwbi9(j)=a7*(C(9*N+j-1)-2*C((9+1)*N+j-1)+C((9+2)*N+j-1))-
((Rm*C((9+1)*N+j-1))/(Ks+C((9+1)*N+j-1)));
    F_Cnwbi2(j)=a7*(C((2+10)*N+j-1)-2*C((2+1+10)*N+j-1)+C((2+2+10)*N+j-
1))-((Rm*C((2+1+10)*N+j-1))/(Ks+C((2+1+10)*N+j-1)));
    F_Cnwbi3(j)=a7*(C((3+10)*N+j-1)-2*C((3+1+10)*N+j-1)+C((3+2+10)*N+j-
1))-((Rm*C((3+1+10)*N+j-1))/(Ks+C((3+1+10)*N+j-1)));
    F_Cnwbi4(j)=a7*(C((4+10)*N+j-1)-2*C((4+1+10)*N+j-1)+C((4+2+10)*N+j-
1))-((Rm*C((4+1+10)*N+j-1))/(Ks+C((4+1+10)*N+j-1)));
    F_Cnwbi5(j)=a7*(C((5+10)*N+j-1)-2*C((5+1+10)*N+j-1)+C((5+2+10)*N+j-
1))-((Rm*C((5+1+10)*N+j-1))/(Ks+C((5+1+10)*N+j-1)));
    F_Cnwbi6(j)=a7*(C((6+10)*N+j-1)-2*C((6+1+10)*N+j-1)+C((6+2+10)*N+j-
1))-((Rm*C((6+1+10)*N+j-1))/(Ks+C((6+1+10)*N+j-1)));
    F_Cnwbi7(j)=a7*(C((7+10)*N+j-1)-2*C((7+1+10)*N+j-1)+C((7+2+10)*N+j-
1))-((Rm*C((7+1+10)*N+j-1))/(Ks+C((7+1+10)*N+j-1)));
    F_Cnwbi8(j)=a7*(C((8+10)*N+j-1)-2*C((8+1+10)*N+j-1)+C((8+2+10)*N+j-
1))-((Rm*C((8+1+10)*N+j-1))/(Ks+C((8+1+10)*N+j-1)));
    F_Cnwbi9(j)=a7*(C((9+10)*N+j-1)-2*C((9+1+10)*N+j-1)+C((9+2+10)*N+j-
1))-((Rm*C((9+1+10)*N+j-1))/(Ks+C((9+1+10)*N+j-1)));
end

F_C=[F_Cg';
    F_CL';
    F_Cwb_interface';
    F_Cwbi2';
    F_Cwbi3';
    F_Cwbi4';
    F_Cwbi5';
    F_Cwbi6';
    F_Cwbi7';
    F_Cwbi8';
    F_Cwbi9';
    F_Cwb_iN';
    F_Cnwb_interface';
    F_Cnwbi2';
    F_Cnwbi3';
    F_Cnwbi4';
    F_Cnwbi5';
    F_Cnwbi6';
    F_Cnwbi7';
    F_Cnwbi8';
    F_Cnwbi9';
    F_Cnwb_iN'];
```

M-file for solution

```
% Kim & Deshusses Modified Model (2003)


% CONTINUOS MODE OF OPERATION for Reactor in Series Model

uL=11.8;                        % Trickling rate (m3/m2.h)
ug=9400;                        % Gas flow rate (m3/m2.h)
N=10;                  % No of segments along the height of BTF/biofilm
FT=(23e-6)/N;                   % Biofilm thickness (m)
Rm=58400;                       % Max reaction rate (g.m3/h)
Ks=0.0279;                      % Michaelis-Menten constant (g/m3)
H=0.387;                        % Henry's constant
D=5.796e-6;                     % H2S Diffusion coefficient (m2/h)
Dg=0.016332;                    % H2S diffusion in gas using Fuller
correlation at 25C and 1 atm (m2/h)
a=600;                          % Specific interfacial area (m2/m3)
Dp=0.04;                        % Size of packing (m)
rhoL=1007;                % Density of water (trickling liquid) (kg/m3)
rhog=1.1845;                    % Density of gas (kg/m3)
mL=3600*0.0008904;              % Viscosity of water at 25C (kg/m.h)
mg=0.0678;                      % Viscosity of gas from HYSYS (kg/m.h)
gc=1.271376e8;                  % Acc. due to gravity (m/h2)
stw=933120;      % Surface tension of water at room temperature (kg/h2)

ab=Dp^2;                        % Cross-sectional area of bed (m2)
FL=uL*ab;                       % Volumetric flow rate of liquid (m3/h)
Fg=ug*ab;                       % Volumetric flow rate of gas (m3/h)
L=uL*rhoL;                     % Superficial liq. mass velocity (kg/m2.h)
G=ug*rhog;                      % Superficial gas mass velocity (kg/m2.h)
V=Dp^3;                         % Volume of bed (m3)
A=a*V;                          % Interfacial Area (m2)

% Finding surface tension term in equation 13

rr=0.2298;                          % Wetting ratio at FL=0.01888 m3/h
uLL=11.8;                           % Trickling rate (m3/m2.h)
FLL=uLL*ab;                       % Volumetric flow rate of liquid (m3/h)
LL=uLL*rhoL;                % Superficial liq. mass velocity (kg/m2.h)
Ree=LL/a/mL;                        % Reynolds number
Frr=(a*LL^2)/gc/(rhoL^2);           % Froude number
Wee=(LL^2)/rhoL/stw/a;              % Weber number
STR=-log(1-rr)/(1.45*(Ree^0.1)*(Frr^(-0.05))*(Wee^0.2));     % Surface
tension ratio term in equation 13

% Finding wetting ratio, wetted area and specific wetted area

Re=L/a/mL;                                          % Reynolds number
Fr=(a*L^2)/gc/(rhoL^2);                                  % Froude number
We=(L^2)/rhoL/stw/a;                                     % Weber number
r=1-exp(-1.45*STR*(Re^0.1)*(Fr^(-0.05))*(We^0.2));       % Wetting ratio
Aw=r*A;                                                % Wetted area (m2)
aw=Aw/V;                                  % Specific wetted area (m2/m3)
```

```
% Finding mass transfer coefficients
kg=5.23*((G/(a*mg))^0.7)*((mg/(rhog*Dg))^(1/3))*((a*Dp)^(-2))*a*Dg;
% Gas-Liq mass transfer coefficient (m/h)
kL=0.0051*((L/(aw*mL))^(2/3))*((mL/(rhoL*D))^(-
0.5))*((a*Dp)^0.4)*((rhoL/(mL*gc))^(-1/3));   % Liq-biofilm mass
transfer coefficient (m/h)


% Finding Gas and Liquid Volumes
VL=(0.00001*FL)+0.0000008;    % Dynamic holdup/liq. phase volume (m3)
Vol_ratio=8.6e4;              % Gas/liquid Volume ratio
Vg=Vol_ratio*VL;              % Gas phase volume (m3)


% Solution

tspan=0:0.0014:0.3;
Cg0(1)=0.164;          % Inlet concentration to the first reactor (g/m3)
C0=zeros(22*N,1);
C0(1,1)=Cg0(1);
C0(N+1,1)=Cg0(1)/H;
C0(12*N+1,1)=Cg0(1)/H;
[t,C]=ode15s(@gLbio_conc_profiles_continuos_RIS_R1,tspan,C0,[],D,H,FT,N
,kg,kL,r,A,Fg,FL,Vg,VL,Rm,Ks);
Ci_out=C(:,N);
plot(t,Ci_out)
hold on
C_Out_SS(1)=C(length(t),N);

n=40;

for I=2:n
ANS=[];
for i=1:length(Ci_out)
M=Ci_out(i);
Css0=zeros(22*N-1,1);
Css=fsolve(@gLbio_conc_profiles_continuos_RIS_Ri,Css0,[],M,D,H,FT,N,kg,
kL,r,A,Fg,FL,Vg,VL,Rm,Ks);
CSS=[M;Css];
ANS=[ANS;M CSS(N)];
end
Ci_out=ANS(:,2);
C_Out_SS(I)=Ci_out(length(t));
plot(t,Ci_out)
hold on
end
xlabel('\bfTime (h)')
ylabel('\bfC_g_,_o_u_t (g/m^3)')
title('\bfOutlet Concentration of H_2S for each reactor','FontSize',12)
hold off
figure (2)
plot(t,Ci_out)
xlabel('\bfTime (h)')
ylabel('\bfC_g_,_o_u_t (g/m^3)')
Z=0:n;
```

```
Cz_ss=[Cg0(1);C_Out_SS'];
figure(3)
plot(Z,Cz_ss)
xlabel('\bfPosition along the length of Reactor')
ylabel('\bfH_2S Concentration at Steady State (g/m^3)')
figure(4)
Lr=0.04*Z;     % Length of reactor (m)
plot(Lr,Cz_ss)
xlabel('\bfDistance along the length of Reactor (m)')
ylabel('\bfH_2S Concentration at Steady State (g/m^3)')
```

Simulink Block Flow Diagrams for Simulation of Data Driven BTF Models

1. BTF transfer function model simulation

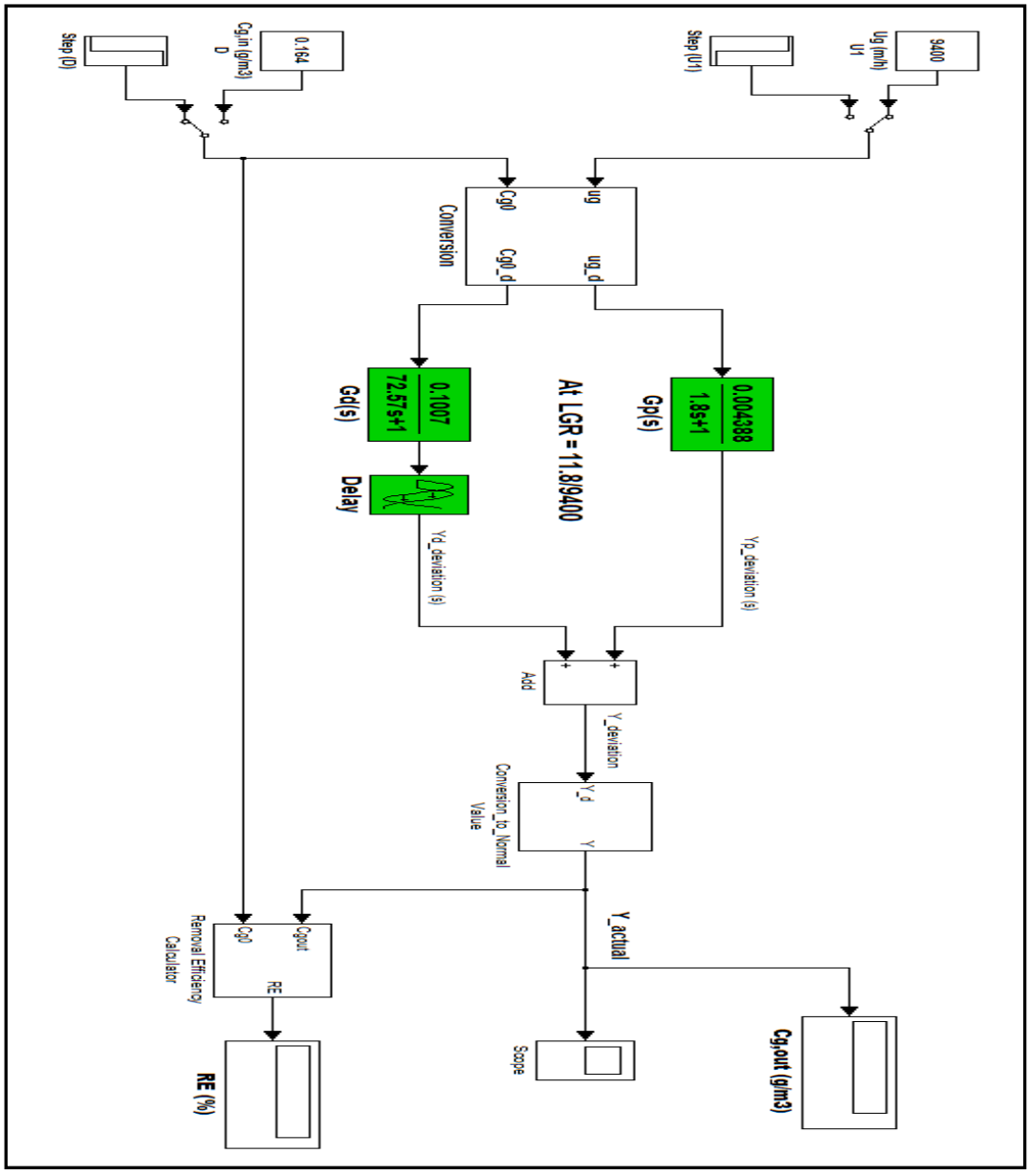

Note: the transfer function models for process and disturbance were obtained from Loop Pro TRAINER 5.1

2. Steady state BTF NN model simulation

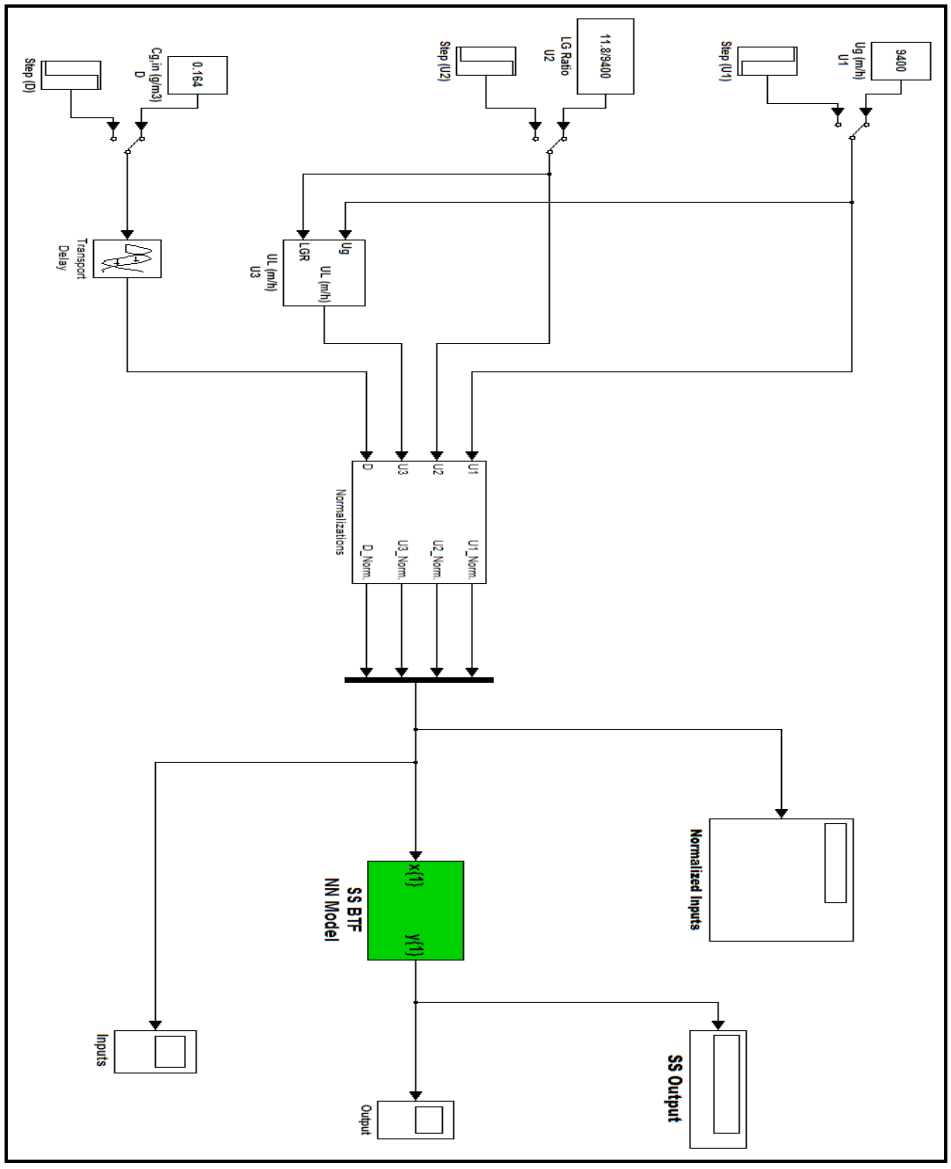

Simulink Block Flow Diagrams for Simulation of Control Systems

1. PI Controller

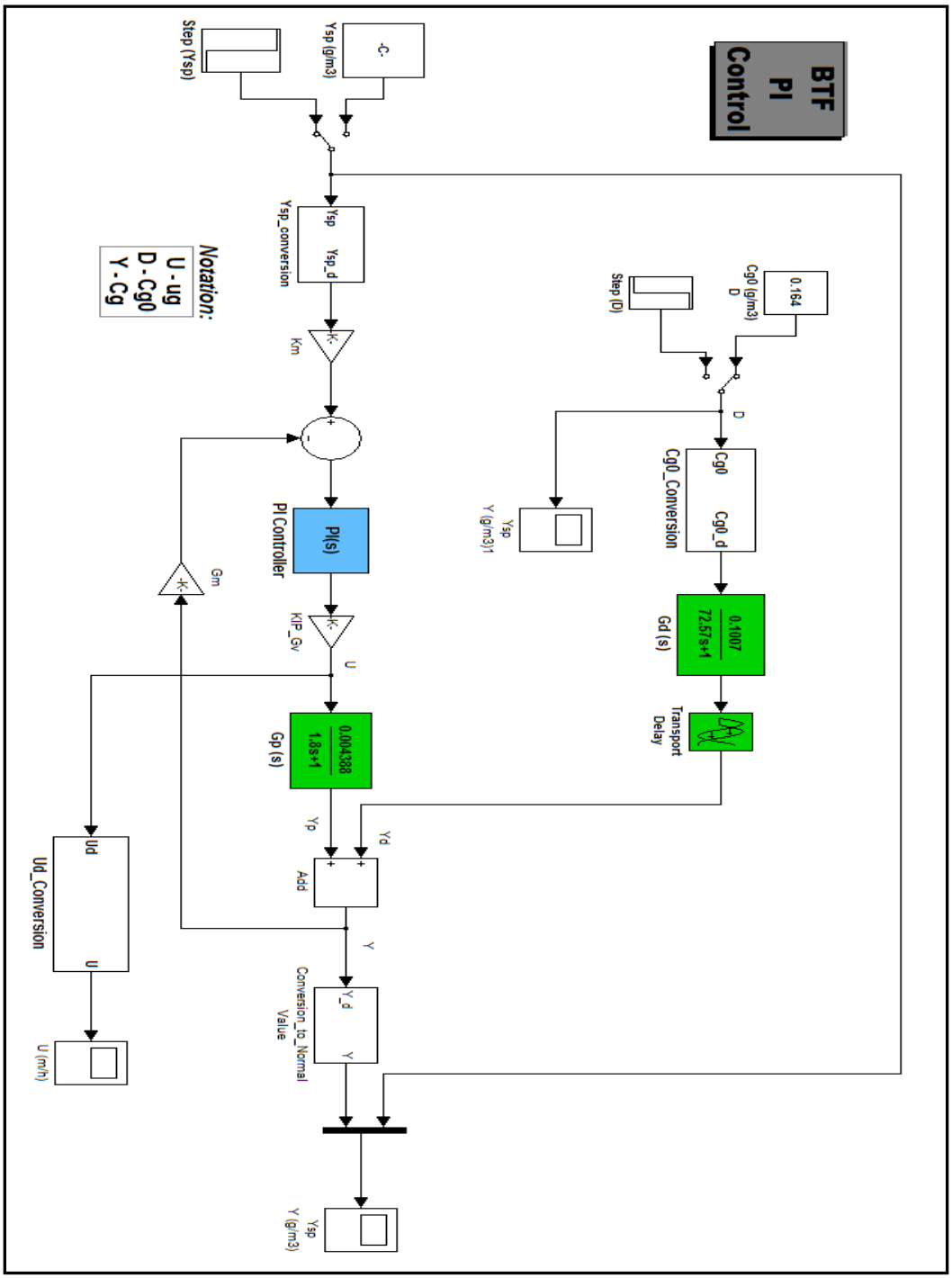

2. FB PI - FF Controller

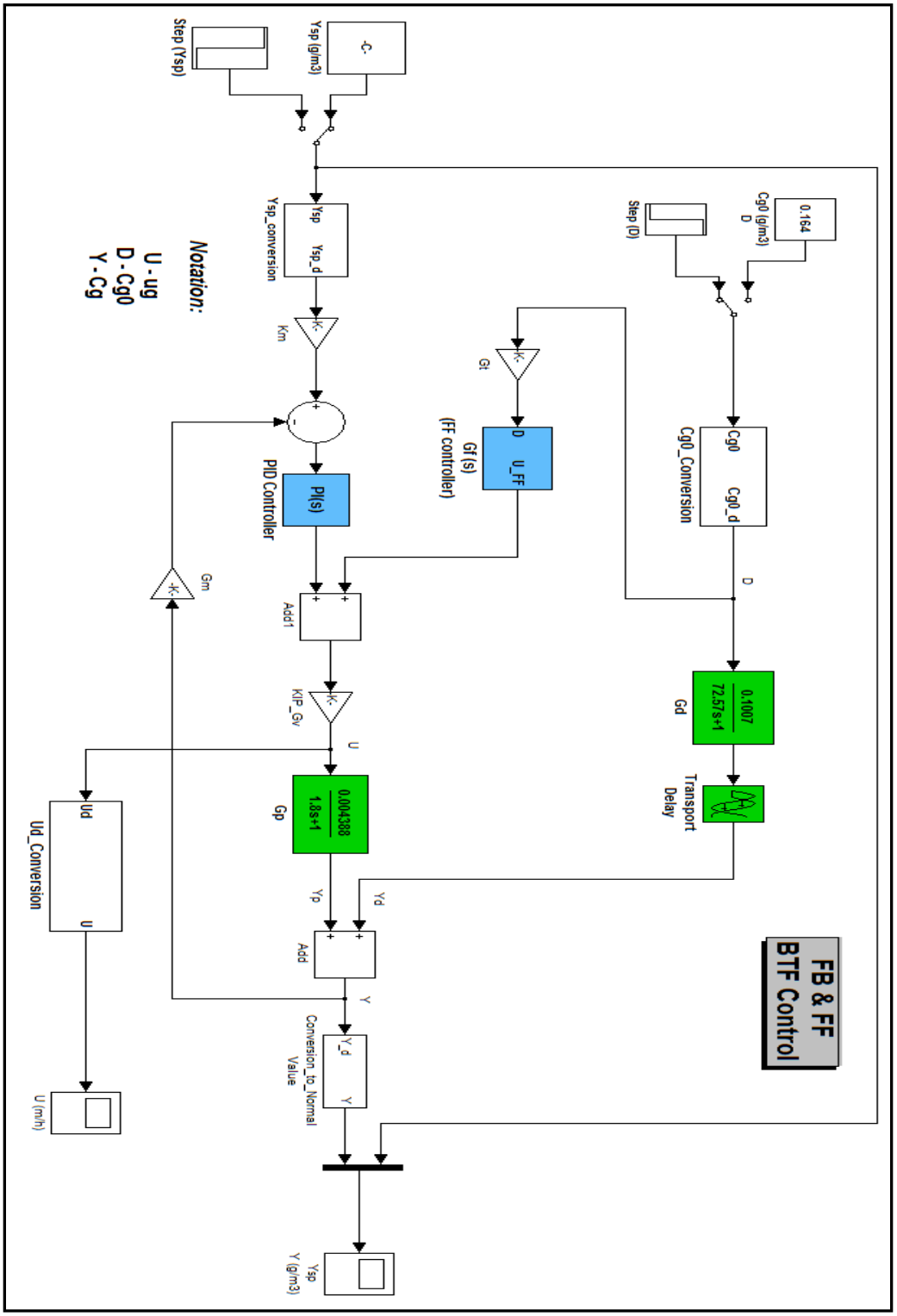

3. TF MPC controller

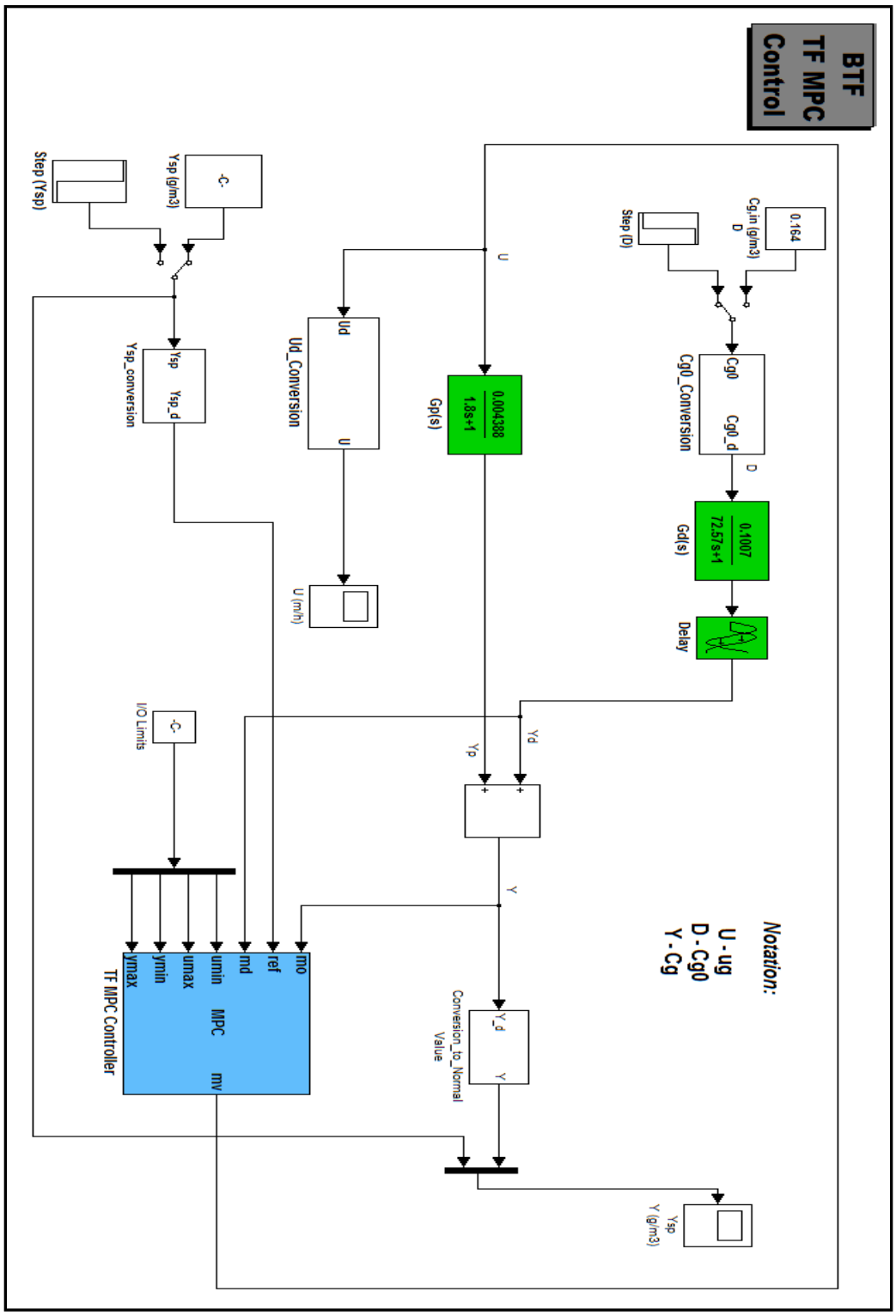

4. NNMPC controller

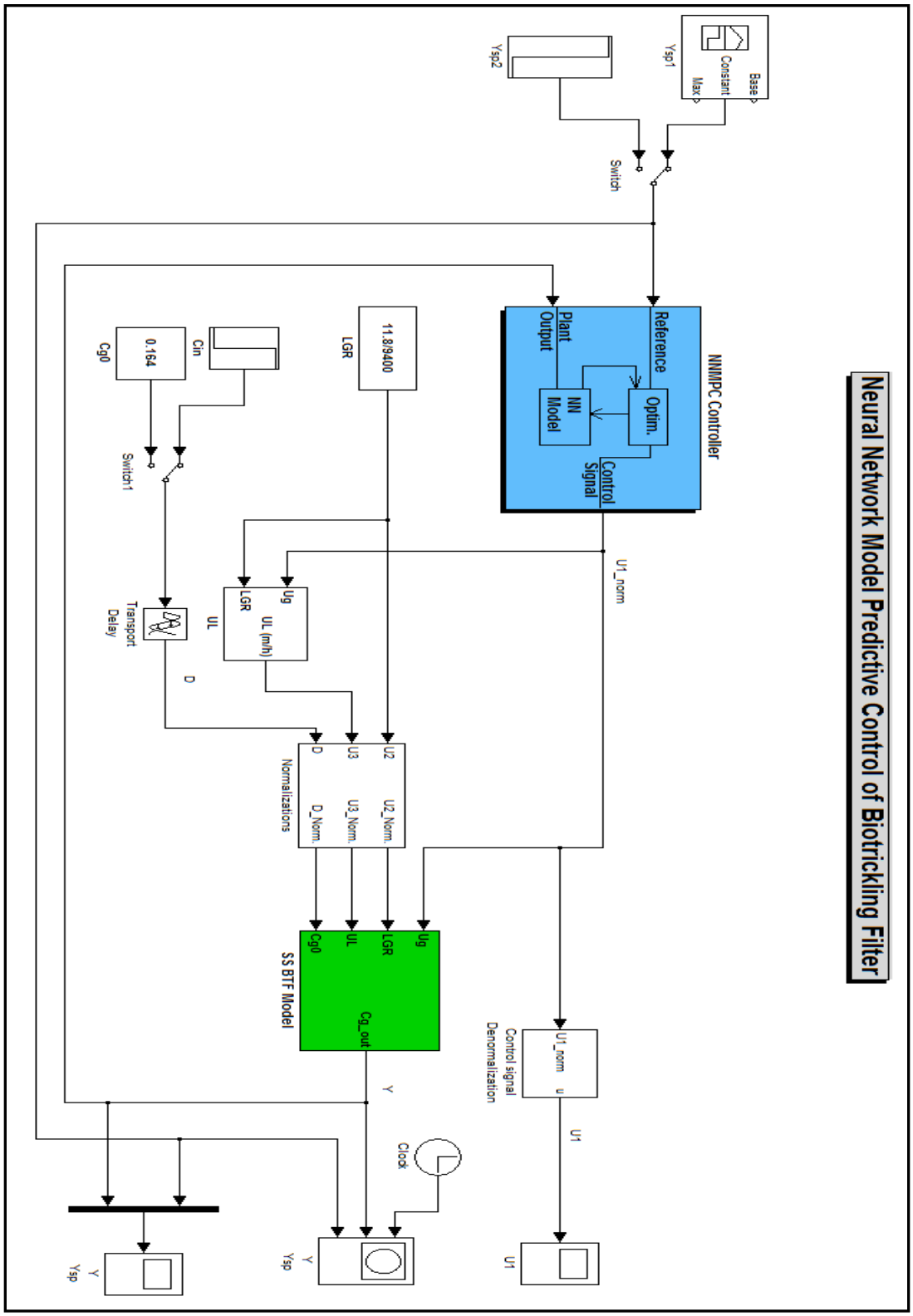

5. NNMPC + Integral controller

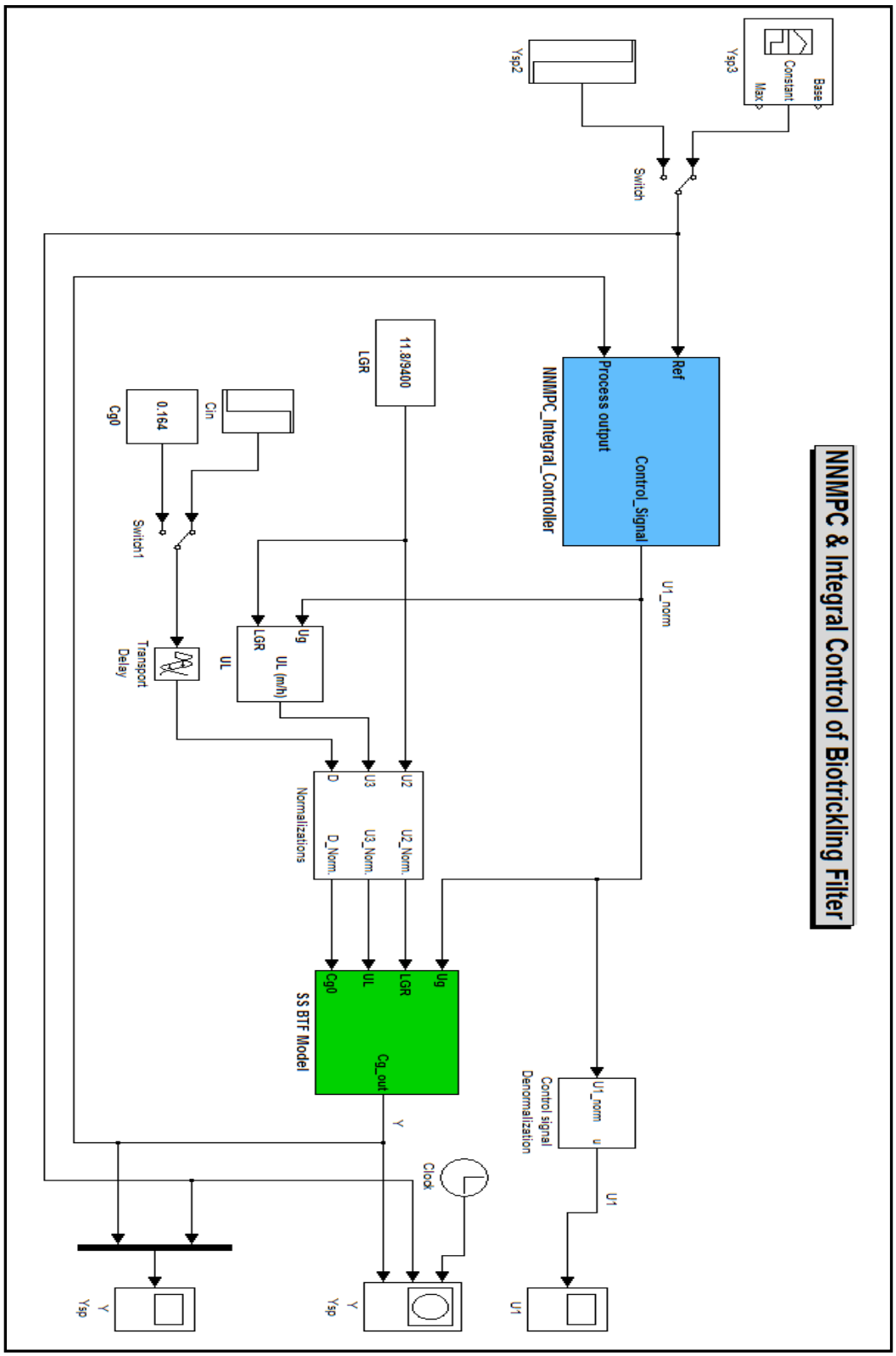

6. Control system comparisons for set-point changes

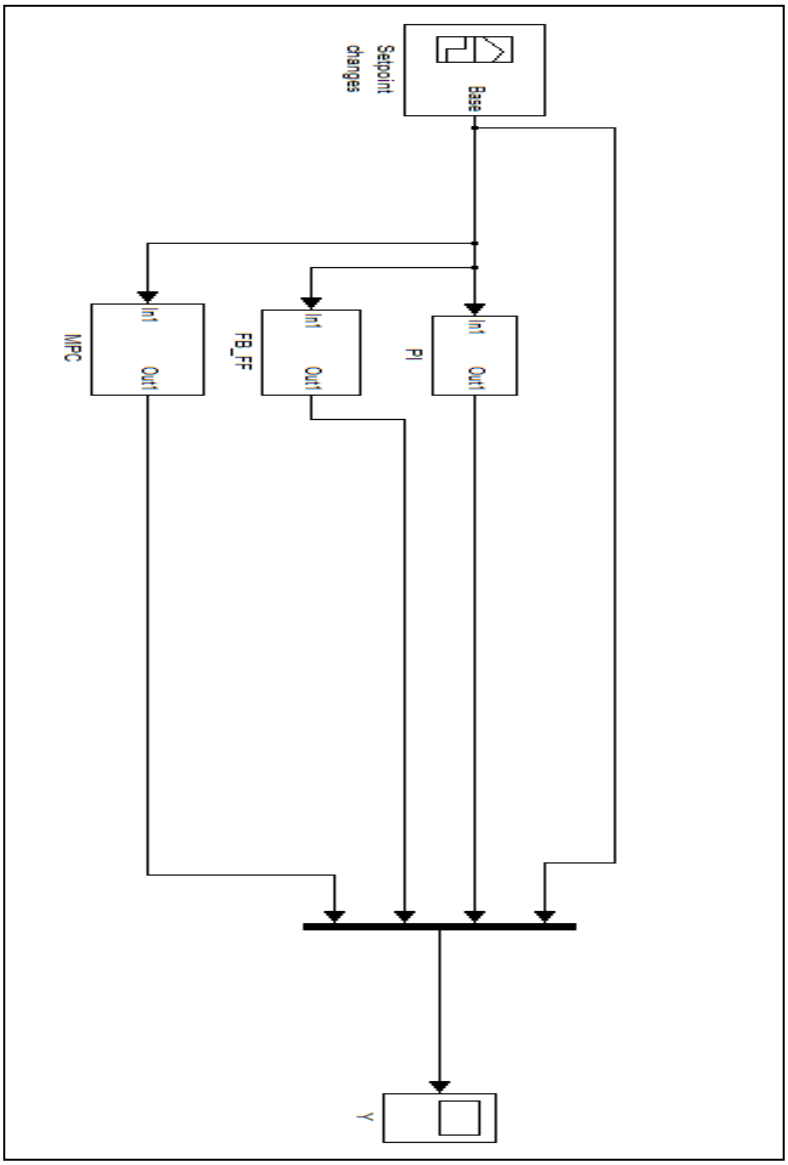

7. Control system comparisons for set-point changes

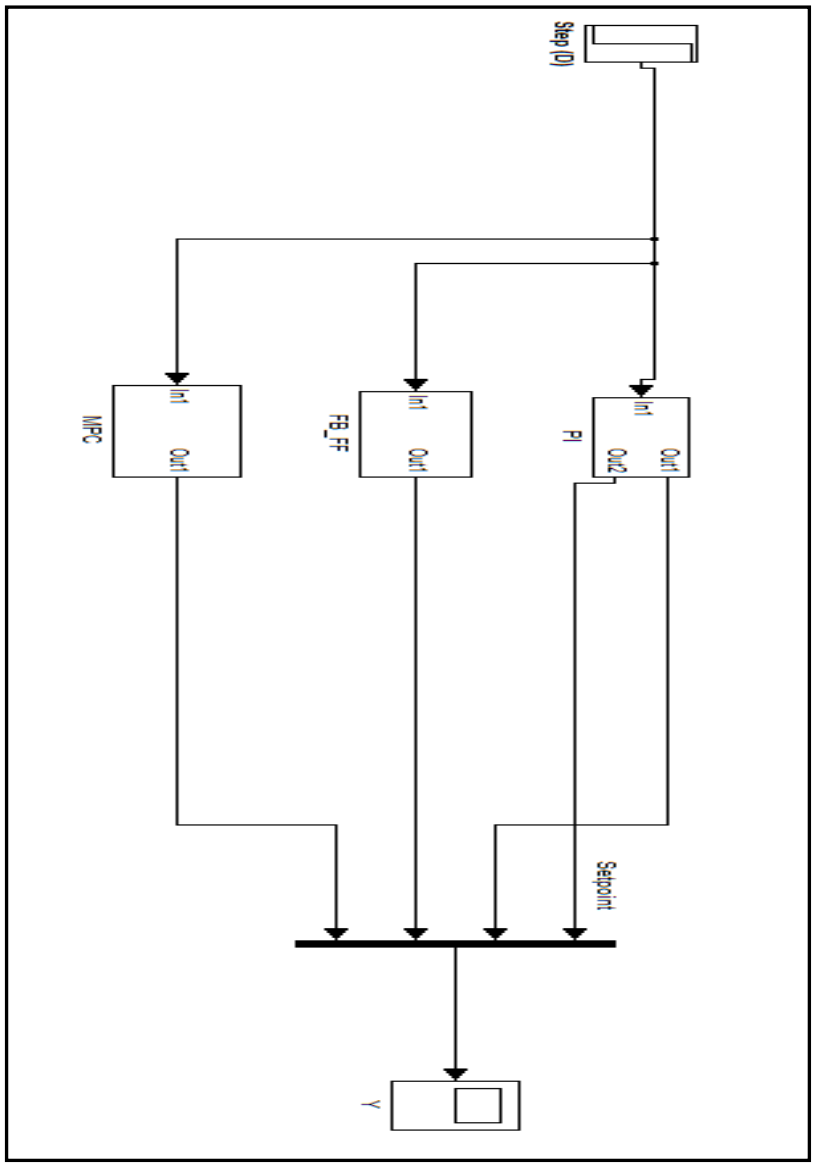

Vita

Originally from Pakistan, Wasim Ahmed Bashir was born on April 28, 1985, in Dubai, United Arab Emirates. He started his primary education from an English school with British Curriculum in Al Sadiq Islamic English School, conveniently located in the city of Dubai. He successfully completed his O' Level and graduated with top position in 2002. Aiming for further education, he enrolled in the English Medium School, where he completed his A' Level and graduated as a science student in 2005.

Mr Ahmed enrolled in American University of Sharjah and graduated *cum laude* with a Bachelor of Science Degree in Chemical Engineering and a Minor in Engineering Management in 2009. During his years as an undergraduate student, he received academic scholarship and had been in the Dean's list for four semesters. From his undergraduate senior design collaborative project on biofilter process, he got to publish two scholarly articles. In 2010, he continued to pursue his education by enrolling in a Master's program in Chemical Engineering at the American University of Sharjah. Under the student assistantship program, he worked as a computer lab assistant at the university for one year and then as a computer lab instructor for a computer methods undergraduate course. He is expected to graduate in 2012.